Retrospective Theses and Dissertations

Iowa State University Capstones, Theses and Dissertations

1976

Investigations of several interference effects in high frequency plasmas of analytical importance

George Frederic Larson

Iowa State University

INFORMATION TO USERS

This material was produced from a microfilm copy of the original document. While the most advanced technological means to photograph and reproduce this document have been used, the quality is heavily dependent upon the quality of the original submitted.

The following explanation of techniques is provided to help you understand markings or patterns which may appear on this reproduction.

1. The sign or "target" for pages apparently lacking from the document photographed is "Missing Page(s)". If it was possible to obtain the missing page(s) or section, they are spliced into the film along with adjacent pages. This may have necessitated cutting thru an image and duplicating adjacent pages to insure you complete continuity.

2. When an image on the film is obliterated with a large round black mark, it is an indication that the photographer suspected that the copy may have moved during exposure and thus cause a blurred image. You will find a good image of the page in the adjacent frame.

3. When a map, drawing or chart, etc., was part of the material being photographed the photographer followed a definite method in "sectioning" the material. It is customary to begin photoing at the upper left hand corner of a large sheet and to continue photoing from left to right in equal sections with a small overlap. If necessary, sectioning is continued again — beginning below the first row and continuing on until complete.

4. The majority of users indicate that the textual content is of greatest value, however, a somewhat higher quality reproduction could be made from "photographs" if essential to the understanding of the dissertation. Silver prints of "photographs" may be ordered at additional charge by writing the Order Department, giving the catalog number, title, author and specific pages you wish reproduced.

5. PLEASE NOTE: Some pages may have indistinct print. Filmed as received.

77-10,325

LARSON, George Frederic, 1949-
  INVESTIGATIONS OF SEVERAL INTERFERENCE
  EFFECTS IN HIGH FREQUENCY PLASMAS OF
  ANALYTICAL IMPORTANCE.

  Iowa State University, Ph.D., 1976
  Chemistry, analytical

Investigations of several interference effects in

high frequency plasmas of analytical importance

by

George Frederic Larson

A Dissertation Submitted to the

Graduate Faculty in Partial Fulfillment of

The Requirements for the Degree of

DOCTOR OF PHILOSOPHY

Department: Chemistry
Major: Analytical Chemistry

Approved:

Signature was redacted for privacy.

In Charge of Major Work

Signature was redacted for privacy.

For the Major Department

Signature was redacted for privacy.

For the Graduate College

Iowa State University
Ames, Iowa

1976

TABLE OF CONTENTS

Page

CHAPTER I. INTRODUCTION

Since the initial studies of the analytical applications
of the inductively coupled plasma (ICP) by Greenfield and
associates (1) and Wendt and Fassel (2,3), the ICP has
emerged as a very useful excitation source for the simul-
taneous multielement determination of trace elements in
solution. The analytical applications of the ICP have been
reviewed recently (4-9). The samples are usually examined
by generating an aerosol out of the solution containing the
analyte. After introduction into the high temperature
plasma, the aerosol particles are rapidly decomposed into
their constituent atoms. The emission spectra emitted by
the released free atoms are dispersed by a spectrometer.
The output of the detector is related to the total concen-
tration in the solution of the analyte whose emission line
impinges on the detector. Because absolute intensity
measurements are not made, analytical calibration curves are
usually established by measurements on a series of reference
solutions of known composition. To obtain accurate results,
the composition of the actual samples must match that of the
reference solutions to the extent that neither the chemical
form nor the presence of concomitants produces a significant
bias in the analytical measure. The presence of varying
concentrations of concomitants in the samples may cause an
interference, i.e., a systematic error in the analytical

measure. Consequently, the ultimate scope of application of the ICP will depend to a great extent on its degree of freedom from the interference effects.

The types of interferences encountered in atomic emission spectrometric techniques based on the vaporization, atomization and excitation of liquid samples may be classified according to several viewpoints (10): transport, solute vaporization, vapor phase, flame or plasma geometry, and spatial distribution interferences; specific and non-specific interferences; physical and chemical interferences; and spectral interferences. These various types of interferences are not mutually exclusive in their actions or mechanisms. The most important types of interferences are the solute vaporization, ionization (a type of vapor phase interference) and spectral interferences.

Solute vaporization interferences occur when the rate of vaporization of the desolvated aerosol particle is altered by the presence of a concomitant (11,12). A reduced efficiency of free atom formation can result from the formation of a less volatile compound. With this type of interference, a plot of the analyte emission intensity versus the concentration of the concomitant exhibits a linear decrease in intensity followed by a "knee" and a plateau region (11-14). The "knee" in the curve usually occurs at concentration ratios of the concomitant to the

analyte equivalent to the formation of a definite refractory compound. The plateau region indicates that the excess interferent is readily vaporized from the aerosol droplet. A solute vaporization interference may also result from the occlusion of the analyte in a refractory matrix of the concomitant which is not completely vaporized in the vaporization-atomization source (11-13,15-17). With this type of interference, the analyte emission intensity drops smoothly toward zero with increasing concentrations of the interferent. The types of solute vaporization interferences discussed above may occur in combination for a given pair of analyte and interferent.

An ionization interference results from a shift in the ionization equilibrium of the analyte (M):

$$M^0 \rightleftarrows M^+ + e^-.$$
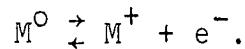
Because the electron number density is relatively low in combustion flames with only a small quantity of metallic species introduced, the presence of easily ionizable elements in the sample may produce significant increases in the electron number density (11,18-20). The resulting shift in the ionization equilibrium will produce an increase in the neutral atom number density and an accompanying (but not necessarily equal) decrease in the ion number density. Although a larger number of analytes will possess significant

degrees of ionization in high temperature plasmas than in combustion flames, ionization interferences are not necessarily more pronounced. This is due to the higher electron number density in the absence of significant quantities of metallic species as well as possible deviations from local thermodynamic equilibrium (21-25). It is also relevant to acknowledge that the addition of easily ionizable elements to various electrically generated, high temperature plasmas has been found to produce significant changes in temperature (26-29) and the spatial distributions of the analyte species (30-32). Thus, the presence of varying concentrations of easily ionizable elements constitutes a significant source of interferences in many electrically generated, high temperature plasmas.

In this dissertation, the results of an investigation of the degree to which several solute vaporization and ionization interferences are observed in the ICP are presented in a quantitative manner. The results of a comparative study of several interference effects in the ICP and in a microwave-excited single electrode plasma are also presented.

When atomic emission spectrometry is employed for the determination of trace elements at concentration levels near the detection limit, the spectral background is normally a large fraction of the total measured signal. Thus, accurate

background correction is a necessity. For samples of varying composition, changes in the concentrations of concomitants often produce changes in background levels. Two specific sources of these background shifts which have received little attention, i.e., stray light and the wings of broadened emission lines, are discussed. Experimental evidence is presented showing various forms of stray light originating from defects in the optical components, design and engineering of optical spectrometers. Experimental evidence is also presented illustrating that in high temperature sources the wings of certain spectral lines may contribute a significant continuum at wavelengths as far removed as 10 nm or more from the line center.

CHAPTER II. INVESTIGATIONS OF SEVERAL INTERFERENCE
EFFECTS IN THE INDUCTIVELY COUPLED PLASMA

Introduction

The presence and degree to which certain interference
effects are observed in ICP's appear to be sensitively
dependent on a number of plasma properties (4-7,33-35). In
view of this dependency, it is instructive to explore some
of the unique properties of the annular shaped ICP (1,4,36,
37) which appear to lead not only to the high degree of
freedom from interference effects but also to some of the
other desirable analytical characteristics. A schematic
diagram of the typical annular shaped ICP configuration,
including the concentric quartz tubes, the Ar flow patterns,
the load coil, and the magnetic fields (H) induced by the
radiofrequency currents (I) in the load coil, is shown in
Figure 1. For the initiation of the plasma, the Ar support
gas is partially ionized by a tesla coil discharge. The
liberated electrons and ions couple to the magnetic fields
and are accelerated on each half cycle of the oscillating
magnetic field. The accelerated ions and electrons flow in
closed annular paths (eddy current) inside the quartz tube.
The electrons (and ions) meet resistance to their flow,
Joule heating results as a natural consequence, and
additional ionization occurs. The steps discussed above

H I I H

ARGON PLASMA
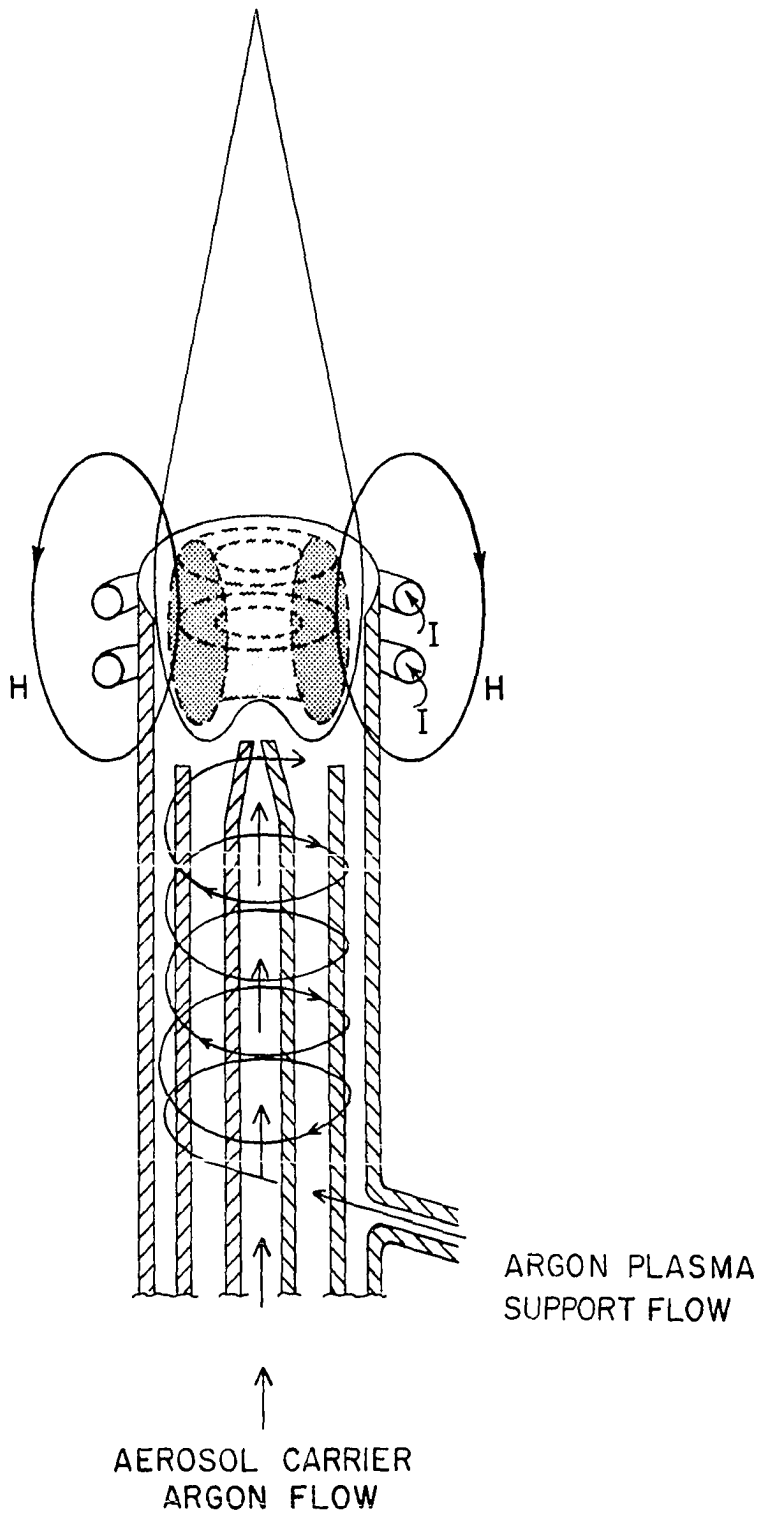SUPPORT FLOW

AEROSOL CARRIER
ARGON FLOW

Figure 1. Schematic diagram of typical annular shaped plasma

lead to an almost instantaneous formation of a plasma of extended dimensions.

Thermal isolation of the plasma is normally achieved with Reed's vortex stabilization technique (38,39), which utilizes a flow of Ar introduced tangentially along the outer quartz tube as shown in Figure 1.

After initiation of the plasma, an additional Ar flow (∿1 l/min) carrying the suspended aerosol particles is introduced through the central quartz tube. In order for the plasma to serve its desired purpose, i.e., the production and excitation of free atoms, the sample particles must be efficiently injected into the plasma and remain in the high temperature environment for as long as possible. This physical situation has been difficult or impossible to achieve in many plasma configurations that have been proposed for analytical (40,41) and other (42-47) purposes. Although the theoretical basis for the rejection of particles by high temperature plasmas has not been refined, there have been numerous observations of the deflection of particles by plasmas. The primary force opposing the injection of particles is the expansion thrust pressure or thermal repulsion (43,48,49). When gases are heated internally, they are accelerated in a direction perpendicular to the exterior surface of the plasma (50). The bombardment of the oncoming particles by the expanding gas results in a deflection of the particles.

The presence of a magnetic thrust pressure in teardrop shaped ICP's sustained by laminar, coaxial gas introduction was originally recognized by Chase (42,43) and has also been studied by Waldie (45) and Boulos (46,47). In an ICP the electric field and, consequently, the induced current density are zero at the center. The magnetic fields induced by the coil and eddy currents reinforce each other in the outer regions and oppose each other at the center. These characteristics lead to a Lorentz force which produces a magnetic compression around the sides of the plasma acting toward the central axis (42-47). The plasma is thus confined in two dimensions. The excess pressure energy can be converted into kinetic energy only by expansion outward along the central axis of the plasma in both the upstream and downstream directions. The resulting flow tends to deflect the oncoming sample particles and transport them around the plasma. However, Chase (42) found that with the vortex stabilization scheme normally used in ICP's designed for analytical applications, the low pressure region along the central axis of the plasma overwhelmed the magnetic thrust pressure.

The skin depth effect of induction heating has been used to good advantage in achieving efficient sample introduction. The skin depth effect, i.e., the depth at which the eddy current is reduced to 1/e of its surface value, is

inversely proportional to the square root of the radio-frequency current frequency. This effect leads to the formation of an incipiently cooler axial channel which offers less resistance to the injection of sample particles than the high temperature annulus. The annular shape may be further developed by optimizing the flow velocity of the aerosol carrier gas.

Thus, by proper optimization of the configuration of the plasma confinement tubes, the tangential velocity component of the plasma sustaining gas, the frequency of the primary current generator, and the flow velocity of the aerosol carrier gas, an annular shaped plasma permitting efficient sample injection along the central axis is formed. It should be realized that there exists no unique configuration of the annular shaped ICP. Investigators have employed different sets of the above mentioned param-eters to achieve varying degrees of annularity and sample residence times. In fact, Greenfield et al. (8) found that an annular shaped ICP may be formed with laminar or tangential introduction of the plasma support gas if the upstream "boundary" of the plasma is flattened with an additional gas flow introduced between the sample injection tube and the intermediate quartz tube. Investigations of the magnetic thrust pressure in ICP's supported by laminar gas introduction (42-47) have not considered the influence of this additional gas flow.

The annular plasma configuration leads to certain unique physical properties that make it a remarkably successful vaporization-atomization-excitation source. Once the sample particles are injected, they are heated indirectly via convection, conduction, and radiation absorption as they travel along the narrow axial channel inside the high temperature annulus. The relatively long residence time (on the order of 2 msec) of the sample in the high temperature region (up to ~7000 K) leads to an exceptionally high degree of atomization, hence solute vaporization interferences should be negligible. Because the free atoms and ions reside at very low concentrations in a chemically inert Ar environment, the formation of molecular species should be minimized, which results in relatively long lifetimes for the free atoms and ions.

Experimental studies of the distribution of the analyte atoms and ions indicate that the sample and its decomposition products are confined to a narrow cylindrical volume along the central axis. This confinement of the analyte atoms and ions appears to be an important factor leading to several of the desirable characteristics of the annular shaped ICP. The interaction of the sample with the sustaining eddy current is minimized by the confinement. For example, with the present ICP facility there was less than a five-watt change in the forward power in the

transmission line leading to the tuning-coupling circuit and only an approximate one watt increase in the reflected power when the solution nebulized was changed from deionized H_2O to 2.3 wt. % Na. At the observation heights normally employed for analytical purposes (15 or 20 mm above the load coil), the zone to which the sample is confined is fairly isothermal. This should minimize the effect of lateral diffusional interferences arising from differences in the vaporization rate (51) or arising from other interfering processes such as ambipolar diffusion (30-32). However, changes in the radial distribution within the axial channel (if present) will have some effect on the measured intensities because of the differences in efficiency of transfer of the emitted radiation to the detector.

The free atoms are generated in the high temperature environment of the core of the plasma which exhibits high spectral background and complex line spectra. For analytical applications the analyte free atoms or ions may be observed downstream in environments ranging downward from ∿6500 K. The optical aperture or viewing field of conventional spectrometers can be readily filled by analyte emission originating in the central channel. In this way, the analyte radiation is used most effectively.

The relatively low number densities of the analyte atoms or ions in the Ar sheath reduce self-absorption which leads

to analytical curves that are linear over 4 to 5 orders of magnitude (52,53). This feature often permits the simultaneous determination of trace, minor and major constituents without variable dilutions of the sample solutions.

In contrast to the desirable physical properties of the annular shaped ICP, the teardrop shaped ICP (2,3,54) has a relatively poor sample introduction efficiency. The expansion thrust pressure and the magnetic thrust pressure (if laminar plasma support gas introduction is employed) act to deflect the sample particles and cause them to by-pass the high temperature region. In addition, other desirable features of the annular shaped ICP discussed above should not be present with the teardrop shaped ICP. Hence, the combination of the low frequency (4.8 MHz), laminar gas flow pattern, and the absence of an aerosol delivery tube (to produce a relatively high injection velocity) may have played a role in producing the interferences reported by Veillon and Margoshes (54).

A further distinguishing factor between various ICP's is the mode in which they are generated. For example, the plasma generator may be a self-excited oscillator, with the plasma acting as part of the resonant circuit, as used by Boumans and de Boer (55,56). Alternatively, the same type of generator may be used and coupled to the plasma via an impedance matching network, as utilized in some of the

earlier published work from Ames Laboratory (36,37). A
third alternative (52), used in the present study, is based
on crystal control of the operating frequency and the use of
a tuning-coupling circuit for impedance matching purposes.
In this case the plasma is a less active circuit element.
A relatively high degree of freedom from interference
effects has also been observed with a generator of the
second type discussed above (57). However, Boumans and
de Boer (33,34) have reported somewhat different interference
effects produced by easily ionizable elements with their
facility.

The extent to which various interelement effects occur
may indeed be dependent on the plasma configuration and on
the method of plasma generation, but there are other factors
that play a role as well. Thus, the power dissipated in the
plasma, the method of sample introduction, the height of
observation, and the viewing field of the optical transfer
system all have an effect.

Experimental Facilities and Procedure

Apparatus

A photograph of the apparatus is shown in Figure 2.
Detailed descriptions of the apparatus, except as modified
for the present study, may be found in reference 52.
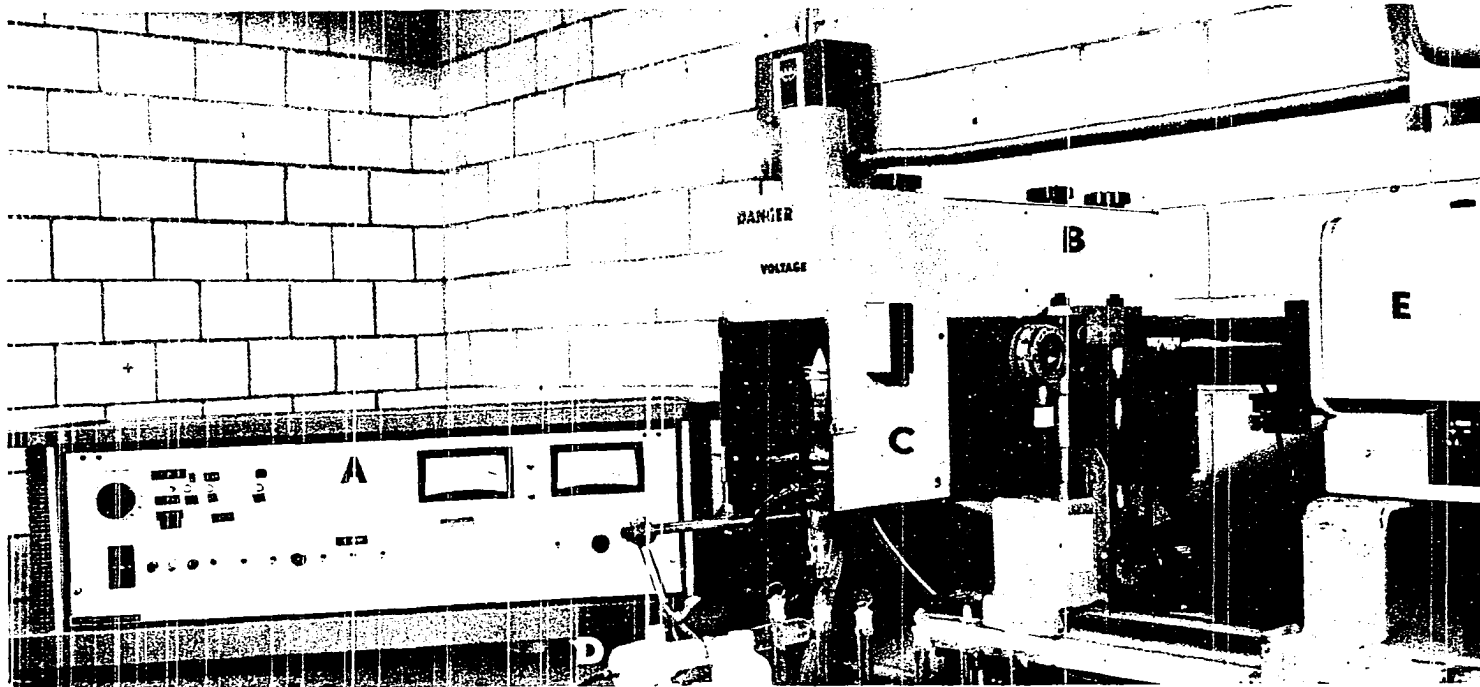
Figure 2. Plasma generation and observation facilities

    A.   Radiofrequency generator;

    B.   Impedance matching network;

    C.   Plasma, with enclosure removed;

    D.   Pneumatic nebulizer;

    E.   Spectrometer

Radiofrequency generator   A feedback circuit was
added to this facility to maintain a constant forward power
in the transmission line to the impedance matching network
by controlling the screen voltage of the oscillator. The
addition of this circuit was necessitated by changes in the
radiofrequency power level produced by fluctuations in the
mains voltage. The extent to which interference effects
occurred was not affected significantly by the presence of
absence of the feedback circuit. The output power waveform
of this generator originally possessed a 60 Hz sinusoidal
ripple resulting from the ac current in the filament of the
power amplifier and 120 Hz sawtooth ripple produced by
incomplete filtering of the dc voltages in the generator.
A constant current supply (11 amp) eliminated the 60 Hz
ripple in the radiofrequency power waveform. The 120 Hz
sawtooth ripple was reduced by increasing the capacitance
in the high voltage filtering network from 4 µF to 12 µF.

An indirect method was employed to estimate the magni-
tude of the ripple in terms of power since only a wattmeter
(Thruline Model 43, 2500 H element, Bird Electronic Corp.,
Cleveland, OH) designed for constant wave power measurements
was available. A calibration curve of the voltage on a
stationary probe positioned inside the impedance matching
unit (which picks up an unknown fraction of the radio-
frequency field) versus the wattmeter reading in the de-
rippled mode was constructed. The peak and minimum power

levels in the rippled mode at a given "average" wattmeter reading were estimated from the wattmeter readings corresponding to the peak and minimum voltages on the probe from the calibration curve. For the "average" wattmeter reading of 1025 W with the 60 Hz and 120 Hz ripple (hereafter called 1025 W with ripple), the peak power was ∿1225 W and the minimum was ∿750 W. In the derippled mode, the residual 120 Hz sawtooth ripple was ∿3% peak to peak of the voltage on the probe or ∿±25 W in the power at an "average" wattmeter reading of 1200 W.

It should be realized that the power levels mentioned in this work are those measured in the transmission line from the radiofrequency generator to the impedance matching unit. They are not equal to the power transferred to the plasma. Power losses in the load coil may amount to as much as 40% of the radiofrequency power in the transmission line (58). Additional losses may occur in the components in the impedance matching unit or from inefficient coupling to the plasma (44,59). Calorimetric measurements on a dummy load have been utilized to measure power levels with ICP facilities (8,33,44,59). These methods possess uncertainties because of differences in the conductivities of the dummy load and the plasma which lead to differences in the coupling efficiencies (8,59). Hence, the calorimetrically measured power of 700 W accepted by Boumans and de Boer (33) as a compromise for simultaneous multielement analysis with the

ICP may represent a similar power dissipation in the plasma to the 1200 W level in the transmission line employed in the present work.

Aerosol generation system   The aerosol generation and delivery system is shown with the torch assembly in Figure 3. The pneumatic nebulizer (60) is attached to a 125 mm Teflon portion of the aerosol chamber that has an i.d. tapering from 28 mm to 18 mm. The Teflon portion is connected to an 18 mm i.d. glass tube about 125 mm long. When compared to the dual tube aerosol chamber (52), this simpler chamber reduced clean-out time between samples and decreased the magnitude of several of the interferences (Ca-PO$_4$ and Ca-Al) discussed later in this chapter.

Gas flow control system   The gas flow control system, except as modified for the present study, has been previously described (52). An additional pressure regulator (Model 93-250 Harris Calorific Co., Cleveland, OH) was added on the Ar manifold. A flow controller (No. 8942, Brooks Instrument Div., Emerson Electric Co., Hatfield, PA) was employed on the nebulizer flow only and no filter was employed. A pressure gauge (0-100 psi) was added immediately upstream from the nebulizer to monitor the pressure drop across the nebulizer orifice. The Ar flow rates were: 12 1/min plasma and 1.0 1/min (or 1.3 1/min where indicated) aerosol carrier.

INSULATING SHIELD

PLASMA Ar →

AUXILIARY PLASMA Ar → (OPTIONAL)

AEROSOL CARRIER Ar
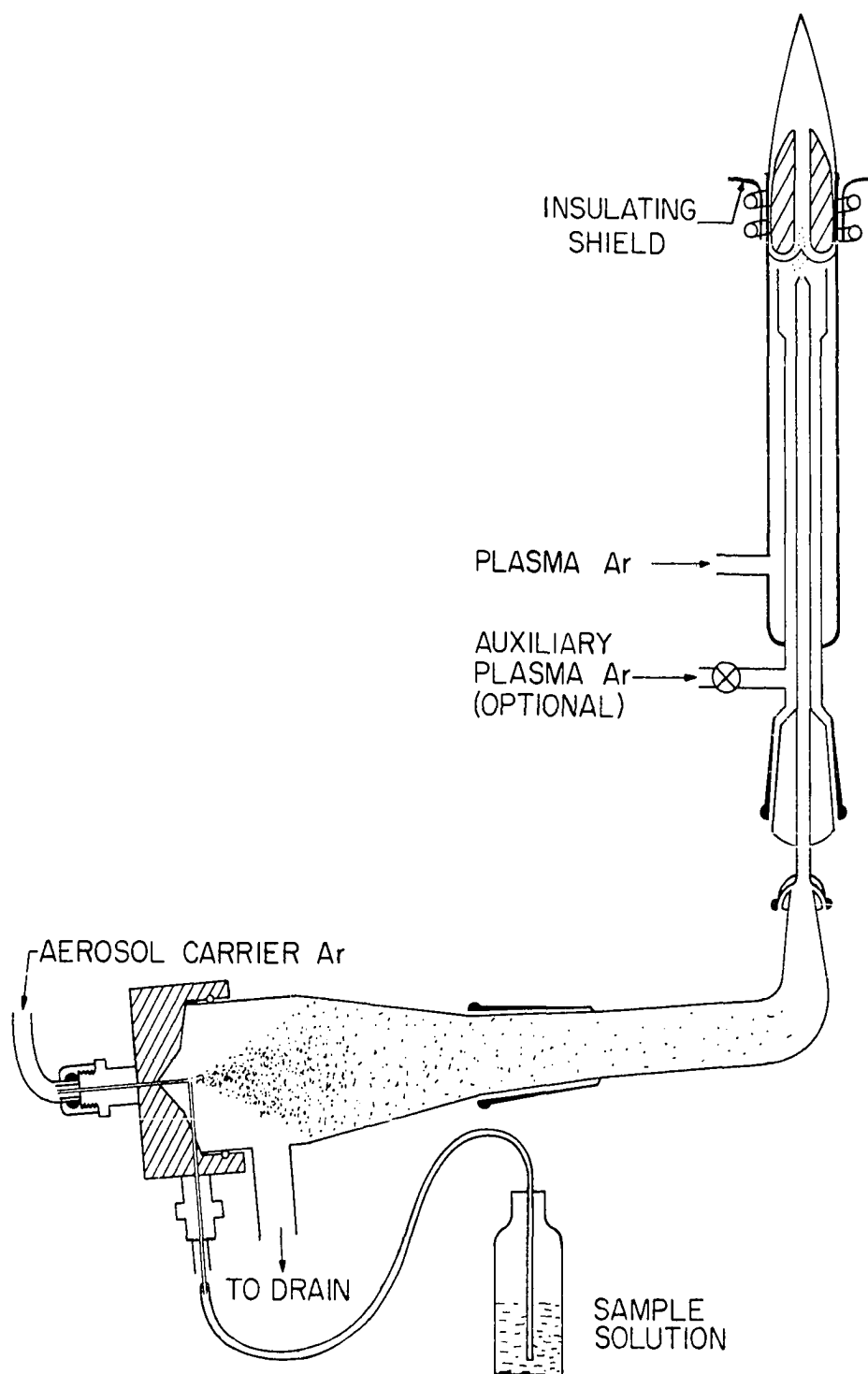
TO DRAIN

SAMPLE SOLUTION

Figure 3.   Schematic diagram of torch and aerosol generation system

Optical system   The emission from the plasma was focused by a 16 cm focal length x 5 cm dia. plano-convex, fused quartz lens positioned at 30.2 cm (twice the focal length at 303.4 nm) from the slit. The center of the plasma was at 60.4 cm from the slit. Fixed 15 μ entrance and exit slits were employed. The entrance slit height was masked to 4 mm.

Procedure

The Ca, Cr, Cd, and Mo analyte solutions were prepared by dissolving reagent grade $CaCO_3$, Cr metal, CdO, or $(NH_4)_2MoO_4$ in dilute HCl. The Na concomitant solution was prepared from NaCl. Ten volume percent of concentrated HCl was added to all solutions so that any acid effects would not bias the results. In preliminary experiments with no excess HCl added to the solutions, no differences in the effects of NaCl and $NaNO_3$ were observed.

Phosphorous was added as reagent grade H_3PO_4 (85%) in the $Ca-PO_4$ system. For the study of the Ca-Al system, $Al(NO_3)_3 \cdot 6H_2O$ or $AlCl_3$ were employed.

For the study of the effects of various concomitants on Mo emission, the concomitants were added as solutions of reagent grade chlorides (K, Na) or as solutions of the metal (Al, Cu, Zn) in dilute HCl.

Intensity data were obtained by peaking the monochromator on the line and integrating the signal for 24

seconds. The signal from the blank was then subtracted to yield the net relative intensity. The concomitant blanks did not differ from the distilled water blank (within 1% of the background signal) except for the Na and Al which contained a measurable residue of Ca.

Results and Discussion

The Ca-PO$_4$ and Ca-Al solute vaporization interference systems

In view of the disparity of results so far reported on the Ca-PO$_4$ and Ca-Al solute vaporization interference systems (4), it is of interest to evaluate these interferences in a facility specifically assembled for analytical purposes (52) and operated under conditions used for analytical purposes.

Ca-PO$_4$ system   The Ca-PO$_4$ solute vaporization interference has been attributed to the formation of a refractory compound, e.g., Ca$_2$P$_2$O$_7$ or Ca$_3$(PO$_4$)$_2$, whose greater thermal stability leads to a reduced efficiency of free atom formation (11-14). In the annular shaped ICP Greenfield et al. (1) reported an absence of the depression effect up to PO$_4^{3-}$/Ca^{2+} molar ratios of 4. Wendt and Fassel (3) and Veillon and Margoshes (54) reported enhancements in free-atom absorption in teardrop shaped plasmas. Veillon and Margoshes (54) also reported an enhancement of about 100% in the calcium free-atom emission at a PO$_4^{3-}$/Ca^{2+} molar ratio of one and even larger enhancements in the calcium ion

emission, while Fassel (4) reported only small changes in free-atom emission in an annular shaped plasma.

The results obtained for the calcium-phosphate system at an observation height of 20 mm above the load coil with the present facility are shown in Figure 4. In this and in subsequent figures, the net emission intensities of a given species in the absence of an interferent are normalized to 100 arbitrary units at each observation height. The results of this study are in general agreement with the observations of Greenfield et al. (1) and Wendt and Fassel (3) and Fassel (4). The precipitous depression and the "knee" in the suppression curve observed in some combustion flames are not detectable, indicating the absence of the classical solute vaporization interference due to compound formation. Similar interference curves were obtained at observation heights of 15 and 25 mm above the load coil. The data presented in Figure 4 were obtained at the forward power of 1025 W with ripple. A comparison of the interference effects produced by concomitant PO_4^{3-} observed at the 1025 W with ripple power level with those obtained at the derippled level of 1200 W is shown in Table I. As demonstrated by the data in Table I, the ripple in the power at the level which was originally present in the generator had no measurable influence on these interferences. The slight suppression that is observed at PO_4^{3-}/Ca^{2+} approaching 1000 is probably attributable to a transport interference resulting from changes in
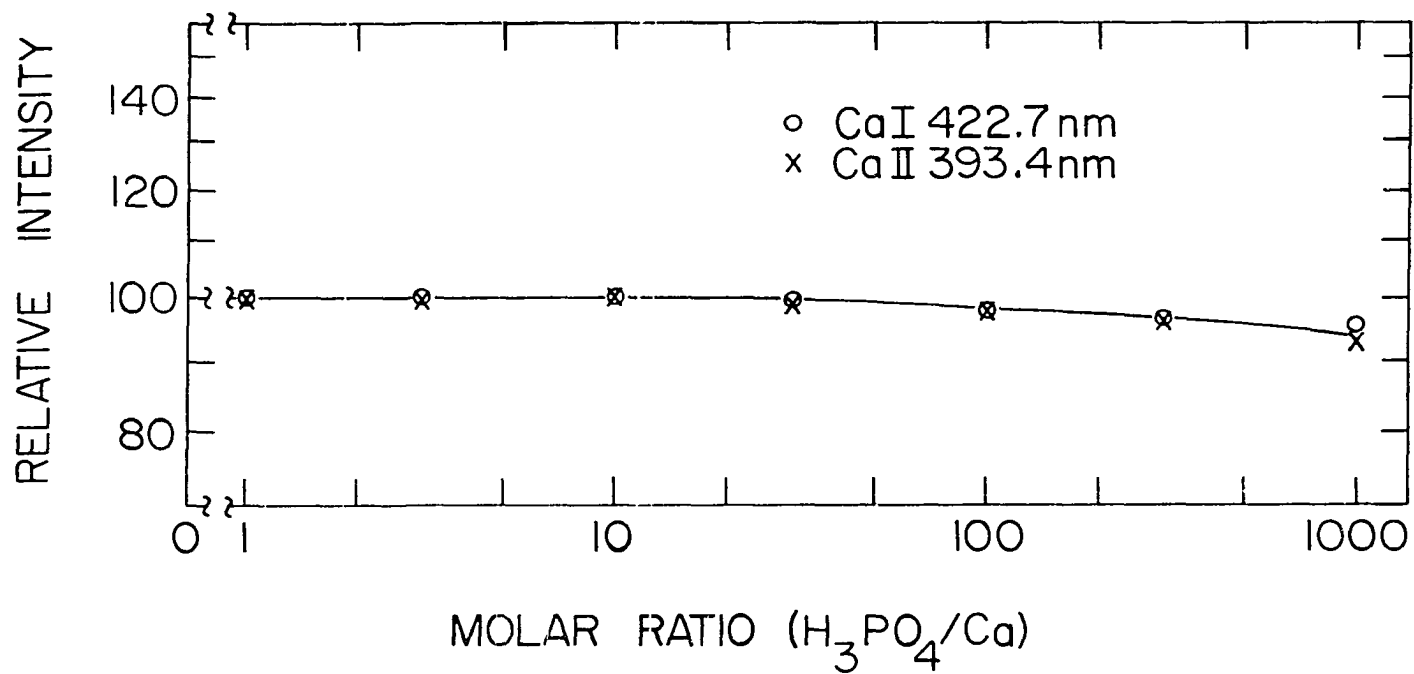
Figure 4. Effect of phosphoric acid on Ca emission intensity at 20 mm above load coil (0.5 μmol/ml Ca)

Table I. Comparison of the effects of phosphate and Al on Ca emission with and without ripple in the radiofrequency power

	Intensity ratio[a]					
Height above load coil (mm):	15		20		25	
	Ripple[b]	Deripple[c]	Ripple[b]	Deripple[c]	Ripple[b]	Deripple[c]
Interference system Emission line						
Ca-PO$_4$[d]						
Ca I 422.7 nm	0.93	0.97	0.93	0.94	0.92	0.95
Ca II 393.4 nm	0.96	0.94	0.97	0.98	0.97	0.97
Ca-Al[e]						
Ca I 422.7 nm	0.92	0.97	0.99	1.04	1.31	1.15
Ca II 393.4 nm	0.92	0.97	0.95	1.00	1.00	1.02
Ca + Na-Al[f]						
Ca I 422.7 nm	0.90	0.89	1.00	1.01	1.04	1.04
Ca II 393.4 nm	0.87	0.91	0.98	0.97	1.01	1.03

[a] Intensity ratio = net intensity with interferent ÷ net intensity without interferent.

[b] Ripple = 1025 W with ripple power level.

[c] Deripple = 1200 W derippled power level.

[d] Molar Ratio PO$_4$/Ca = 1000.

[e] Molar Ratio Al/Ca = 100.

[f] Molar Ratio Al/Ca = 300; 200 μ mol/ml Na present.

the physical properties of the solutions. It is important to note that a PO_4^{3-}/Ca^{2+} molar ratio of 1000 here is equivalent to approximately 5 wt. % H_3PO_4, which may be considered the analytical equivalent of determining Ca in H_3PO_4.

Ca-Al system   The suppression of Ca free-atom forma-- tion in the presence of increasing concentrations of Al has also been attributed to the formation of a refractory com- pound ($CaAl_2O_4$, $Ca_3Al_2O_6$, etc.) and to the occlusion of Ca in a refractory aluminum oxide matrix (11,12). In combustion flames, with the Al present in solution as $AlCl_3$, several investigators have reported a "knee" followed by a plateau in the suppression curve indicating the formation of a refractory compound (15,16). With the Al present as $Al(NO_3)_3$, the Ca emission or absorption in flame atomizers has been observed to decrease smoothly toward zero with increasing concentrations of Al indicating the occlusion of the Ca in a refractory aluminum oxide matrix (13,15-17). In these studies with the ICP, no differences in the behavior of $AlCl_3$ and $Al(NO_3)_3$ were observed.

The Ca-Al interaction has been studied by Greenfield et al. (1) and by Fassel (4) in annular shaped plasmas, and also by Wendt and Fassel (3) and Veillon and Margoshes (54) in teardrop shaped plasmas. These investigators reported significantly different results. Greenfield et al. (1)

initially reported no change in calcium atom emission up to
Al/Ca molar ratios of 50. Wendt and Fassel (3), and Veillon
and Margoshes (54) observed enhancements in calcium free-
atom absorption in their plasmas. Later, Fassel (4)
observed a slight enhancement of both the calcium atom and
ion emission and Veillon and Margoshes (54) reported an
approximate five-fold enhancement of the calcium atom
emission when the Al/Ca molar ratio was increased from zero
to 8.

The results of the present study are shown in Figure 5.
These data were obtained at the forward power of 1025 W with
ripple. The absence of any depression at low molar ratios
indicates that no measurable solute vaporization inter-
ference due to compound formation occurs. At Al/Ca molar
ratios approaching 100 (1350 µg/ml Al) slight suppressions
are observed in the calcium atomic and ionic line emission
at 15 mm above the load coil. This suppression may at first
glance be attributed to the occlusion of the Ca in a refrac-
tory aluminum oxide matrix formed during the aerosol droplet
evaporation process, because the suppression of the Ca II
emission decreased with increasing observation height until
at 25 mm above the load coil it is virtually absent.
However, the observation that $AlCl_3$ and $Al(NO_3)_3$ solutions
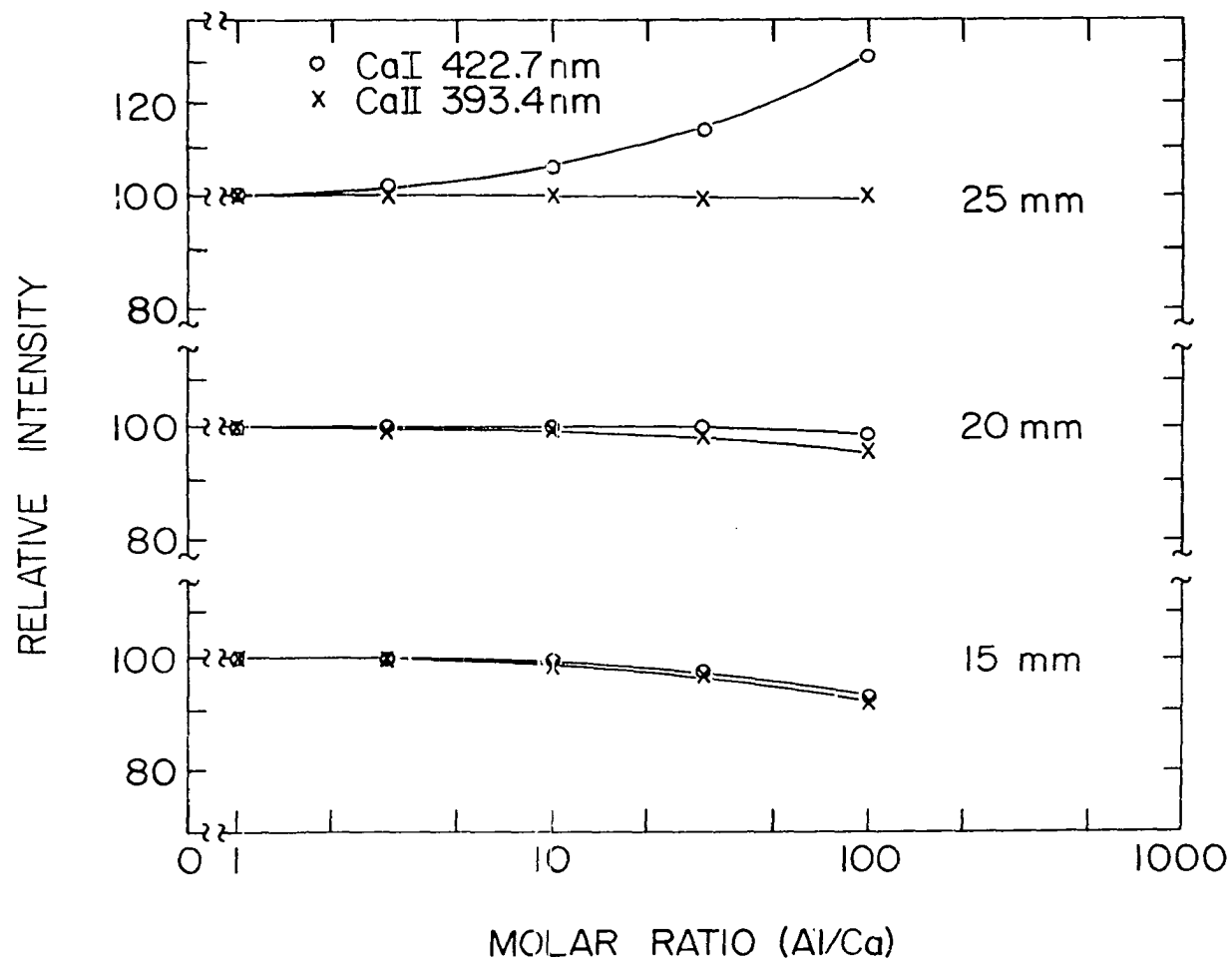produced essentially identical results in the ICP does not
support this hypothesis.

Figure 5. Effect of Al on Ca emission intensity at three heights
of observation above load coil (0.5 μmol/ml Ca)

The interpretation of the experimental results on the Ca-Al interactions is rendered difficult by the possibility that ionization suppression of Ca and other interactions occasioned by the presence of increasing concentrations of Al in the plasma may obscure solute vaporization interference. Thus, the enhancement of Ca I emission at 25 mm above the load coil may be rationalized as a manifestation of a shift of the Ca ionization equilibrium

$$Ca^{o} \rightleftharpoons Ca^{+} + e^{-}$$
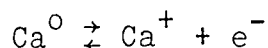
toward the free atom, because ionization of the increasing Al concentrations in the plasma might increase the number density of electrons. The absence of a significant simultaneous depression of the Ca II emission can also be rationalized since the degree of ionization of Ca has been found to be exceptionally high [>99% (24,25)] in the absence of Al.

To buffer whatever interactions are occurring through the presence of relatively high concentrations of easily ionizable elements, Na was added at a concentration of 4600 µg/ml (as NaNO$_3$) to another set of otherwise identical solutions. The results obtained for these solutions are shown in Figure 6. The addition of this quantity of Na virtually eliminated the interference effects produced by up to 1350 µg/ml Al (molar ratio Na/Al = 4). Although higher Al concentrations produced depressions of both the Ca I and
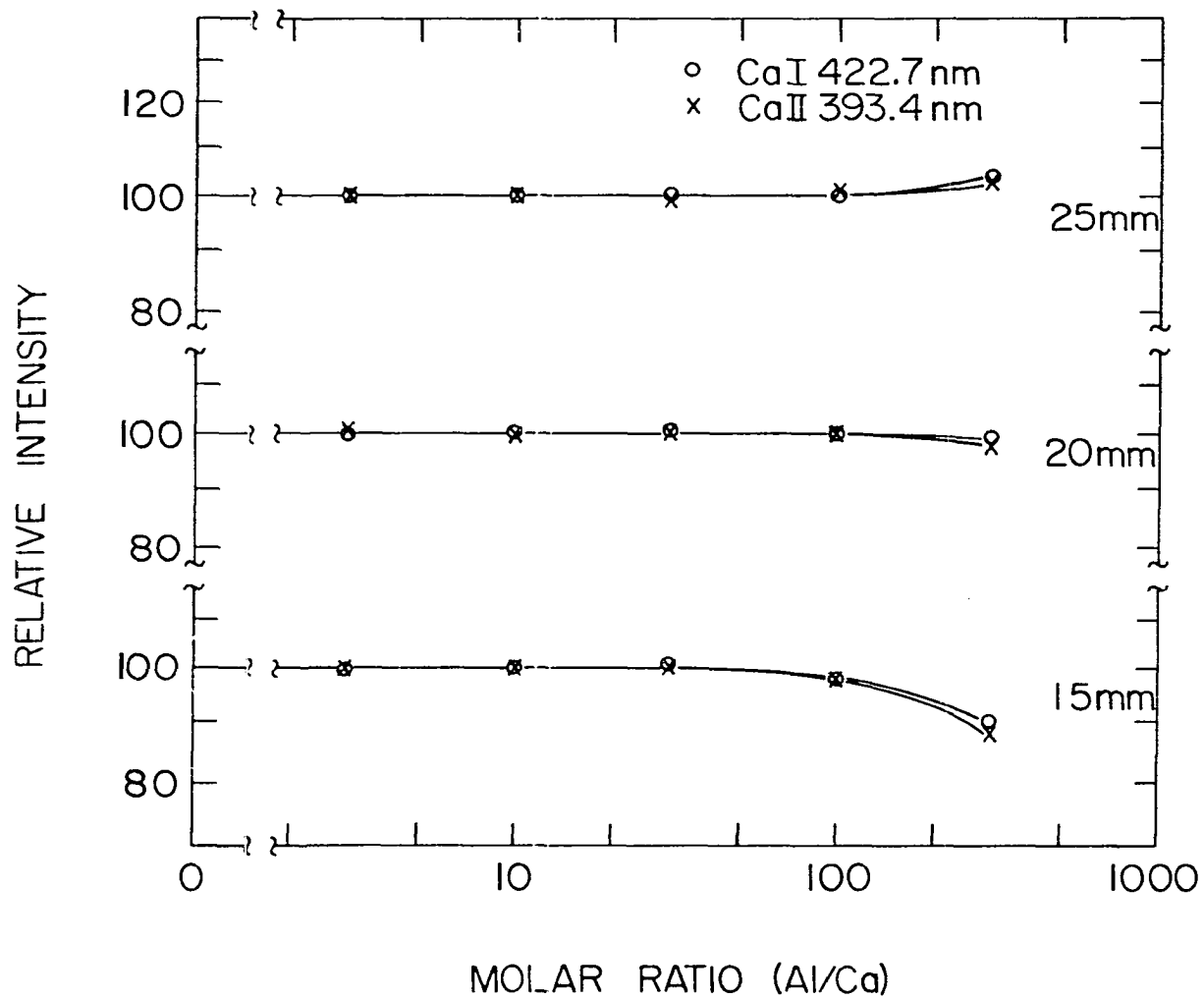
Figure 6. Effect of Al on Ca emission intensity in the presence of Na at three heights of observation above load coil (0.5 μmol/ml Ca; 4600 μg/ml Na)

Ca II emission at 15 mm, these depressions were essentially absent at the 20 mm observation height.

The comparison of the interferences produced by concomitant Al with and without excess Na at forward powers of 1025 W with ripple and 1200 W derippled shown in Table I indicate that the ripple in the power had no major influence on the interferences. The enhancement of the Ca I line at 25 mm at 1025 W with ripple level is measurably larger than that observed at the 1200 W derippled level. The same trend was observed with concomitant Na discussed below. However, unequivocal interpretations of the role of solute vaporization and the interactions occasioned by increasing concentrations of Al in the nebulized solution and in the plasma await a better understanding of the nebulization and transport processes and of the physical environment prevailing in the plasma.

Interference effects produced by easily ionizable elements

Reports in the literature on the existence and degree to which interference effects may occur in the ICP from changing concentrations of easily ionizable elements have been rather limited, considering the possible severity of such effects and the great degree to which they have been observed in other electrically generated plasmas (27-32,61-64).

Hoare and Mostyn (65) reported that 1000 µg/ml Na did not affect the emission intensity of B and that 10,000 µg/ml

Li produced only slight enhancements of atomic lines and slight depressions of ionic lines for an annular shaped inductively coupled plasma. Kirkbright and associates (66, 67) briefly reported that 50-fold weight excesses of K or Na did not affect the emission intensities from 100 μg/ml S, 100 μg/ml P, 100 μg/ml I, 10 μg/ml As, 10 μg/ml Se, and 10 μg/ml Hg in their annular shaped ICP. Since the initial disclosure (68) of a portion of the results presented below, several other studies on the interferences produced by easily ionizable elements have been published. The recent studies of Abdallah et al. (35) are in general agreement with the present work. Agreement with the recent results of Boumans and de Boer (33,34) exists to the extent that under the operating conditions chosen by the authors as "compromise" conditions for simultaneous multielement analysis, the ICP possesses a high degree of freedom from interelement interactions produced by concomitant easily ionizable elements.

The results of the present study on the effect of 300 μmol/ml Na (6900 μg/ml) on the emission intensities of atomic and ionic lines of three selected elements of different ionization energies (Ca, Cr, and Cd) are presented in Figure 7. The ionization potentials of Ca, Cr, and Cd are 6.11, 6.76, and 8.99 eV (69), respectively (with no correction applied for temperature effects on the partition functions). These data were obtained with an aerosol carrier

Figure 7. Variation of effect of Na on analyte emission
intensity with an aerosol carrier gas flow
rate of 1.0 l/min

Net intensities of a given species in the
absence of Na are normalized to 100 arbitrary
units at each height and power. (Analyte
concentration: 0.5 μmol/ml; Na concentra-
tion: 6900 μg/ml)

☐   900 W

O   1200 W
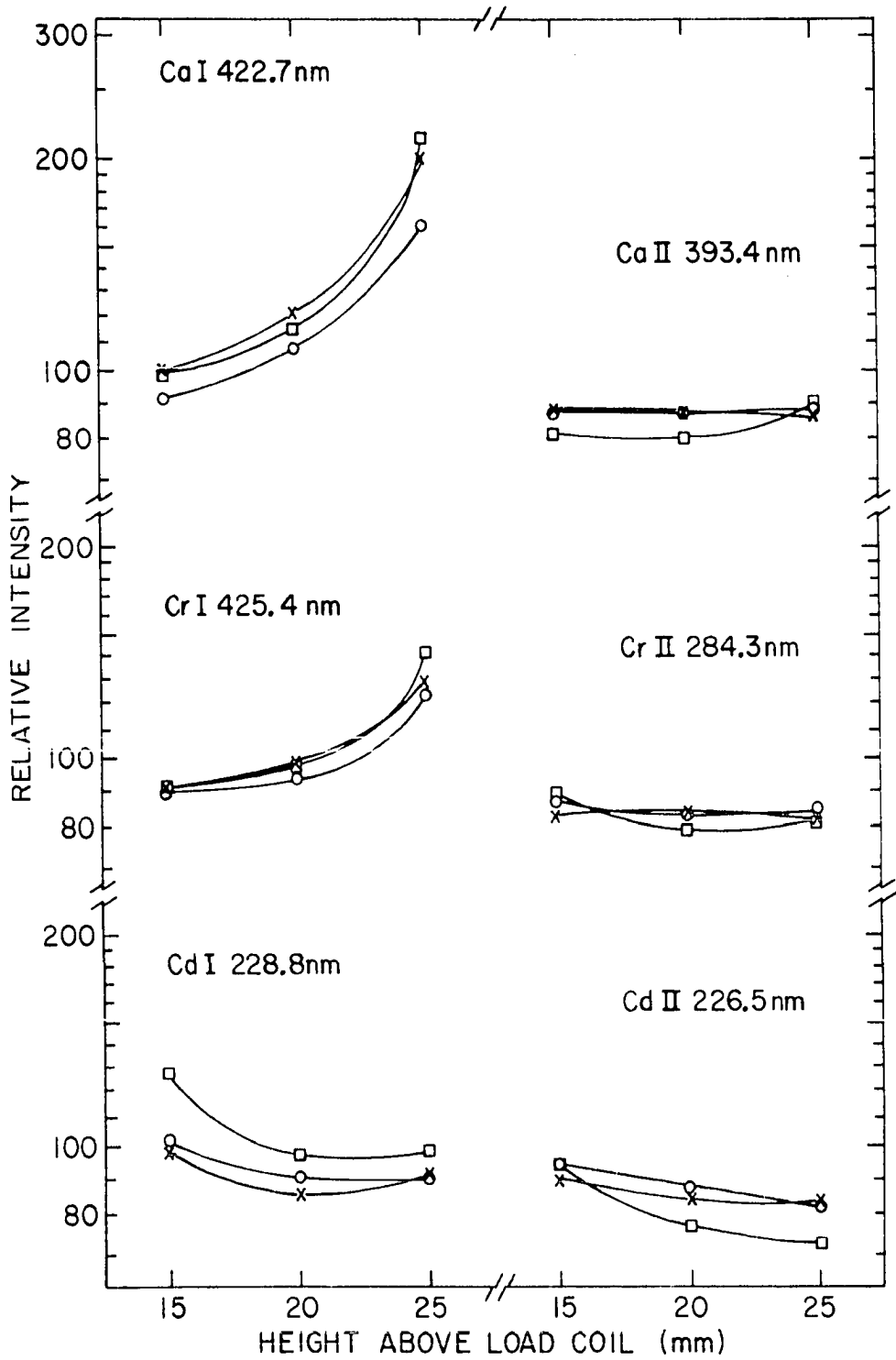
X   1025 W with ripple

gas flow rate of 1.0 l/min and at forward power levels of

1025 W with ripple and the derippled levels of 900 and 1200 W.

The magnitudes and trends of these interferences did not

differ significantly with the forward power level or waveform

as shown by the data in Figure 7. Hence, a small to moderate

ripple in the forward power waveform with an aerosol carrier

gas flow of 1.0 l/min may be tolerated without significant

influence on the interference effects produced by concomitant

Na. In this context it is important to note that enhance-

ments in the time integrated intensities of the Ba I 553.6,

Ba II 455.4, Cu I 324.8, Zn I 213.9, and Zn II 206.2 nm lines

were observed with the addition of Na by Kniseley et al. (70)

in an ICP facility (system III of reference 53) which pos-

sessed an ∿50% peak-to-valley 120 Hz ripple on the radio-

frequency voltage envelope. A series of oscilloscope

tracings of the time resolved emission indicated that the

ripple in the power waveform played an important role in pro-

ducing the enhancements observed with this facility. However,

the addition of Na to the nebulized solution had no signifi-

cant influence on the time resolved emission waveforms for

the spectral lines shown in Figure 7 with the ICP facility

employed in the present study when an aerosol carrier gas

flow of 1.0 l/min was utilized. To resolve this discrepancy

additional information on the instantaneous power dissipated

in the plasma is required.

The effects of increasing Na concentrations from 69 µg/ml to 6900 µg/ml on the emission intensities of Ca, Cr, and Zn with a forward power of 1025 W with ripple are presented in Figures 8-10. Before attempting some rationalizations of the trends of the data plotted in Figures 8 to 10, it is appropriate to recall that the additions of relatively high concentrations of Na to the nebulized solution affected the forward and reflected power levels to a very small extent, i.e., without the stabilizing feedback circuit there was less than a five-watt change in forward power in the transmission line and only an approximate one watt increase in the reflected power when the solution nebulized into the plasma was changed from deionized water to a solution containing 2.3 wt. % Na. Under the conditions employed in this study, effective iron excitation temperatures were observed to change only ∿3 K/watt (71). Thus changes in power absorbed by the plasma do not appear to be responsible for the effects observed. As noted above, the electrons released by the ionization of the increasing concentrations of an easily ionizable element such as Na may increase the number density of electrons to a sufficient degree to suppress the ionization of the analyte species. The trends of the curves plotted in Figures 8 to 10 tend to indicate the presence of a small degree of ionization suppression, i.e., for the more easily ionized Ca and Cr
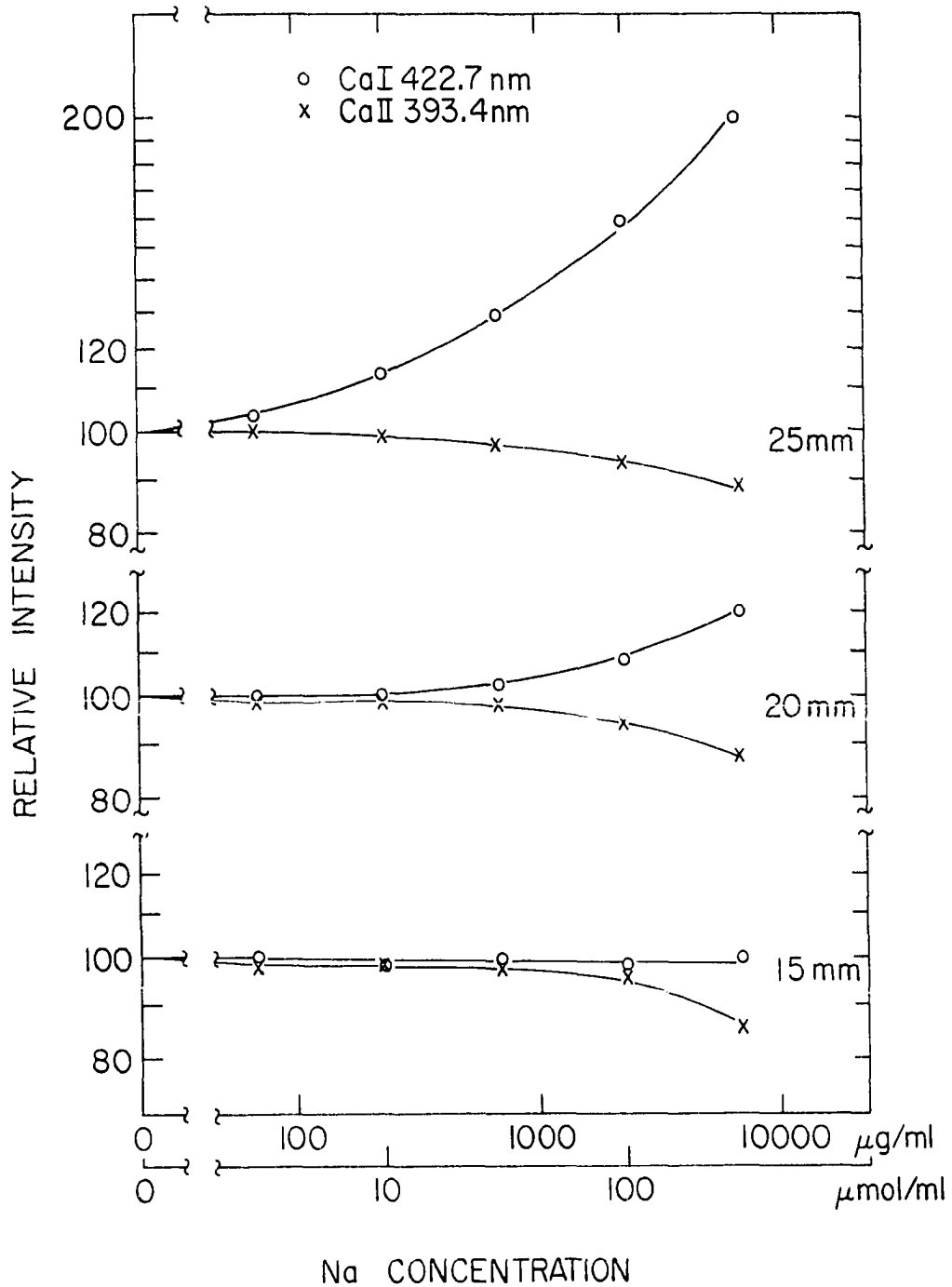
Figure 8. Effect of Na on Ca emission intensity at three heights of observation above load coil (0.5 μmol/ml Ca)
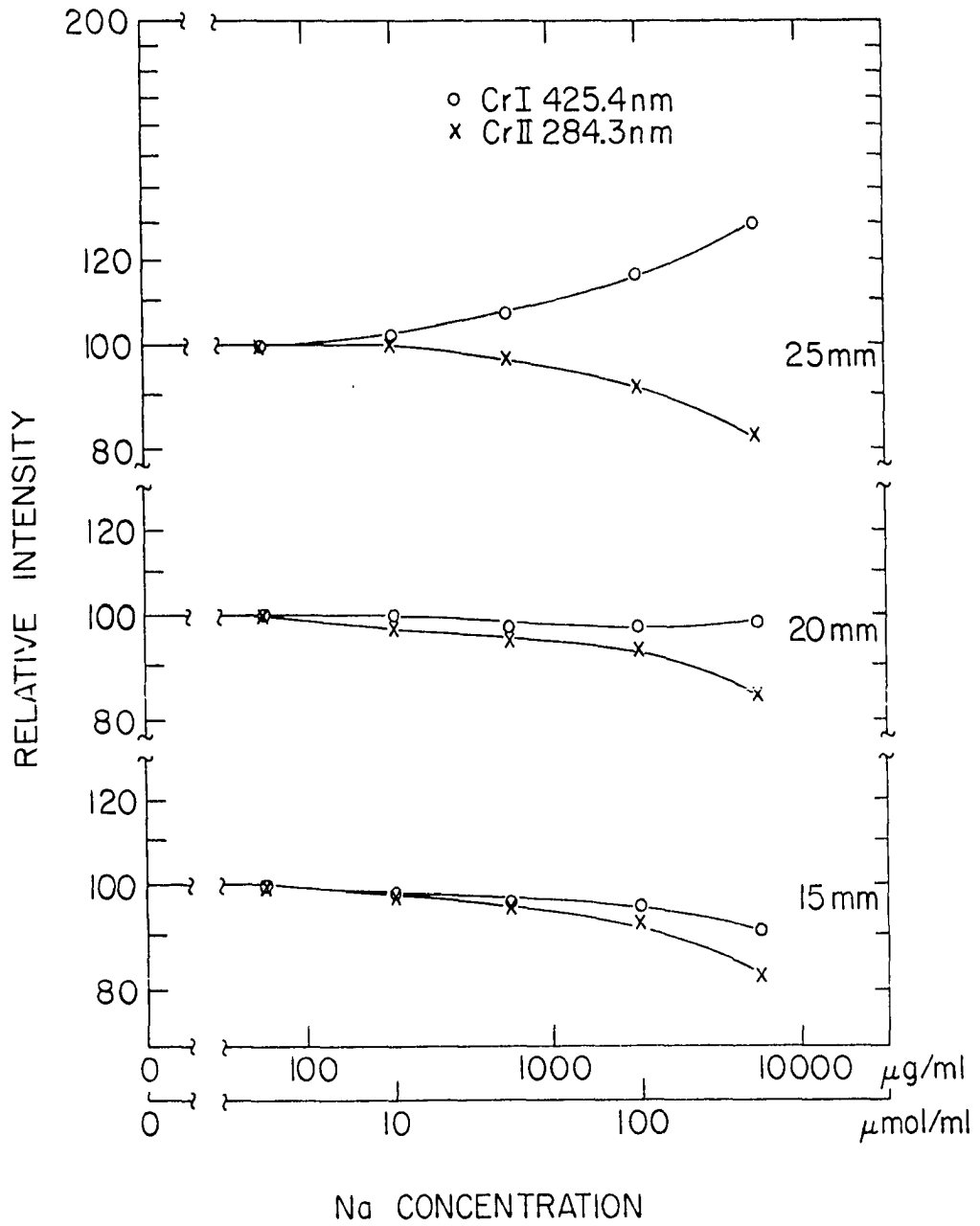
Figure 9.   Effect of Na on Cr emission intensity at
three heights of observation above load coil
(0.5 μmol/ml Cr)
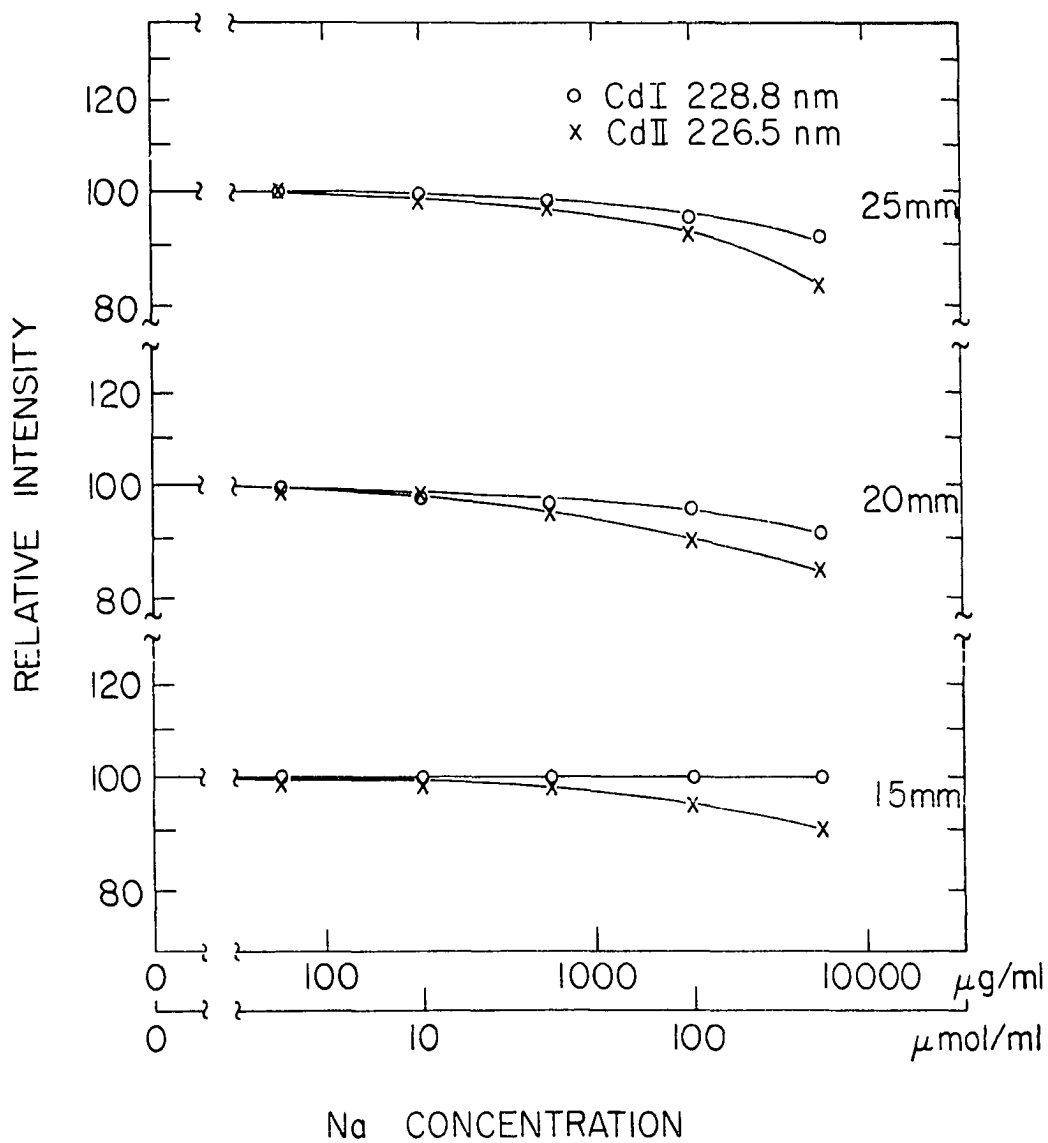
Figure 10. Effect of Na on Cd emission intensity at
three heights of observation above load coil
(0.5 μmol/ml Cd)

species, there is indeed an enhancement in neutral atom line intensities with increasing concentrations of Na, especially at an observation height of 25 mm. If the analyte ionization suppression by the addition of large concentrations of Na were a dominant process, then for an analyte which is highly ionized (Ca) the large enhancements observed in the atomic lines should be accompanied by much smaller depressions in the ionic lines. For a species such as Cd, which is ionized to a lesser degree [∿85% (24,25)], smaller enhancements in the atomic line and larger depressions in the ionic lines would be observed with the suppression of ionization. The existence of some ionization suppression is suggested by the observation that the ionic lines are suppressed to a greater extent than the atomic lines in Figures 8-10 and that the enhancements of both Ca I and Cr I emission are observed high in the plasma (25 mm above the load coil).

Hence, ionization suppression resulting from increases in the electron number density (n_e) plays only a minor role in the interferences shown in Figures 7 to 10. The absence of significant increases in the n_e which may be inferred from the data in Figures 7 to 10 was also found by Kalnicky (24) who determined spatially resolved n_e's with and without 6900 µg/ml Na in the nebulized solution (25). Abdallah et al. (35) and Mermet and Robin (72) have also observed no significant increases in the n_e with the addition of Na.

These observations are in conflict with the n_e's calculated
from the theoretical plasma model of Barnett et al. (73) and
of Mermet and Robin (72). In the theoretical plasma model of
Barnett et al. (73), the sample (Mg) was found to be the
predominant source of electrons at the temperatures [≲7000K
(24,25)] which prevail in the analytically useful observa-
tion zone. According to this model, the addition of Mg
(or elements with lower ionization potentials) above a
certain Mg/Ar ratio leads to an increase in the electron
number density. However, uncertainties in the Mg/Ar ratios
due primarily to the lack of knowledge of the quantity of
Ar which mixes with the sample preclude a comparison of the
model and real plasmas. Mermet (22,23), Kalnicky (24), and
Kalnicky et al. (25) have suggested that ionization equilib-
rium does not exist in the ICP. Thus, the absence of
ionization equilibrium, which is assumed to exist in the
theoretical models, may also contribute to the discrepancies
in the model and real plasmas.

Greater effects would be observed on the Cd II 226.5 nm
and Cr II 284.3 nm lines than on the Ca II 393.4 nm line if
changes in the effective excitation temperatures were the
dominant interfering process. This is due to the high exci-
tation potentials of the Cd II [5.47 eV (69)] and Cr II
[5.88 eV (69)] lines, the low excitation potential of the
Ca II line [3.15 eV (69)], and the high degree of ionization

of Ca [>99% (24,25)]. The similar behavior of these lines in Figures 8-10 suggests that changes in effective excitation temperatures do not appear to be a dominating factor. This suggestion has been confirmed by Kalnicky (24), who found that the addition of 6900 μg/ml Na to the nebulized solution had only a minor effect on the spatially resolved excitation temperatures under similar operating conditions (25).

It should be emphasized that the reported relative intensities in Figures 7-10 represent the effective values within the viewing field of the transfer optics. The importance of this factor is illustrated by the effective horizontal emission profiles at 20 mm above the load coil plotted in Figure 11. The profiles were obtained with the optical transfer system described in reference 71 and no Abel inversion has been applied. It is seen that the Ca I emission is greatly enhanced by the addition of Na at a distance of approximately 4 mm from the central axis of the plasma, while the Ca II emission is only very slightly enhanced by Na in this region. The Cd I emission is also slightly enhanced off axis by the addition of Na while the Cd II emission is not significantly affected in this region.

It is quite certain that other factors play a role in the trends of the interference effects plotted in Figures 8 to 10. For example, the concentration of Na employed may have been great enough to produce a transport interference

Figure 11. Effect of Na on analyte horizontal emission
distribution

(Analyte concentration: 0.5 μmol/ml;
height of observation: 20 mm above load
coil; forward power: 1025 W with ripple)

-O- no Na
--△-- 6900 μg/ml Na

RELATIVE INTENSITY

CaI 422.7 nm

CaII 393.4 nm

CdI 228.8 nm

CdII 226.5 nm

HORIZONTAL DISPLACEMENT FROM CENTER
(mm)
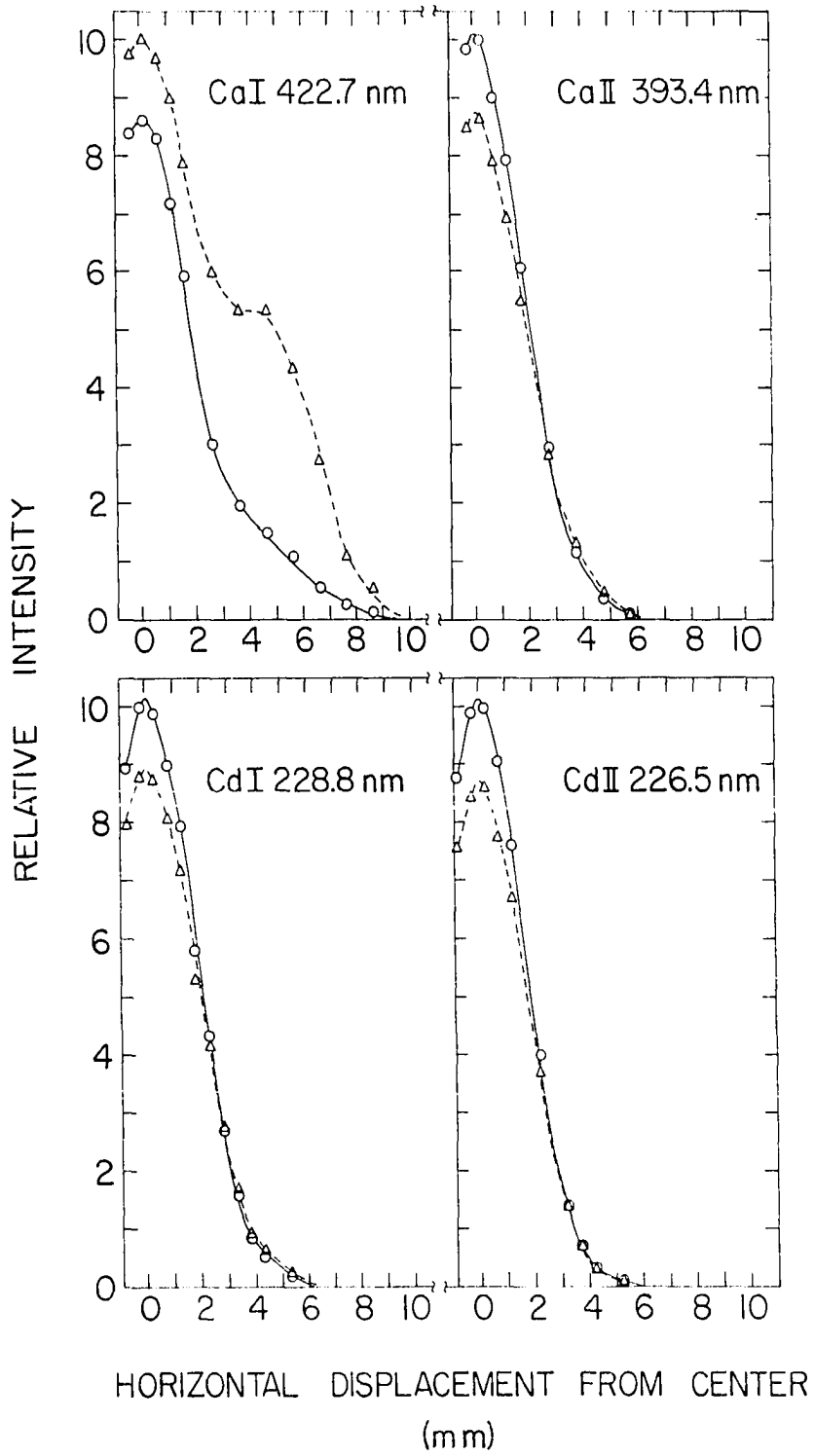
caused by changes in the physical properties of the nebulized solutions.

The influence of increasing the aerosol carrier gas flow rate to 1.3 l/min on the interferences produced by 6900 µg/ml Na at the forward power of 1025 W with ripple and derippled levels of 900 and 1200 W is shown in Figure 12. In contrast to the observations discussed above, relatively large interferences and significant variations of these with power level and waveform are present with an aerosol carrier gas flow rate of 1.3 l/min. The enhancements of all lines (from ∿15 to 280%) at the 15 mm observation height may be rationalized in part by an increase in the effective excitation temperature. Indeed, Kalnicky (24) measured an increase in the excitation temperature from ∿4150 to 4400 K in the center of the plasma with the addition of 6900 µg/ml Na to the nebulized solution at the 15 mm observation height with an aerosol carrier gas flow rate of 1.3 l/min at 1000 W forward power (25). This change in excitation temperature would result in an increase in the Cd I 228.8 nm line intensity of 136% at the center of the plasma (ignoring shifts in the ionization equilibrium). The existence of ionization suppression is suggested by the large decreases in the Cd II 226.5 nm line at the 25 mm observation height. Other interfering processes are important as suggested by the large enhancements of both the Ca atom and ion lines (which are

Figure 12. Variation of effect of Na on analyte emission
            intensity with an aerosol carrier gas flow
            rate of 1.3 l/min

            Net intensities of a given species in the
            absence of Na are normalized to 100
            arbitrary units at each height and power.
            (Analyte concentration: 0.5 µmol/ml;
            Na concentration: 6900 µg/ml)

                          □   900 W
                          ○   1200 W
                          X   1025 W with ripple
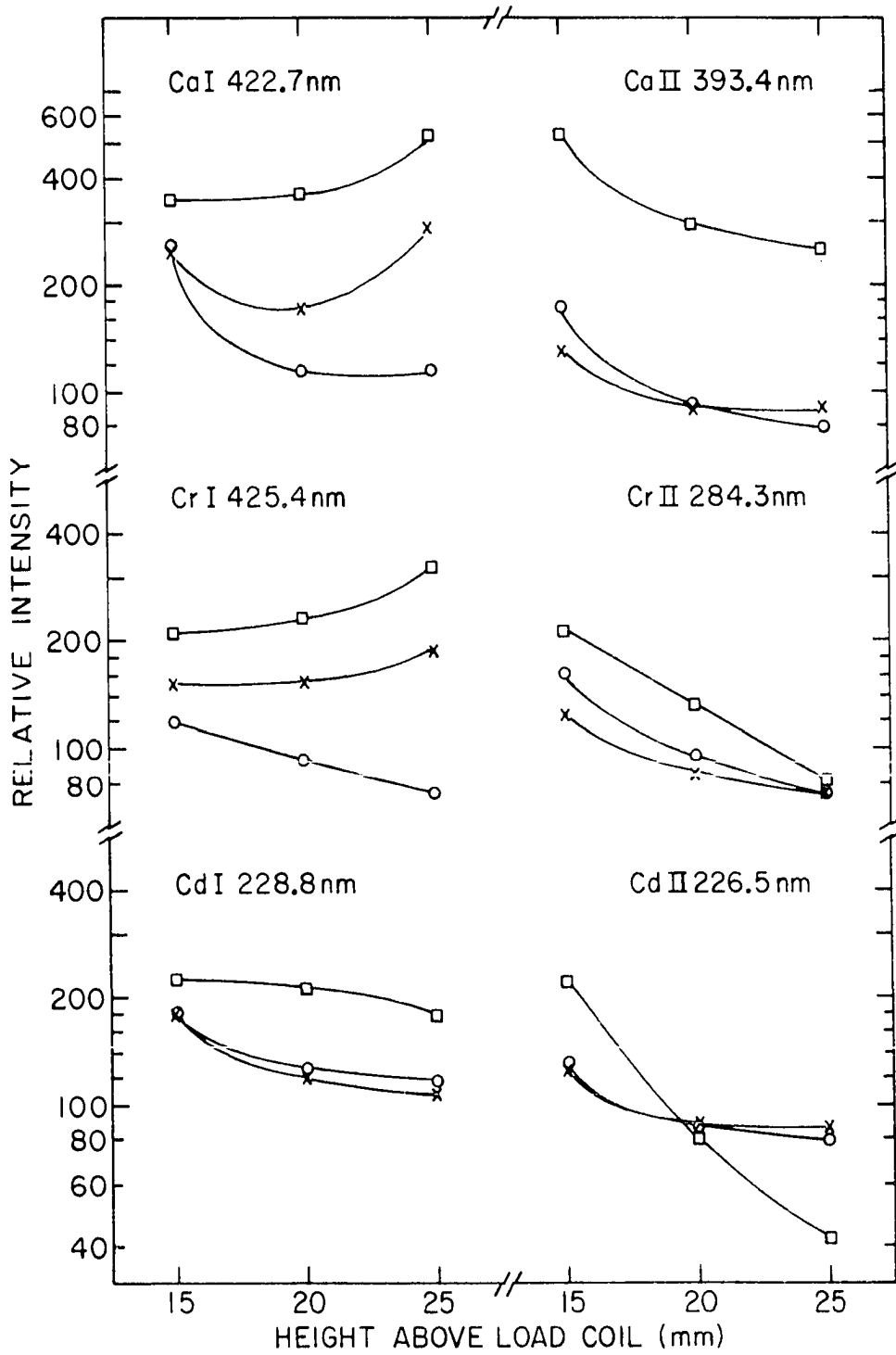
relatively insensitive to excitation temperature) at 900 W.
These enhancements are greater than those observed for lines
which are significantly more sensitive to temperature changes,
e.g., the Cd I 228.8, Cd II 226.5, and Cr II 284.3 nm lines.

Boumans and de Boer (33) have reported relatively large
interferences produced by concomitant easily ionizable
elements with aerosol carrier gas flow rates of 1.5 l/min or
greater especially at lower power levels but not with the
1.3 l/min flow rate. This discrepancy may be the result of
any one or the combination of the differences in the experi-
mental facilities and operating conditions. For example,
if the initial aerosol carrier gas velocity is an important
factor in producing the larger interferences at the higher
flow rate, the larger aerosol delivery tube orifice diameter
of 1.80±0.02 mm employed by Boumans and de Boer in their
most recent studies (34) (compared to the 1.5 mm orifice
used in the present study) may indeed be a factor contribu-
ting to the discrepancies. However, in the absence of a
more detailed knowledge of the origins of these interferences
and of the influence of various experimental parameters on
the physical environment prevailing in the ICP, any attempt
to reconcile the disparity in the observed interference
effects must rely on speculation.

The injection velocity of the aerosol carrier gas is
determined not only by the gas flow rate and diameter of the

orifice of the aerosol delivery tube but also by the configuration of the delivery tube. In this context it is relevant to distinguish between the aerosol delivery tube which terminates in a 1.5 mm diameter jet-like orifice (74) used in the present work (fabricated by collapsing a 4 mm i.d. quartz tube onto a Pt wire of 1.5 mm diameter) and the tube which terminates in a section of straight-walled capillary tubing. Greenfield et al. (1,75) have utilized an aerosol delivery tube terminating in a 2.0 mm i.d. capillary tube which they describe as the "correctly shaped injector" (75). Scott and Kokot (76) advocate the use of a capillary tube with a smaller i.d. of 1.4 mm. The results of some preliminary studies of the interferences produced by 6900 µg/ml Na with an aerosol delivery tube terminating in a 50 mm section of 1.5 mm i.d. quartz tubing (hereafter called "capillary aerosol tube") are presented in Table II along with data obtained with the "standard" aerosol tube. The reproducibilities of the intensity ratios with the standard aerosol tube are generally within acceptable levels, i.e., ∿5%. The most notable features of the intensity ratios for the capillary aerosol tube are the substantially higher variations for the Ca I 422.7 and Ca II 393.4 nm lines and to a lesser extent for the Cr I 425.4 nm line. For example, the intensity ratios observed for the Ca II 393.4 nm line at the 15 mm observation height varied between 0.68 and 1.15

Table II. Influence of aerosol tube configuration on
           interference effect due to Na

Species	Height of observation (mm)	Intensity ratio[a]	
		Standard aerosol tube	Capillary aerosol tube
Ca I 422.7 nm			
	15	0.91 ± 0.03[b](4)[c]	0.77 ± 0.21(9)
	20	1.02 ± 0.04(4)	0.83 ± 0.13(9)
	25	1.61 ± 0.19(4)	1.18 ± 0.18(9)
CaII 393.4 nm			
	15	0.87 ± 0.03(3)	0.93 ± 0.18(10)
	20	0.87 ± 0.02(3)	0.79 ± 0.12(10)
	25	0.88 ± 0.02(3)	0.76 ± 0.09(10)
Cr I 425.4 nm			
	15	0.90 ± 0.05(4)	0.87 ± 0.11(4)
	20	0.94 ± 0.02(4)	0.87 ± 0.05(4)
	25	1.23 ± 0.05(4)	1.05 ± 0.06(4)
CrII 284.3 nm			
	15	0.87 ± 0.03(4)	1.14 ± 0.02(3)
	20	0.83 ± 0.03(4)	0.87 ± 0.02(3)
	25	0.85 ± 0.02(4)	0.81 ± 0.01(3)
Cd I 228.8 nm			
	15	1.01 ± 0.01(5)	1.49 ± 0.05(3)
	20	0.90 ± 0.004(5)	1.00 ± 0.04(3)
	25	0.91 ± 0.02(5)	0.92 ± 0.02(3)
CdII 226.5 nm			
	15	0.94 ± 0.02(4)	1.16 ± 0.06(3)
	20	0.87 ± 0.03(4)	0.91 ± 0.02(3)
	25	0.82 ± 0.02(4)	0.79 ± 0.01(3)

[a]Intensity ratio = net intensity with 6900 μg/ml Na ÷ net intensity without Na.

[b]Standard deviation of observed intensity ratios.

[c]Values in parentheses are the number of determinations.

with an average of 0.93±0.18 over the course of these experiments in contrast to the range of 0.84 to 0.89 with an average of 0.87±0.03 with the standard aerosol tube. These data were obtained over a period of more than a year and represent variations in torch placement within the load coil, in nebulizer performance, and in numerous other experimental parameters. The relatively large variations in the intensity ratios shown in Table II suggest that adequate control of an unidentified experimental parameter(s) was not maintained over the course of these experiments. Regardless of the origins of these variations, this situation should be resolved if the capillary aerosol tube is to be utilized for analytical purposes. Systematic investigations of these two aerosol tube configurations are needed to determine their relative merits, i.e., detection limits, interference effects, deposition of sample material in the orifice, and memory effects.

A definitive interpretation of the magnitudes and trends of the analyte line behavior discussed in this chapter requires a far more detailed knowledge of the spatial distributions of the temperatures and the analyte free atoms and ions, of the influence of possible deviations from local thermodynamic equilibrium (22-25), the ionization processes occurring, on the role played by the Ar sustaining gas, and of the influences of the sample nebulization and transport

processes. The present inability to interpret these results in a more definitive manner should not detract from the fact that at the height of observation ($\sim$15 to 20 mm) and flow rate (1.0 l/min) selected for excellent powers of detection for a majority of elements (77) these interferences are small or insignificant for reasonable changes in the concentrations of easily ionizable elements. In fact, these interferences are far smaller than those generally observed in combustion flames (18-20) and other plasmas (26-32).

Effect of matrix change on analyte emission

The experimental results summarized above suggest the interesting and potentially very valuable possibility of establishing single analytical curves for the determination of an analyte in a variety of matrices. Documentary evidence that this excitation source, operated under the conditions described in this paper, offers this promise is shown in Table III. These data show that a complete change in the matrix in solution induced a maximum change in signal of only -6% (Na matrix). In contrast, in a high temperature $N_2O-C_2H_2$ flame the matrix effects ranged from -70 to +50% (51).

Table III. Effect of concomitants on emission of 25 µg/ml Mo

Height above load coil (mm):	15		20		25		$N_2O-C_2H_2$ flame (51)
Concomitant (2500 µg/ml)	Mo I[a]	Mo II[b]	Mo I	Mo II	Mo I	Mo II	Mo I
None	100	100	100	100	100	100	100
K	102	99	102	97	117	96	30
Na	107	95	105	94	119	94	30
Al	102[c]	97[c]	103[c]	95[c]	119[c]	97[c]	150
Cu	100	100	100	100	102	98	150
Zn	100	100	101	100	104	98	120

[a]Mo I 390.3 nm.

[b]Mo II 281.6 nm.

[c]Data corrected for emission by concomitant.

Suggestions for Future Research

A newly developed ultrasonic nebulizer-desolvation system has produced improvements in detection limits by an order of magnitude or more (78) over the pneumatic nebulizer employed in this dissertation research. Because of the greater mass transport rate of the ultrasonic nebulizer-desolvation system and the important influences of the entire sample introduction apparatus on interference effects, the interference systems studied in this dissertation research should be investigated with the ultrasonic nebulizer-desolvation system. These investigations may be more con-firmatory than exploratory in nature, since Boumans and de Boer (33,34) and Abdallah et al. (35) have observed a high degree of freedom from interference effects with their ultrasonic nebulizer-desolvation systems coupled to ICP's. However, because of the often subtle or unexpected dependence of interference effects on various experimental parameters, these studies are necessary before the ultra-sonic nebulizer-desolvation system is adopted. Additional interference systems should also be investigated, particularly those which may occur in the desolvation apparatus (34,35,79,80).

CHAPTER III. COMPARISON OF INTERFERENCE EFFECTS

IN A MICROWAVE SINGLE ELECTRODE PLASMA

AND IN A RADIOFREQUENCY INDUCTIVELY

COUPLED PLASMA

Introduction

In the preceding chapter it was shown that the ICP possesses a high degree of freedom from several interference effects. In addition to the ICP, the single electrode plasma (SEP) has recently emerged as a promising atomization and excitation source for the optical emission determination of trace elements in solution. The SEP is sustained by capacitive coupling of the plasma to the high frequency field concentrated at the tip of a single electrode. A radiofrequency (43 MHz) version of such a plasma was first employed for the determination of elements in solution by Bădărău et al. (81), and a microwave-excited version, in which the plasma was formed on the central conductor of a co-axial waveguide, was first employed by Mavrodineanu and Hughes (82) for the same purpose. The analytical applications of these plasmas have been recently reviewed by Fassel (4), Greenfield et al. (83), Boumans (9), and Skogerboe and Coleman (84). Although such terms as "capacitively coupled plasma", "electronic torch", "high frequency brush discharge", and "ultra high frequency plasma torch" have been

employed to describe these plasmas, the term "single electrode plasma" or SEP will be used here in accordance with reference 10.

Although the promise of these plasmas as atomization and excitation sources for optical emission spectroscopy resides primarily in their excellent powers of detection (4-6,9,78, 83,84), their freedom from interelement interferences or matrix effects will be an important factor in determining their eventual scope of application for the determination of trace metals in samples of widely varying composition. Thus, it is of interest to make direct comparisons of the relative magnitudes of interference effects in plasmas operated under experimental conditions either recommended or commonly used for the analysis of samples, even though these effects may be dependent on such experimental parameters as the exciting frequency, the nature of the support gas, the method of coupling the high frequency power supply to the plasma, the characteristics of the power generator, the power dissipated in the plasma, the torch configuration and gas flow rates, the viewing field of the optical transfer system, and the method of sample transport and injection.

Presented in this chapter are the results of a comparative study of the interelement effects observed in both the SEP and the ICP (similar to those which are commercially available) produced by: (a) an easily ionizable element

(Na) on the emission intensities of neutral atom and ion
lines of Ca, Cr, Mo, and Zn; (b) concomitants of different
ionization potential on Mo neutral atom and ion line
emission; and (c) the well-known phosphate on calcium and
aluminum on calcium solute vaporization interferences. The
results of this study are in basic agreement with those of
another comparative study (79) in which greater freedom from
interference effects was found in an ICP than in a SEP
sustained in N_2 (rather than Ar as employed in the present
study).

Experimental Facilities and Procedure

SEP facility

The Hitachi UHF Torch Generator employed was similar to
the version described in references 61 and 85. The magnetron
(H3032L, 2.45 GHz) was operated at an anode current of 260 mA
at 2 KV. The Ar sheath or coolant gas flow between two
quartz tubes concentric with the electrode was 5.6 l/min.
The aerosol carrier gas flow rate between the electrode and
the inner quartz tube was set at 2.6 l/min; the interferences
discussed in this chapter were not strongly dependent on
the aerosol carrier gas flow rate between 2 and 3 l/min. The
nebulizer (60), dual tube aerosol chamber (52), and desolva-
tion facility (74) have been previously described. The
aerosol transport rate into the plasma was equivalent to

∿0.06 ml/min with a solution uptake rate of 1.7 ml/min. These conditions correspond to those recommended by the manufacturer.

The spectrometric instrumentation has been previously described (86), except that the following modifications were made: (a) 20 μm entrance and exit slits masked to a height of 3 mm were employed; (b) the external optics consisted of a 15 cm x 5 cm diameter plano-convex fused quartz lens positioned at 28.3 cm (twice the focal length at 303.4 nm) from the slit and 28.3 cm from the plasma; and (c) a Keithley Model 417 picoammeter and a Texas Instruments Model FWD recorder were employed.

ICP facility

The ICP facility has been described in the preceding chapter. The forward power was 1025 W with ripple and the reflected power was approximately 10 W. The aerosol carrier gas flow rate was 1.0 l/min. No external desolvation apparatus was employed.

Procedure

The preparation of solutions and data collection procedures have been described in the preceding chapter, except that relative intensity measurements for the SEP were obtained from strip chart recordings.

Results and Discussion

Interference effects produced by easily ionizable elements

There have been numerous reports of rather severe inter-
ference effects caused by changing concentrations of easily
ionizable elements in various versions of the SEP. Bădărău
(81) reported depressions of Pb I 405.7 nm emission with
increasing concentrations of alkali and alkaline earth
elements in a radiofrequency-excited (43 MHz) SEP sustained
in air. Tappe and van Calker (62,87) observed severe inter-
ferences on Mn I 403.0 nm emission with increasing concen-
trations of the alkali elements in a radiofrequency-excited
(27 MHz) SEP sustained in air. Jantsch (88) has described
interferences produced by increasing concentrations of Na
on Fe I 371.99 nm and Al I 396.2 nm emission intensity in a
microwave-excited (2.45 GHz) SEP supported by N_2. At the
observation height where maximum intensity for Fe I 371.99 nm
was observed (18 mm above electrode tip), the addition of
1840 µg/ml Na produced enhancements of ∿20% in the Fe I
intensity and ∿300% in the Al I intensity. In contrast to
the observations of Jantsch, Kessler (89) reported that in a
similar SEP several easily ionizable elements (Na, K, Cs, Ca,
Sr, and Ba) had little influence on the Fe I 371.99 nm line
but produced enhancements of the Al I 396.2 nm line. In a
more extensive study with a very similar SEP sustained by N_2,
Sermin (90) found that the interference effects produced by

Na were quite dependent on the analyte. For example, Ni neutral atom emission was only slightly affected (<10% change) by up to 100 µg/ml Na but increasing concentrations of Na produced a steady depression ($\sim$50% with 1000 µg/ml Na). Similar effects were observed with neutral atom lines of Fe and Mo. Neutral atom lines of Cr were enhanced with increasing concentrations of Na up to 1000 µg/ml ($\sim$100%), whereas a decrease in intensity was observed with a further increase to 10,000 µg/ml Na. Similar effects were observed with neutral atom lines of Al and Mn. Steady decreases in intensity with increasing Na concentration were also observed for neutral atom lines of B and Co. Kitagawa and Takeuchi (28) have described interferences produced by Na in a Hitachi SEP (2.45 GHz) supported by N_2 or Ar. For the N_2 supported plasma, the interferences appeared to be less severe than for the Ar supported plasma but were much worse than those observed with the ICP employed in the present study. Murayama (27,85) and Murayama et al. (61) have also described interferences produced by easily ionizable elements in micro-wave-excited SEP's supported by Ar.

The use of a spectrochemical buffer (an additive such as an alkali or alkaline earth element added to both the sample and reference solutions for the purpose of making the measure of the analyte less sensitive to variations in inter-ferent concentration) with the SEP has been recommended by

Murayama (27), Kessler (89), and Boumans et al. (79).
Indeed, Govindaraju et al. (91) have utilized an approximate
ten-fold excess of Sr as a spectrochemical buffer in the
analysis of silicate rocks with a microwave-excited SEP
sustained in N_2. However, since the interference curves
(analyte intensity vs. interferent concentration) from
various SEP's have not exhibited plateau regions (27,28,88,
90), it is reasonable to presume that the buffer must be
present in a large excess to overcome variations in the
interferent concentrations in the samples.

Reports in the literature on the interference effects
produced by easily ionizable elements in the ICP were dis-
cussed in the preceding chapter.

The results of the present comparative study on the
effects of Na on the emission intensities of neutral atom
and ion lines of Ca, Cr, Mo, and Zn for two heights of obser-
vation in the SEP and in the ICP at the height normally
employed for analytical applications for this facility are
presented in Figures 13-16. In these and in subsequent
figures, the net emission intensities of a given species in
the absence of the interferent are normalized to unity at
each observation height for each plasma. Because the relative
intensity data are plotted on a logarithmic scale, the
excursions of the curves from the unity value give a direct
comparison of the interelement effects. The ion lines of Mo

Figure 13. Comparison of effect of Na on Ca emission in
            SEP and ICP

            (Concentration of Ca: 0.5 µmol/ml; height of
            observation: SEP 3 or 7 mm above electrode,
            ICP 20 mm above load coil)

                              O   Ca I 422.7 nm
                              X   Ca II 393.4 nm

Figure 14. Comparison of effect of Na on Cr emission in
SEP and ICP

(Concentration of Cr: 0.5 µmol/ml; height of
observation: SEP 3 or 7 mm above electrode,
ICP 20 mm above load coil)

O   Cr I 425.4 nm

X   Cr II 284.3 nm
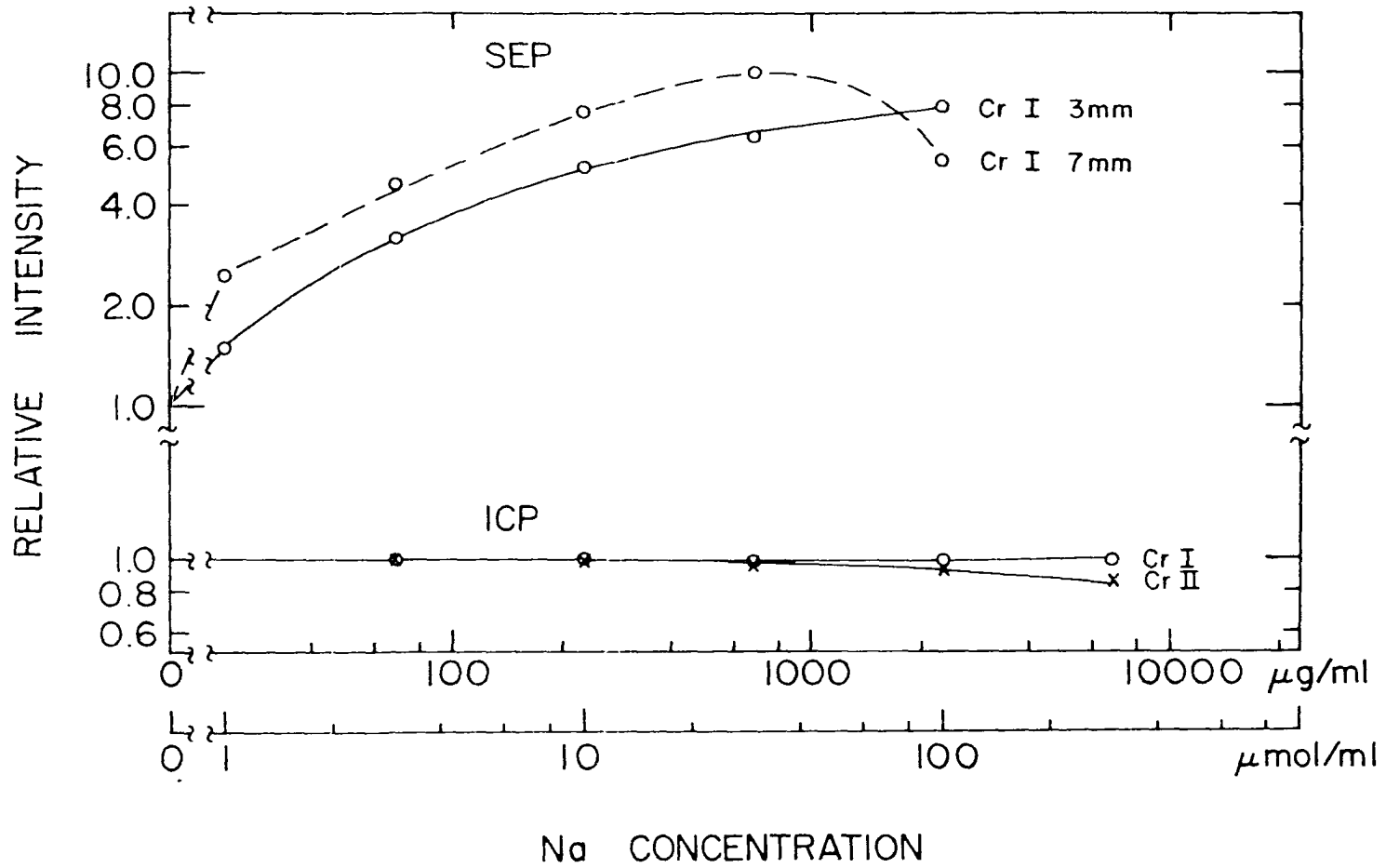
Figure 15.   Comparison of effect of Na on Mo emission in

SEP and ICP

(Concentration of Mo: 25 µgm/ml; height of

observation: SEP 3 or 7 mm above electrode,

ICP 20 mm above load coil)

O   Mo I 390.3 nm
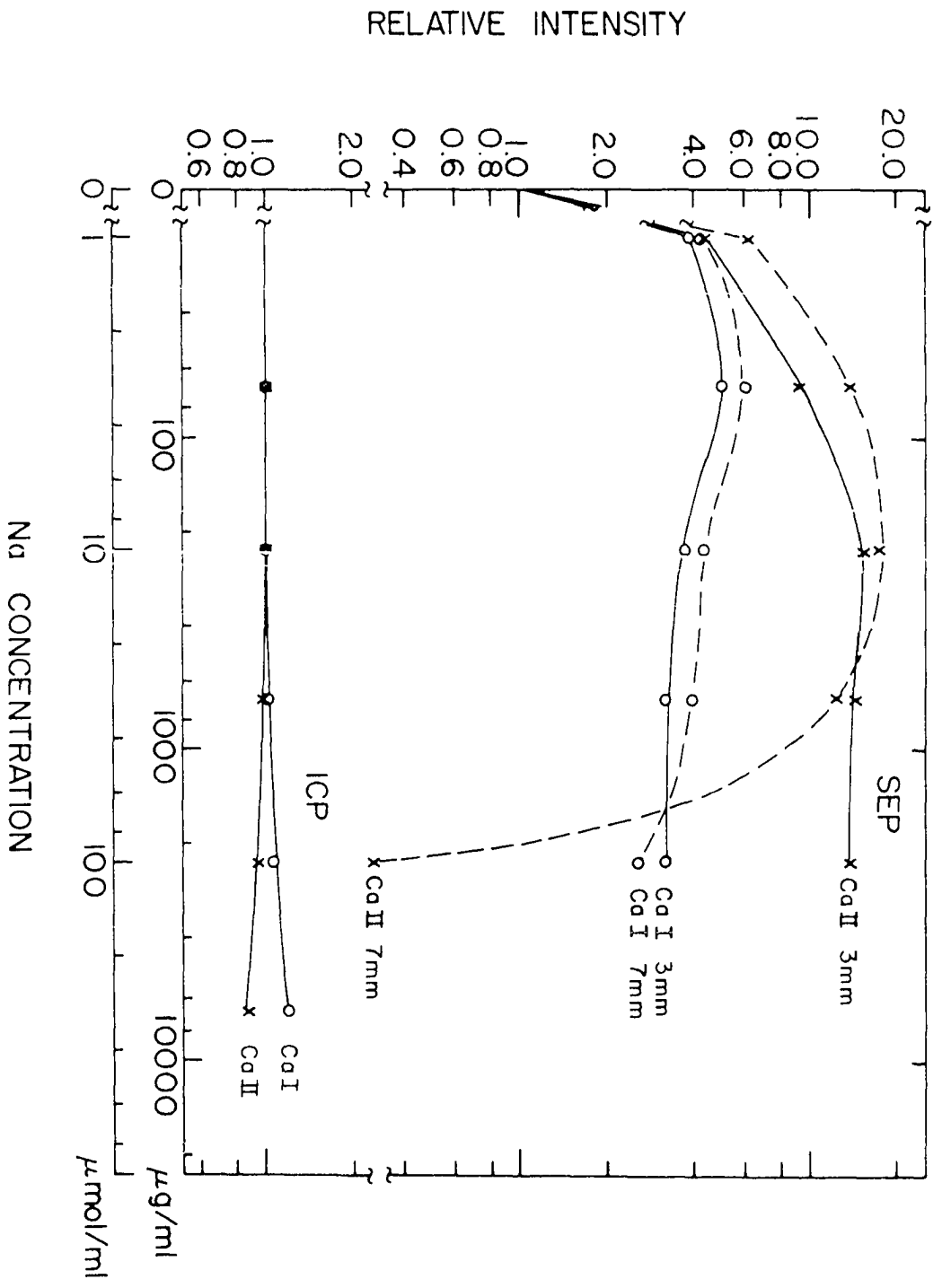
X   Mo II 281.6 nm

Figure 16. Comparison of effect of Na on Zn emission in
            SEP and ICP

            (Concentration of Zn: 0.5 μmol/ml; height
            of observation: SEP 3 or 7 mm above
            electrode, ICP 20 mm above load coil)

                        ◯   Zn I 213.9 nm
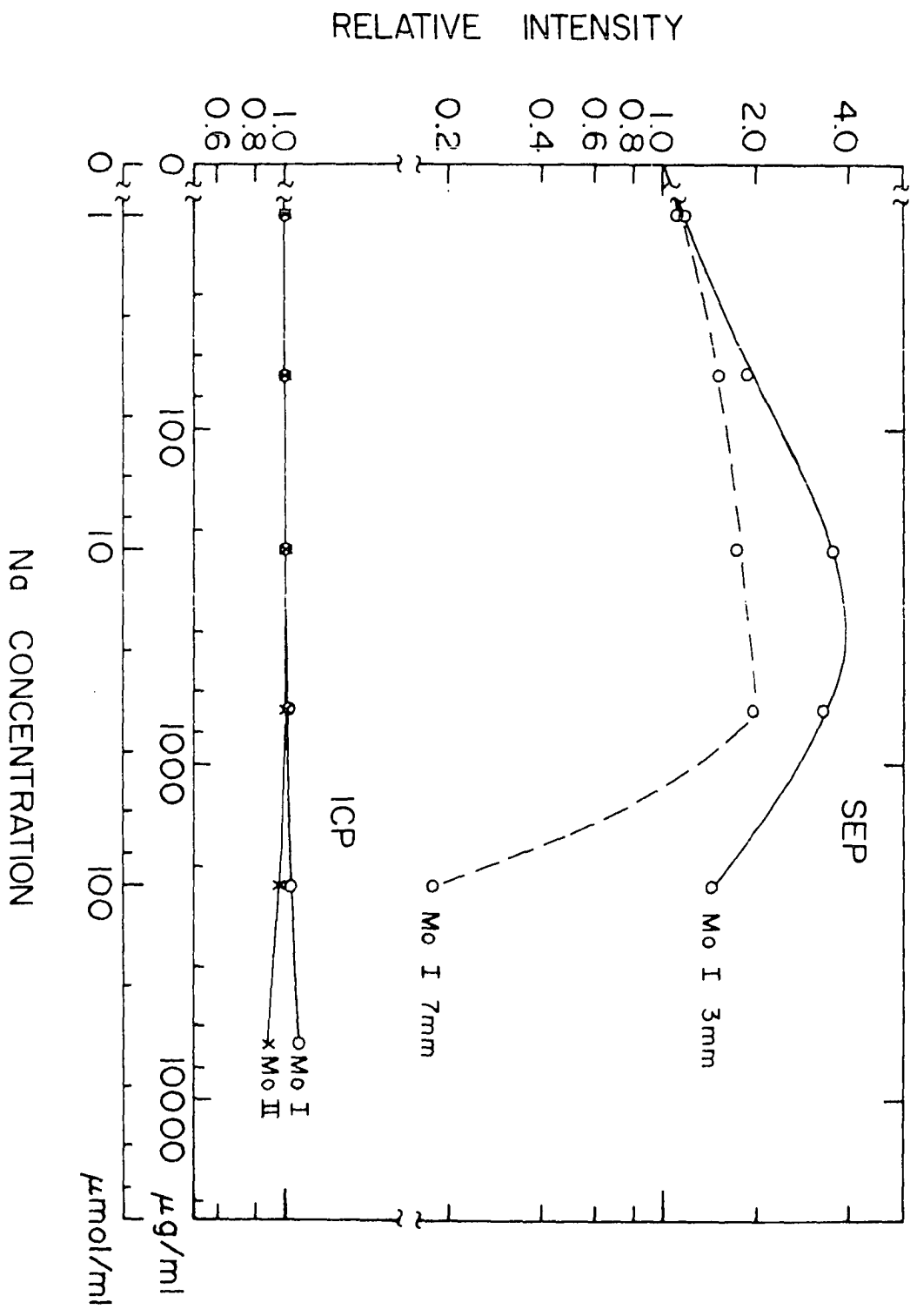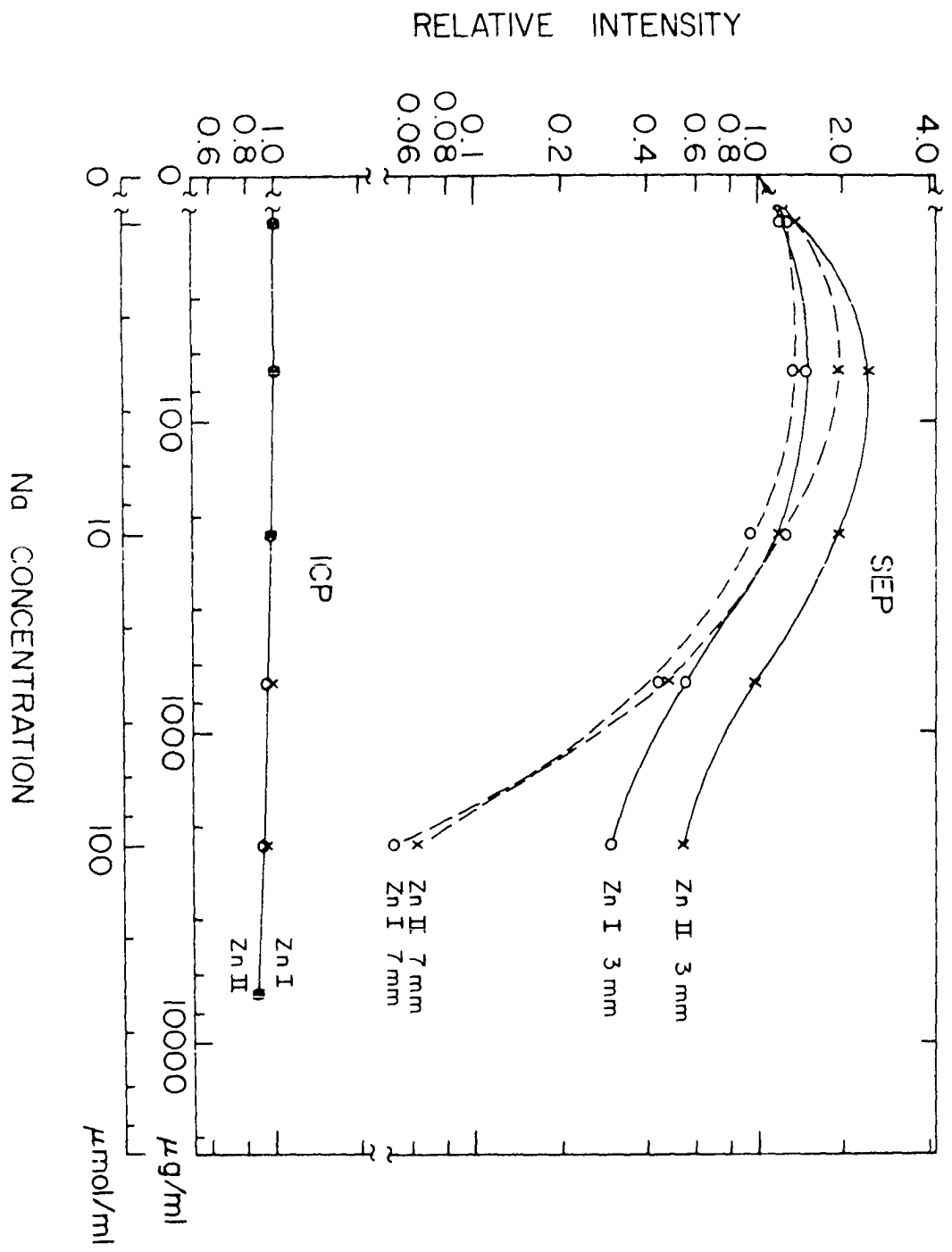   X   Zn II 202.6 nm

RELATIVE INTENSITY

Na CONCENTRATION

SIEP

ICP

ZnI
ZnII

Zn II 7 mm
Zn I 7 mm

Zn I 3 mm
Zn II 3 mm

μmol/ml
μg/ml

89

and Cr in the SEP are not included because of their low signal
to noise ratio.

The trends reported here for the SEP are in general
agreement with those previously described by Murayama (27,85),
Murayama et al. (61), and by Kitagawa and Takeuchi (28) for
microwave SEP's sustained in Ar. The most striking features
of Figures 13-16 are the large relative changes in analyte
emission intensities observed with the SEP for changes in Na
concentration whereas only minor changes are observed in the
ICP over the entire range of Na concentrations studied. The
large enhancements observed in the SEP for Na concentrations
of only 23 µg/ml (corresponding to 1 µmol/ml) suggest that
considerable difficulty would be encountered if samples
contain even minor but variable concentrations of an easily
ionizable element. Equally significant is the observation
that at higher concentrations of concomitant Na large
relative changes in analyte emission intensity are observed
even for relatively small changes in Na concentration. The
absence of a plateau region in the interference curves for
the SEP suggests that additions of an excess of an easily
ionizable element to the sample and reference solutions to
buffer the interactions to a constant level would only be
marginally successful. Moreover, when solutions containing
2300 µg/ml Na or greater were nebulized into the SEP, a Na
deposit formed on the electrode tip and caused the plasma to

become unstable. When solutions containing 6900 μg/ml Na
are nebulized into the SEP, the plasma tended to degenerate
into a ribbon-like discharge maintained between the center
conductor or electrode and the surrounding quartz tube.
Concentrations of Na as high as 23,000 μg/ml do not affect
the stability of the present ICP in any apparent way although
deposits may form on the aerosol injection orifice.

It is worth noting that the changes in the emission
signals for the Ca II 393.4 nm, Cr II 284.3 nm, Mo II
281.6 nm, and Zn I 213.9 nm (lines for which best detection
limits are observed in the ICP) are only -6, -7, -5, and
-8 percent, respectively, for the analytical equivalents of
determining these elements in deionized water and in a
0.23 wt. % of Na. Thus, synthetic reference solutions pre-
pared by the incremental additions of these analytes to
distilled water would provide reasonably accurate analysis
for their determination in sodium salts.

Effect of concomitants on Mo emission

The effects of various concomitants with differing
ionization potentials on Mo emission in the SEP and the ICP
are presented in Table IV. All of the concomitants produced
significant interference on the Mo I emission in the SEP.
In the ICP, small interferences were observed with the more
easily ionizable concomitants (K, Na, Al) whereas the con-
comitants with higher ionization potentials (Cu, Zn) produced

Table IV. Effect of concomitants on emission of 25 µg/ml Mo
          in SEP and ICP

| | | Relative intensities | | |
| | | SEP[a] | ICP[b] | |
Concomitant[c] (Ionization Potential, eV)		Mo I[d]	Mo I[d]	Mo II[e]
None		100	100	100
K	(4.34)	47	102	97
Na	(5.14)	68	105	94
Al	(5.98)	154	103	95
Cu	(7.72)	309	100	100
Zn	(9.39)	150	101	100

[a]Observation height: 5 mm above electrode tip.

[b]Observation height: 20 mm above load coil.

[c]Concomitant concentration: 2500 µg/ml.

[d]Mo I 390.3 nm.

[e]Mo II 281.6 nm.

essentially no interference. These results suggest the inter-
esting and very valuable possibility of establishing single
analytical curves for the determination of an analyte in a
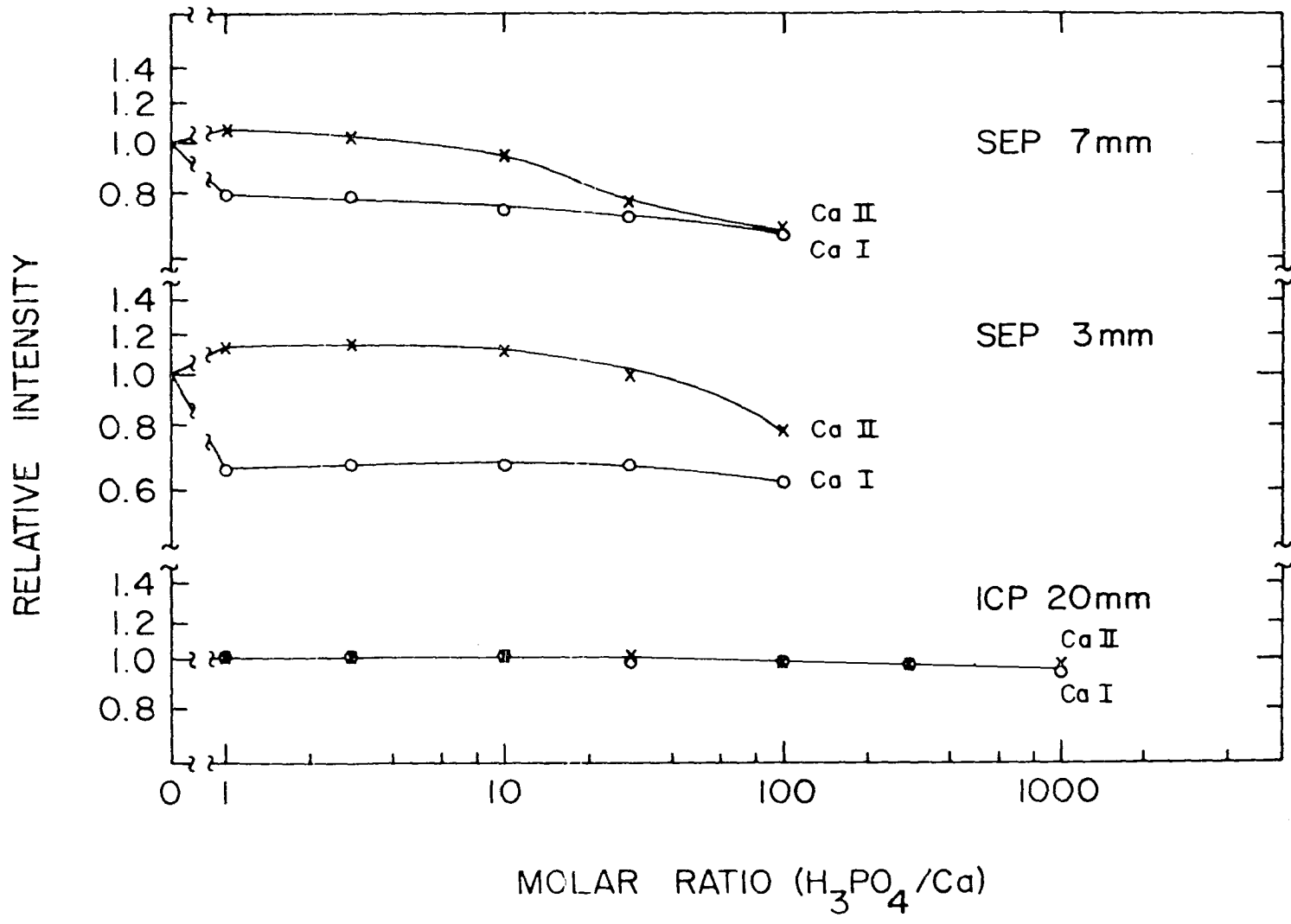variety of matrices in the ICP.

Ca-PO$_4$ interference system

A literature review on the origins of this interference and its occurrence in the ICP was presented in the preceding chapter of this dissertation. The author is not aware of any reports on the existence of interference on Ca emission by the presence of PO$_4^{3-}$ in microwave-excited SEP's whereas West and Hume reported an absence of interference in a radiofrequency-excited SEP in N$_2$ (92). The results of the present study are shown in Figure 17 for two heights of observation in the SEP and for the normal observation height in the ICP. The precipitous depression and the "knee" in the interference curves for Ca I emission with the SEP is reminiscent of the solute vaporization interference as observed in some combustion flames. However, the enhancements of Ca II emission at low PO$_4$/Ca molar ratios and the depression at high molar ratios are not consistent with this interpretation. Changes in analyte distribution produced by changes in the rate of vaporization of the aerosol particles in the presence of PO$_4^{3-}$ (93) may be partially responsible for the interactions reported in Figure 17. In marked contrast to the SEP, the interference on Ca I and Ca II by concomitant PO$_4^{3-}$ is essentially negligible in the ICP.

Figure 17. Comparison of effect of H_3PO_4 on Ca emission
in SEP and ICP

(Concentration of Ca: 0.5 μmol/ml; height of
observation: SEP 3 or 7 mm above electrode,
ICP 20 mm above load coil)

○   Ca I 422.7 nm

X   Ca II 393.4 nm

Ca-Al interference system

A literature review on the origins of this interference and its occurrence in the ICP was presented in the preceding chapter of this dissertation. The author is unaware of reports of any investigations of the Ca-Al system in a microwave-excited SEP in Ar. In microwave-excited SEP's in N_2, enhancements at Al/Ca molar ratios greater than $\sim$20 have been reported by Govindaraju et al. (91), whereas depressions ($\sim$30%) have been observed with additions of Al with Na present as a spectrochemical buffer (90). West and Hume (92) reported an absence of interference in their radiofrequency-excited SEP in N_2.

The results of the present study are shown in Figure 18. The interference on Ca I and Ca II emission by concomitant Al in the SEP is probably a combination of the solute vaporization interference and other interactions occasioned by the addition of the easily ionizable element Al to the plasma. Concomitant Al has little effect on Ca I or Ca II emission in the ICP as shown in Figure 18. Identical results were obtained with the Al added as $AlCl_3$ or $Al(NO_3)_3$. The small interference that is observed in the ICP may be virtually eliminated by the addition of Na to all solutions as was shown in the preceding chapter.

Figure 18. Comparison of effect of Al on Ca emission in

SEP and ICP

(Concentration of Ca: 0.5 µmol/ml; height of

observation: SEP 3 or 7 mm above electrode,

ICP 20 mm above load coil)

O   Ca I 422.7 nm

X   Ca II 393.4 nm

Conclusion

Definitive interpretations of the interference effects observed in various versions of the SEP are rendered exceedingly difficult by the nonuniform distributions of the composition, "temperature", and electron number density in these plasmas. To provide a physically meaningful basis for an interpretation, spatially-resolved, radial distributions of these physical parameters must be employed rather than the experimentally measured, spatially averaged distributions (27,28). In an SEP-type discharge, especially those supported by noble gases, the electronic or excitation temperature may far exceed the gas temperature (26,82,85, 94-96). The apparent absence of local thermodynamic equilibrium adds further complications and may also be a significant factor in producing the relatively high degree of interference effects which have been reported for SEP-type discharges.

In the present version of the SEP, the sample particles are transported to the plasma region by a gas flowing between the electrode and a concentric quartz tube. Thus, the sample particles must overcome the expansion thrust pressure (43, 48,49) to be injected efficiently into the plasma. The advantages of efficient sample introduction were apparently realized by Pforr (97), who introduced the sample aerosol through the center of the electrode tip. However, in order

to maintain a stable, symmetrical plasma, the maximum carrier gas flow was found to be only ∿0.07 l/min. Further work on this approach may result in reduction of some of the inter-element effects observed in SEP-type plasmas.

That the microwave-excited SEP in Ar does not produce efficient atomization of thermally stable compounds is suggested by the suppression of Ca I emission by the addition of PO_4^{3-} or Al to the nebulized solution, as shown in Figures 17 or 18, although the behavior of the Ca II line indicates that other processes are important. In this context it is interesting to note that West and Hume (92) reported an absence of an interference effect on Ca emission with the addition of more than 100-fold excesses of aluminum and phosphate in a radiofrequency-excited SEP in N_2. This absence may have been due to the higher gas temperature prevailing in the N_2 supported discharge. The exciting frequency as well as other experimental parameters apparently play an important role as evidenced by the depression of Ca emission (in the presence of excess Na) with the addition of Al reported by Sermin (90) in a microwave-excited SEP in N_2. Indirect evidence that the microwave-excited SEP in Ar does not produce efficient atomization of thermally stable compounds can be found in an early comparison of detection limits in the SEP and the ICP (4). The detection limits reported for elements which form stable monoxides

$[D_o(MO) > 7 \text{ eV}]$ are generally one to two orders of magnitude
greater for the SEP than the ICP although the detection
limits for most other elements with these plasmas are
similar.

CHAPTER IV.   THE STRAY LIGHT/BACKGROUND SHIFT PROBLEM

IN ULTRATRACE ANALYSES BY OPTICAL

EMISSION SPECTROMETRY

Introduction

When atomic emission spectroscopy is employed for the
determination of trace elements at concentrations near the
detection limit, the spectral background will normally be a
large fraction of the total measured signal. Thus, accurate
analyses require precise background corrections. In samples
of varying composition, changes in the concentration of
concomitants may produce subtle changes in the background
level. These background shifts may be caused by true
spectral line or band interferences, by indirect effects on
the spectral background underlying the analysis line, or by
stray light contributions. These shifts will lead to an
analytical bias unless appropriate corrections are applied.
If this bias results from stray light contributions, it may
masquerade as an interelement interference or matrix effect
when, in reality, limitations in the spectrometer components
or defects in engineering design or construction are the
primary causes. Although there have been excellent dis-
cussions on various stray light effects in absorption (98-
101), fluorescence (102-105), and Raman (106,107) spectros-
copy, the nature and magnitude of these effects have received
little attention when trace element determinations are

performed by atomic emission spectroscopy. In this chapter examples of various forms of stray light originating from grating and optical design defects in spectrometers are illustrated and the biases these effects may produce on the final analytical result are assessed if proper corrections are not made.

Stray light

Stray light is broadly defined as the unwanted radiation that reaches the detector in unintended ways (108). Stray light originating from grating imperfections may occur as Rowland (109-111), worm (112-114), or Lyman (110,111,115) ghosts produced by periodic errors in the grating groove spacing, as satellites, "grass", or "near scatter" $(\Delta\lambda \lesssim 2.5-5.0 \text{ nm})$ (110,111) produced by regular or irregular grating defects, or as "far scatter" $(\Delta\lambda \gtrsim 5 \text{ nm})$ produced by local or microscopic groove or blank imperfections as well as by roughness in the faces or edges of the grooves (110,111).

Progressive improvements in grating production and replication in recent years have significantly reduced stray light originating from grating imperfections. For instance, the intensities of first order Rowland ghosts have been reduced from as great as 2% of the parent line for gratings ruled under mechanical control to <0.001% for gratings ruled under interferometric control (110,111). Although some of the early gratings ruled under interferometric control

exhibited high levels of far scatter due to jitter in the
ruling diamond as the servo-control system sought the null-
position, refinements in the control systems have resulted
in significant reduction in far scatter (111). Holographi-
cally recorded gratings, which are recordings of an
interference phenomenon, do not exhibit line ghosts and,
through the use of virtually grainless photopolymers, also
exhibit low levels of scattered light (111).

In principle, there is a theoretical lower limit that
can be achieved in the relative levels of near and far
scatter. Even a "perfect" diffraction grating with N_r
rulings, where N_r represents an even number, will form N_r-2
secondary interference maxima between the principal or
ordinal maxima of adjacent orders (116-118). Near each
principal maximum, this interference pattern is approximated
by the diffraction pattern produced by an aperture of width
equal to the grating width projected through the angle
between the normal of the grating and the diffracted ray
(110,116-118). Hence, this interference pattern has been
described as the diffraction pattern of the (effective)
grating aperture (110,117). A reduction of the relative
intensity of the "feet" of this diffraction pattern may be
achieved by apodization of the grating aperture with an
appropriate mask. For instance, a diamond shaped mask will
decrease the relative intensities of the "feet" of the

grating aperture diffraction pattern when narrow slits are employed (110,119,120). Fortunately, the theoretical lower limits for far scatter resulting from the secondary maxima are much lower than the far scatter usually observed in high quality spectrometers. Thus, the stray light arising from grating imperfections discussed above and from the other sources discussed below presents a far more serious problem.

Instrumental line broadening effects and stray light may originate from various sources other than grating imperfections. Finite widths of slits, imperfections in the slit jaws, aberrations of the optical system, diffraction by mirror apertures, and optical misalignment may broaden concomitant spectral line images to a sufficient degree to cause spectral interferences. In addition, the primary radiation entering the spectrometer, as well as zero and other order diffracted rays, may be scattered from dust particles and from imperfections in optical surfaces or may be reflected or scattered from interior surfaces of the spectrometer to produce general stray light.

Multiple diffractions (reentry spectra) have also been identified as a significant source of stray light in some in-plane Littrow (106,121), Ebert (122,123), and Czerny-Turner (124-126) spectrometers. For certain component arrangements in Ebert or Czerny-Turner mountings, once-diffracted radiation is returned to the grating by the reflecting optics. This once-diffracted light will undergo

a second diffraction, ultimately striking the camera mirror
and reaching the detector. The problem of multiple dif-
fractions, once identified, may be eliminated by masking a
portion of the grating (which reduces the throughput) or, in
some cases, by employing a grating with a different groove
spacing (124-126).

Finally, the detectors in polychromators are not
normally positioned in individual light tight channels
immediately behind the exit slits. Thus, stray light may
result from leakages and reflections along the optical path
as well as from reflections and scattering in the secondary
optics. The majority of the data obtained with the direct
reading polychromators presented in this chapter was obtained
by R. K. Winge of the Ames Laboratory-ERDA and is presented
here to provide a complete discussion of the various sources
of stray light.

Line broadening

In high temperature sources, such as the ICP, the
emitted lines may be broadened to the extent that the wings
produce a significant contribution to the spectral background
as far removed as 10 nm or more. The identification of the
broadening mechanisms [presumably the strongly perturbing
close collisions (127,128)] which give rise to the signifi-
cant intensity in the extreme wings of spectral lines is
beyond the scope of the present discussion. The spectral

interferences which arise from the wings of very strong emission lines have not been generally recognized in optical emission spectroscopy, in part due to the high stray light rejection factors which are required for their identification. These high rejection factors may be readily achieved with double monochromators (129). However, this type of spectral interference may be quite important in ultratrace analysis when excitation sources with low background emission are employed.

It is also important to realize that spectral inter-ferences from continuum radiation may also be produced by processes other than line broadening. Such sources as recombination reactions, molecular continua, and blackbody radiation from incompletely vaporized particles (130-132) may give rise to significant spectral continua. In addition, concomitants may also induce indirect effects on the spectral background, e.g., through changes in temperature and electron number density (26,130).

Experimental Facilities

Spectrometers

The spectrometers employed in this study are described in Table V.

Table V. Spectrometric instrumentation

Spectrometer I-A:	0.5 m Ebert mount (Model No. 82000, Jarrell-Ash Division, Fisher Scientific Co., Waltham, MA) Grating, (1180 grooves/mm) blazed for 250 nm in first order, was replicated from a master (No. 1227, Jarrell-Ash) which was ruled under interferometric control. This master was retired some years ago because of its high stray light characteristics. Fixed 15 μm entrance and exit slits were employed and masked to a height of 4 mm. The detector and readout electronics have been described previously (52).
Spectrometer I-B:	Same instrument as I-A except for grating. Grating (1180 grooves/mm) was replicated from a more recent master (No. 1370, Jarrell-Ash), which was ruled under interferometer control and blazed for 240 nm.
Spectrometer I-C:	Same instrument as I-A except for grating. Grating (1200 grooves/mm) was holographically recorded with optimized efficiency for 200-700 nm. (J-Y Optical Systems, Metuchen, NJ).
Spectrometer II-A:	Applied Research Laboratories QVAC 127 polychromator. The optical path consists of a field lens, an entrance slit, a grating, and 47 exit slits, after which 45° mirrors deflect the appropriate wavelengths to photomultipliers located above and below the focal plane. The grating, replicated from Bausch & Lomb master #845, has 2160 grooves/mm and is blazed for the 170-215 nm region. Wavelength scans over small intervals are achieved by moving the entrance slit along the Rowland circle.

Table V. (Continued)

Spectrometer II-B:	Same instrument as II-A except for grating. Grating was holographically recorded as a replacement for grating in II-A (J-Y Optical Systems, Metuchen, NJ).
Spectrometer III:	0.5 m Czerny-Turner double mono-chromator (Model 285, GCA/McPherson, Acton, MA). The grating, replicated on both sides of blank, has 1200 grooves/mm and is blazed for 300 nm in first order. The entrance, intermediate, and exit slits were set at 10 μm and masked to a height of 2 mm. Stray light rejection ratios of $<10^{-10}$ at 0.5 nm and $<10^{-11}$ at 1.0 nm from Ar laser line at 514.5 nm are specified by the manufacturer. The detector and readout electronics have been described previously (52).

Excitation sources

Inductively coupled plasmas (ICP) were used as the
excitation sources. The ICP facility employed with spectrom-
eters I-A, -B, and -C was described in Chapter II. The
forward power reading was 1200 W and the reflected power
reading was ~5 W. The Ar flow rates were 1.0 l/min for the
aerosol carrier and 12.5 l/min for the plasma gas. The 4 mm
high observation zone was centered 15 mm above the load
coil.

The ICP generator (Model MN-2500E, Plasma-Therm, Inc.,
Kresson, NJ) employed with spectrometers II-A and -B and III
was operated at a forward power level of 1100 W at a crystal
controlled frequency of 27.12 MHz. The Ar flow rates were
1.0 l/min for the aerosol carrier and 15 l/min for the plasma
gas. The observation zones were centered 15 mm above the
load coil, and their heights were 6+ mm for spectrometer II
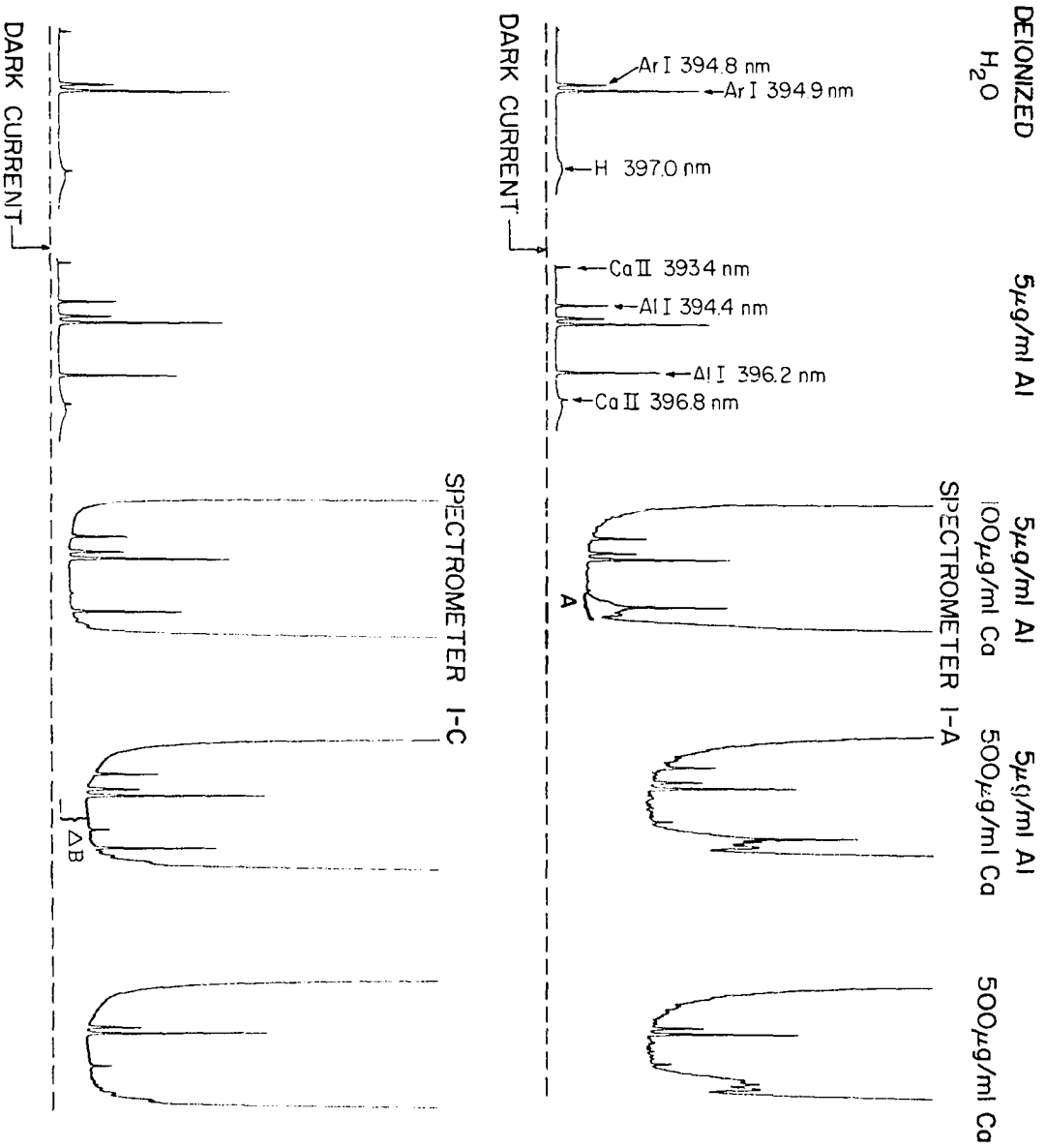and 2 mm for spectrometer III.

Results and Discussion

Near scatter, satellites, and Rowland ghosts

The problems encountered in ultratrace analyses that may
be caused by these sources of stray light are illustrated for
the case of Al in the presence of Ca. Two of the most useful
lines of Al occur at 394.40 and 396.15 nm, in close proximity
to the sensitive ion lines of Ca at 393.37 and 396.85 nm.

Calcium is highly ionized [>99% (24,25)] in the ICP and the
two ion lines are emitted in unusually high intensity, even
at relatively low concentrations of Ca. As shown by the
recordings in Figure 19, these lines are detectable as
impurities when the solutions containing 5 μg/ml of Al are
introduced into the plasma. When solutions containing
appreciable concentrations of Ca are nebulized, e.g., the
100 to 500 μg/ml contents indicated in Figure 19, the Al lines
reside in a deep canyon between the Ca II 393.37 and 396.85 nm
lines. Significant upward shifts in the background underlying
both Al lines accompany these increases in Ca concentration.
Although the background shifts are considerably less in
spectrometer I-C than in I-A, the shift (ΔB) caused by
500 μg/ml Ca in spectrometer I-C was still equivalent to
2 μg/ml Al. The grating in spectrometer I-B produced a
similar shift. Thus, a significant portion of the background
shift for spectrometer I-C (and I-B) may be due to a com-
bination of the diffraction effects of the grating aperture
(the peak intensity of the secondary maximum at a position
corresponding to 396.156 nm would be $\sim 9 \times 10^{-6}$ of the peak
intensity of the principal maximum at 396.847 nm when
infinitely narrow slits are employed with a grating with
60,000 grooves), diffraction by the mirror apertures, scat-
tering from the mirror, aberration and slit broadening, and
misalignment of the optical components rather than grating

Figure 19. Effect of stray light on the observed background signal between the Ca II 393.4 and 396.8 nm lines

DEIONIZED H₂O

Ar I 394.8 nm
Ar I 394.9 nm

H 397.0 nm

DARK CURRENT

5 μg/ml Al

Ca II 393.4 nm
Al I 394.4 nm
Al I 396.2 nm
Ca II 396.8 nm

5 μg/ml Al
100 μg/ml Ca

SPECTROMETER I-A

A

5 μg/ml Al
500 μg/ml Ca

500 μg/ml Ca

DARK CURRENT

SPECTROMETER I-C

ΔB

DARK CURRENT

imperfections. Astigmatism and slit broadening effects played a minor role because a reduction in slit widths from 15 to 5 µm and slit heights from 4 to 2 mm produced only a slight reduction in background shift relative to the Al I lines.

The stray light adjacent to the Al I 396.15 nm line for spectrometer I-C was found to be $\sim$7 x 10^{-5} of the peak intensity of the Ca II 396.85 nm line, which is approximately the same fraction as observed at a $\sim$0.6 nm displacement from the Ne 632.8 nm line of a He-Ne laser (Model S-203-H, C. W. Radiation Inc., Mountain View, CA 94040) when an auxiliary lens was employed to fill the full aperture of the grating. These data indicate that the background shifts between the Ca II lines shown in Figure 19 were produced primarily by stray light and instrumental broadening effects with some possible contribution from plasma line broadening effects discussed below.

Two minor aspects of the recording in Figure 19 are worthy of mention. First, the background shifts (ΔB) observed with these spectrometers were not proportional to the Ca concentrations. Self-absorption of the Ca II lines may contribute to this nonlinearity (see discussion in a later portion of thesis), because a concentration of 500 µg/ml Ca is more than 6 orders of magnitude greater than the detection limit for Ca. Second, the broad band "grass", marked "A" in the

I-A recordings, arose from reflections and scattering of the Ca II 393.37 nm line in the exit slit assembly. This "grass" was eliminated (see spectrometer I-C recording) by blackening the entire assembly.

The recordings in Figure 20 show an example of stray light contributions from near scatter and other sources and from Rowland ghosts. The presence of 50 or 100 µg/ml Ca in the nebulized solution contributes both a shift in the under-lying background and two interfering "lines". There are no known lines or bands attributable to Ca at these wavelengths. The "lines" are, in fact, the 7th and 8th order Rowland ghosts of the Ca II 396.85 nm line. Although the grating used in spectrometer II has an unusually high ghost intensity and is not generally acceptable for ultratrace analytical applications, the shoulders of the Rowland ghosts contribute less background to the Al I 396.15 nm line than the general upward shift in the underlying background contributed by near scatter and instrumental and plasma line broadening effects (see discussion below).

Line broadening

The scan between the Ca II ion doublet for the 1000 µg/ml Ca solution obtained with the double monochromator, spectrom-eter III, also exhibits a significant background shift as shown in Figure 21. The shift at the Al I 396.15 nm line, which is equivalent to ∿0.4 µg/ml Al for the solution
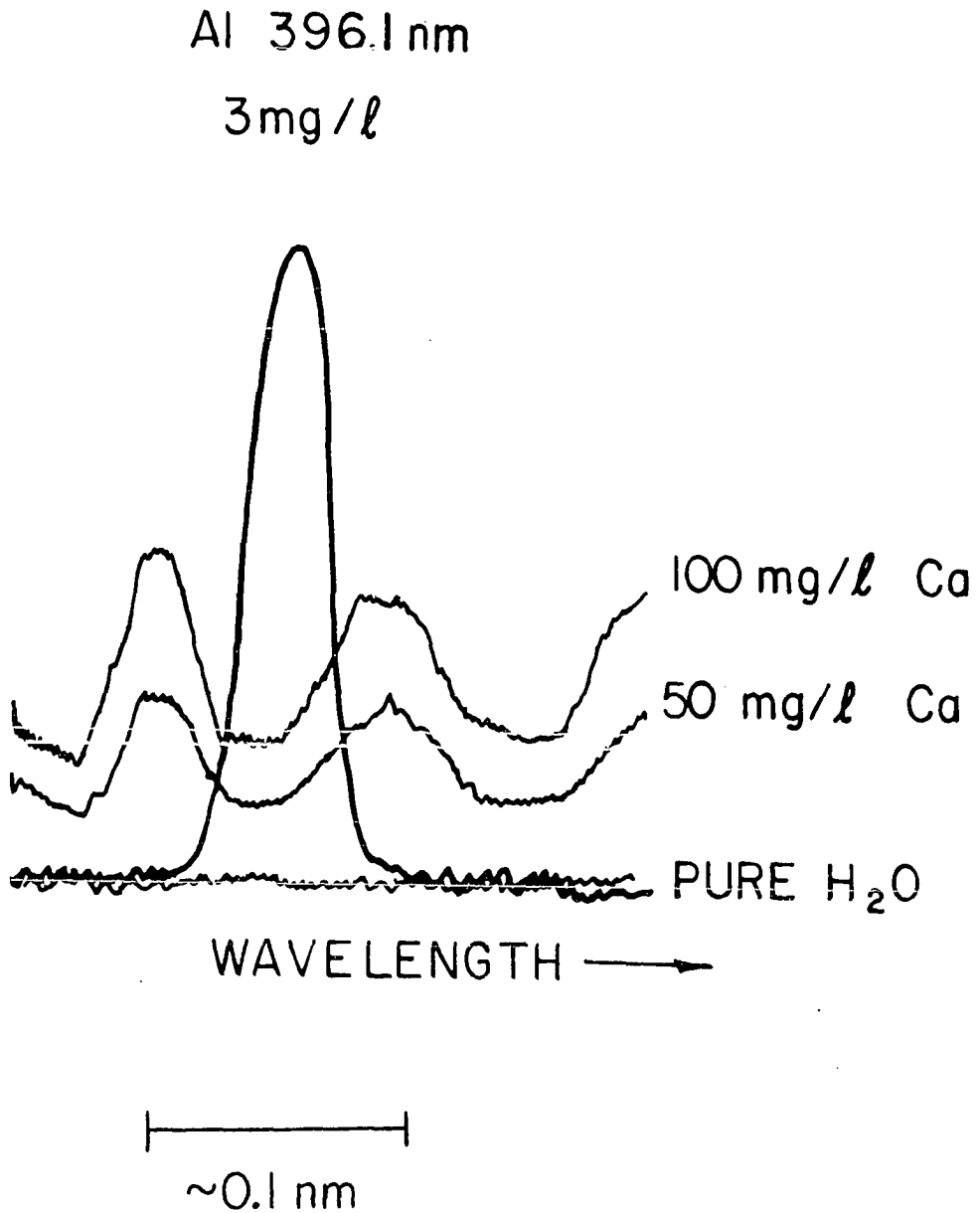
Figure 20. Effect of Rowland ghosts and stray light on the background signal observed with spectrometer II-A in the region of the Al I 396.1 nm line

I μg/ml Al

I μg/ml Al
1000μg/ml Ca

CaII 393.4 nm

CaII 396.8 nm

Ar I 394.9 nm

Al I 396.2 nm

AlII 394.4 nm

ArI 394.8 nm

H 397.0 nm

DARK CURRENT

CaI 395.7 nm

AlI 394.4 nm

AlI 396.2 nm

X 7×10^{-5}

Figure 21. Background shift produced by broadening of the
Ca II 393.4 and 396.8 nm lines in the plasma
observed with spectrometer III

containing 1000 μg/ml Ca, is ~1 x 10^{-5} of the measured peak

intensity of the Ca II 396.85 nm line. This background shift

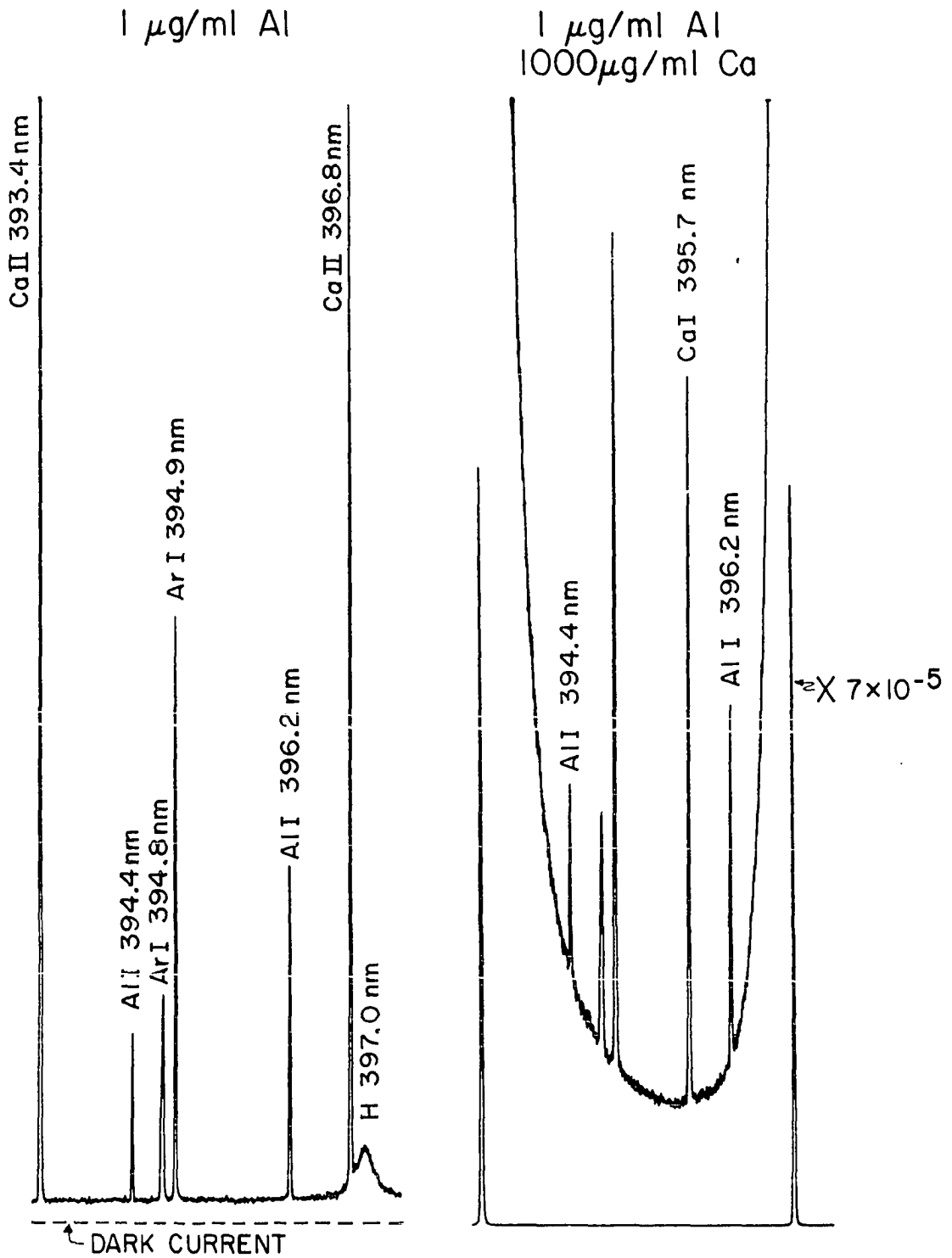is not due to stray light or instrumental broadening, since

the 10^{-5} ratio is much larger than the stray light rejection

ratio of $<10^{-10}$ at 0.5 nm from the parent line specified by

the manufacturer or the experimentally measured (see Figure

22 and related discussion below) ratio of <2 x 10^{-7} at 0.4 nm.

Thus, the background shift shown in Figure 21 is due to line

broadening occurring in the plasma.

An extended wavelength profile for the region of the

Ca II 393.37 and 396.85 nm lines, which was constructed

from the net signals observed for a solution containing

1000 μg/ml Ca at discrete wavelength positions (chosen to

exclude various spectral features such as weak Ca lines),

is shown in Figure 22. The instrument profile, obtained

with the Ne 632.8 nm line from a He-Ne laser, is also shown

in Figure 22. As stated above, since the instrument profile

is narrower than the Ca line profiles at intensity levels

$\lesssim10^{-3}$ of the peak intensities, the intensities in the wings

of the Ca lines do not represent an instrumental artifact

but line broadening in the plasma. (This conclusion is

based on the assumption that the instrument profile is not

strongly wavelength dependent.) The data in Figure 22

demonstrate that the wings of very strong emission lines may
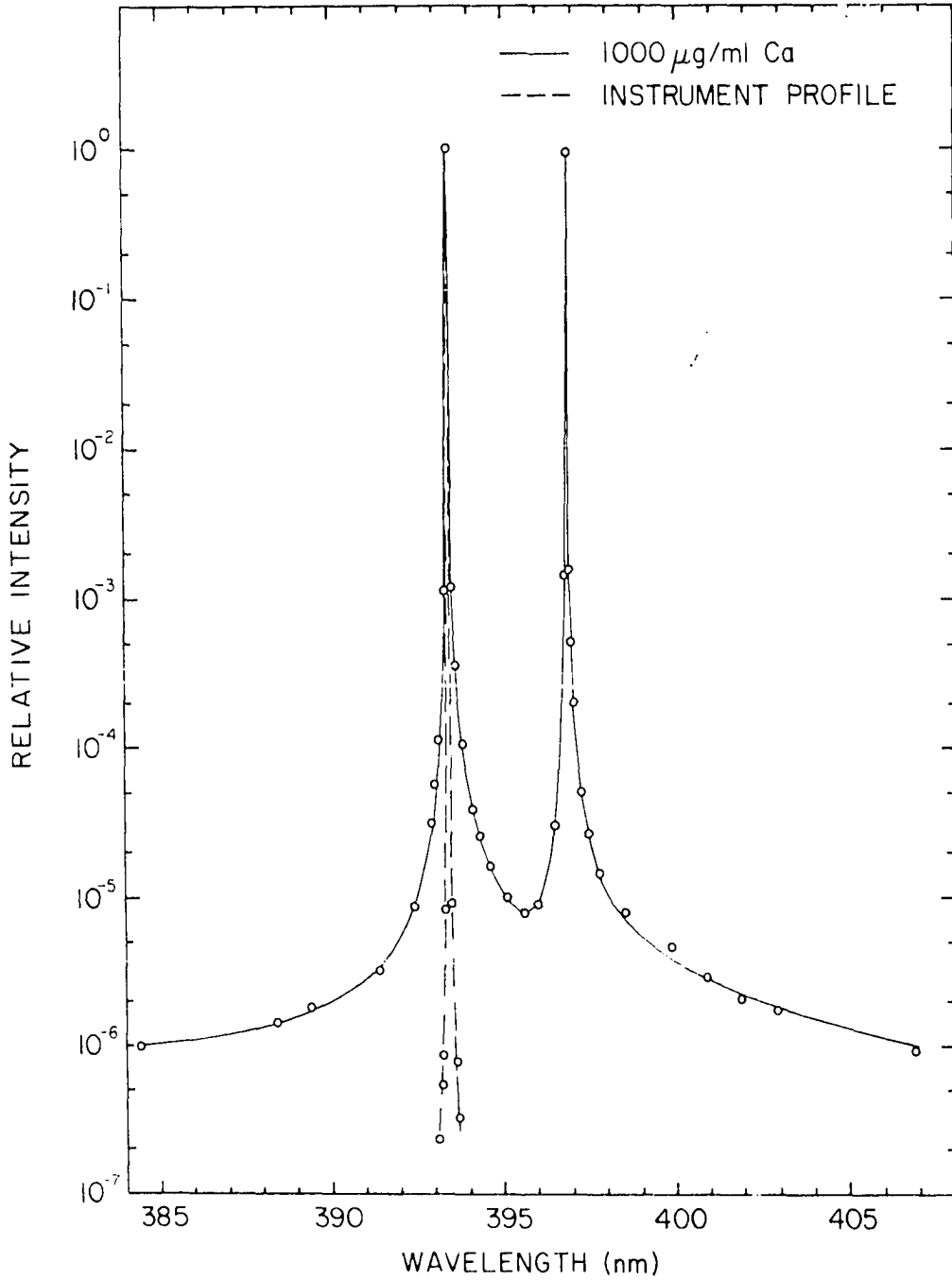
produce significant spectral interferences as far as 10 nm

Figure 22. Extended profile of the Ca II 393.4 and 396.8 nm
lines

or more from the line center. For example, the net signal for the 1000 μg/ml Ca solution at the lowest wavelength shown in Figure 22, 384.1 nm, is ~30% of the signal observed with the introduction of deionized H_2O, although this net signal is only 10^{-6} of the net signal at the Ca II 393.37 nm line center. This fraction would be somewhat less than 10^{-6} if corrections were applied for the self-absorption occurring in the central portion of the Ca II 393.37 nm line.

The results presented in Figures 21 and 22 indicate that proper consideration must be given to spectral interferences arising from the wings of very strong lines (in addition to stray light) in the selection of analysis lines for certain matrices. Thus, another Al line such as the Al I 308.22 nm line should be employed for the determination of trace levels of Al in the presence of variable concentrations of Ca, unless suitable wavelength scanning or other empirical correction procedures are employed. Only a small loss in detection power, from 0.006 to 0.02 μg/ml, would be involved in this alternate line choice.

Replacement of the grating in spectrometer II-A with a holographically recorded grating (designated II-B) resulted in a decrease of the background shift underlying the Al I 396.15 nm line by a factor of only ~5. To determine if a significant portion of this shift arose from stray light or instrumental broadening, the effect of varying Ca concentrations on the observed shifts was investigated. This

approach was necessary because a direct comparison with results obtained with spectrometer III was not possible due to differences in the instrumental bandpasses, in portions of the plasma from which the emission is sampled, and in plasma operating conditions, etc. The analytical curve obtained from the central portion of the Ca II 396.85 nm line exhibits unity slope up to a concentration of ∿100 μg/ml as shown in Figure 23. Above this concentration, significant curvature toward the concentration axis is observed, which indicates the presence of self-absorption. The log-log plot of the equivalent Al concentration versus the Ca concentration obtained with spectrometer III shown in Figure 23, displays unity slope up to 10,000 μg/ml Ca. This curve is essentially an analytical curve for Ca obtained from the wing of the Ca II 396.85 nm line. These experimental results are in agreement with several theoretical treatments (133-135) which have shown that self-absorption by atoms possessing an absorption line profile identical to or narrower than the emission line profile yields a greater relative decrease in the central portion of the emission line profile than in the wings. The plot of the Ca concentration versus the equivalent Al concentrations obtained with spectrometer II-B shown in Figure 23 displays unity slope up to ∿100 μg/ml, above which significant curvature toward the concentration axis is shown. Since similar curvature is observed in the central portion of

Figure 23. Background shifts at 396.2 nm expressed in terms
            of equivalent Al concentration and analytical
            curve for the Ca II 396.8 nm line

            X   Spectrometer III, 396.8 nm
            O   Spectrometer III, 396.2 nm
            □   Spectrometer II-B, 396.2 nm

RELATIVE INTENSITY (ARBITRARY UNITS)

Ga CONCENTRATION (μg/ml)

EQUIVALENT Al CONCENTRATION (μg/ml)
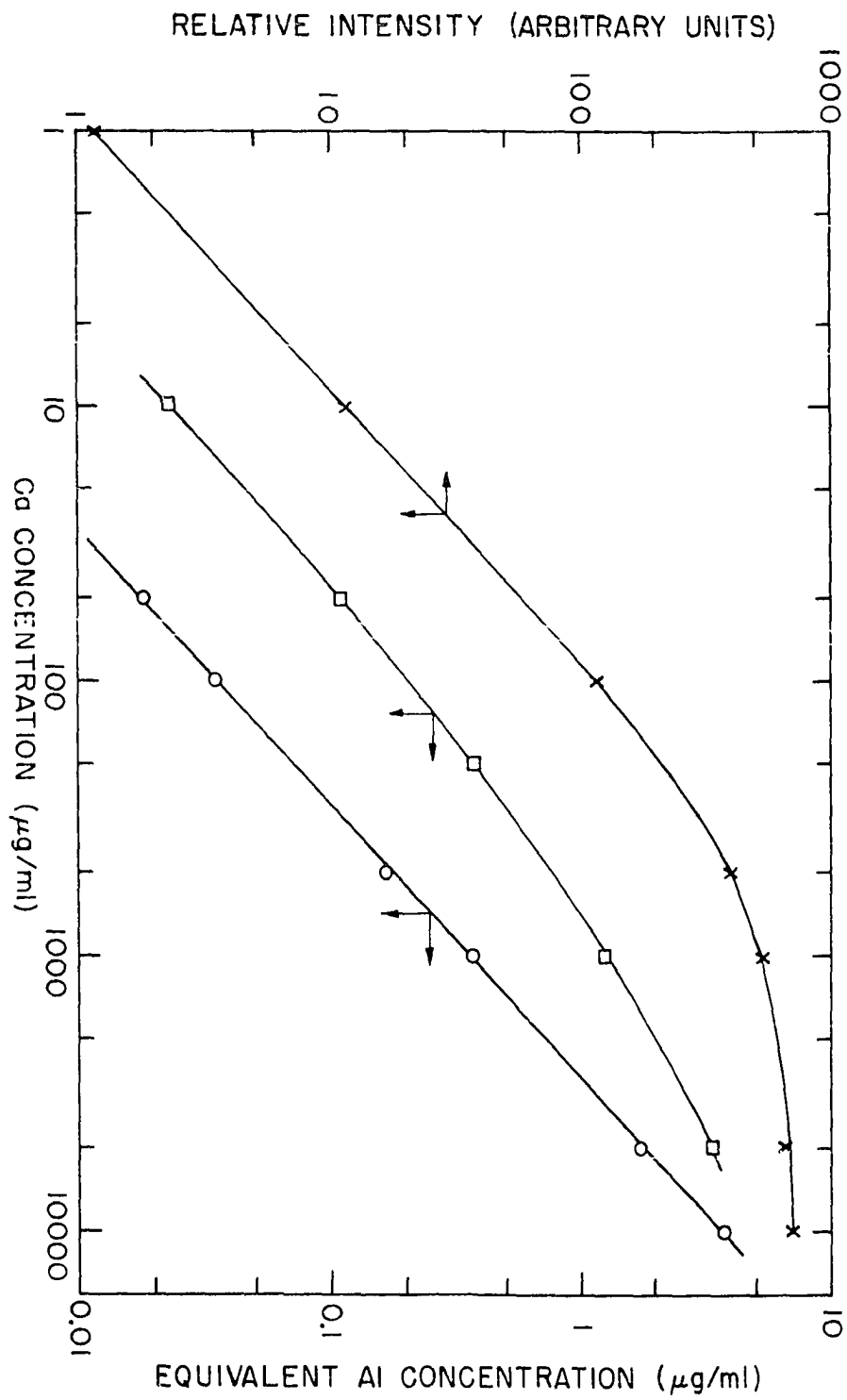
the Ca II 396.85 nm line but not in the wing (as measured with spectrometer III), a significant portion of these background shifts observed with spectrometer II-B must be due to stray light from or instrumental broadening of the central portion of the emission line.

Far scatter

The scans in Figure 24 illustrate the effects of increasing concentrations of Ca on the observed background in the region of the Zn I 213.86 nm line with spectrometers I-A and I-C. The structure observed when deionized water was nebulized arose from NO_γ bands. Even though the Zn 213.86 nm line is coincident with one of these band components, this line is still useful for quantitative determination at concentrations less than 0.1 µg/ml Zn. With increasing Ca concentrations, upward shifts in the baseline background were observed with each of the spectrometers, but to a much greater extent for spectrometer I-A. That these upward shifts were due to stray light is clearly evident for the scans with 1000 µg/ml Ca with a borosilicate glass filter (transmittance $<10^{-4}$ at 213.9 nm) in the optical path (C and C' in Figure 24).

For spectrometer I-A the relatively large stray light contribution from the Ca concomitant has structure as well. Considerable far scatter structure was also observed with spectrometer I-A with a He-Ne laser when an auxiliary lens was employed to fill the full aperture of the grating.
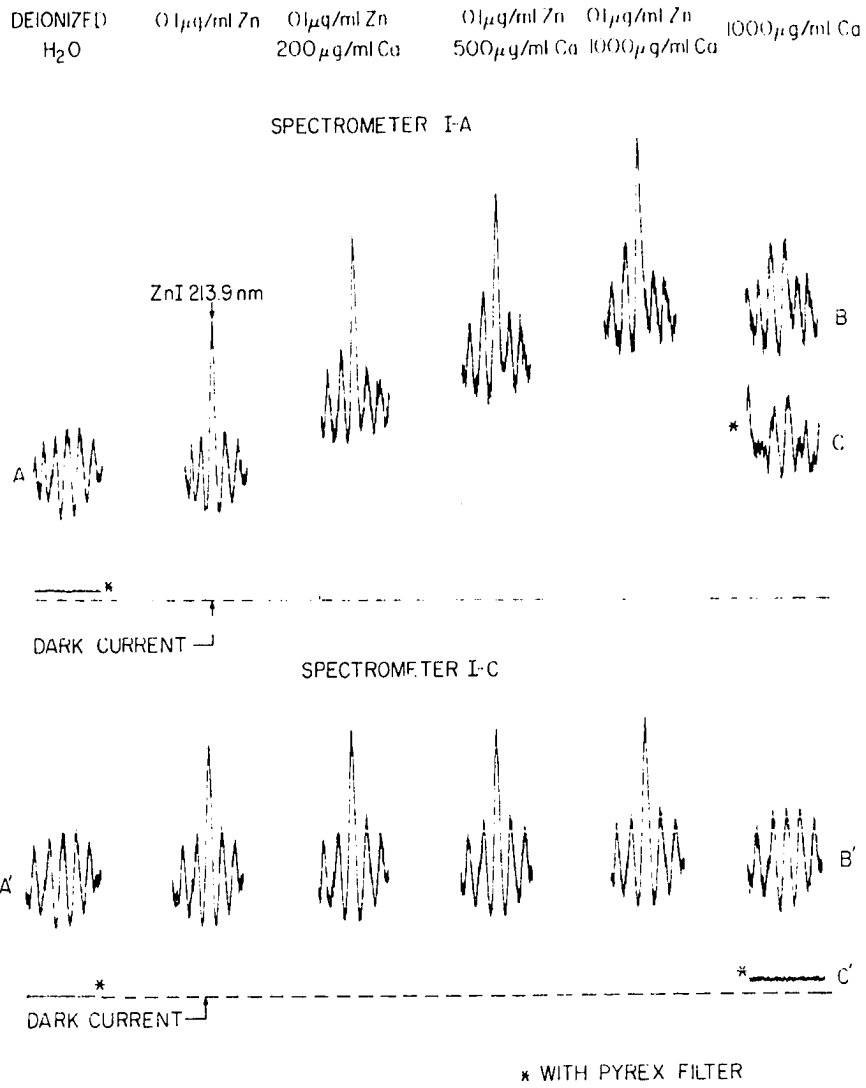
Figure 24. Effect of far scatter from Ca emission on the observed background signal in the region of the Zn I 213.9 nm line

The far scatter observed with spectrometer I-A at a
wavelength setting in the region of the Zn I 213.86 nm line
was on the order of 2×10^{-6} of the sum of the measured first
order peak intensities of the Ca II 393.37 and 396.85 nm
lines. The 2×10^{-6} fraction level is in harmony with other
observations on some of the early gratings ruled under inter-
ferometric control (111) and is unacceptably high. It is
also interesting to note that $\sim 5\%$ of the H_2O background
signal (A in Figure 24) observed with spectrometer I-A was
due to stray light from radiation passed by the borosilicate
glass filter, whereas introduction of solutions containing
1000 µg/ml Ca produced an approximate two-fold increase in
the measured background.

A reduction of stray light by a factor of ~ 10 relative
to the Zn I line resulted when the grating in spectrometer
I-A was replaced with a holographically recorded grating
(designated I-C) as shown in Figure 24. Even with this
reduction the background shift observed for solutions con-
taining 1000 µg/ml Ca (recording C' corrected for the
transmittance of the filter) was still equivalent to 0.02
µg/ml Zn, which is an order of magnitude greater than the
detection limit for Zn. When the stray light generated by
the Ca concomitant was expressed in terms of equivalent Zn
concentration (to take into account the differences in
efficiencies of the gratings), spectrometer I-B gave
essentially the same performance as spectrometer I-C.

Although the major portion of the stray light shown in Figure 24 for spectrometer I-A was due to far scatter from the grating, other sources of stray light may produce significant contributions with the superior gratings in spectrometers I-B and I-C. To eliminate the contributions to the total stray light signal from the far scatter from the grating and the scattering from the exit portion of the mirror, a black velvet cloth was placed over the exit portion of the mirror. With the covered exit mirror, only ∿0.1% of the baseline background signal (recording A' of Figure 24) was observed. Thus, 0.1% represents the upper limit for scattering of reflection from the black velvet. When 1000 µg/ml Ca solutions were nebulized with the exit mirror covered, approximately 10% and 25% respectively of the total stray light signals, i.e., difference between recordings B' and A' in Figure 24, for spectrometer I-B and -C were observed. Thus, 90% and 75% of the stray light signals observed with these spectrometers for 1000 µg/ml Ca solutions were presumably due to a combination of far scatter from the grating and scattering from the exit mirror.

The recordings obtained with spectrometer II (shown in Figure 25) are very similar to those recorded for spectrometer I-C. The ICP employed with spectrometer II was operated under slightly different operating conditions than the ICP employed with spectrometer I-A, -B, and -C so that precise comparison
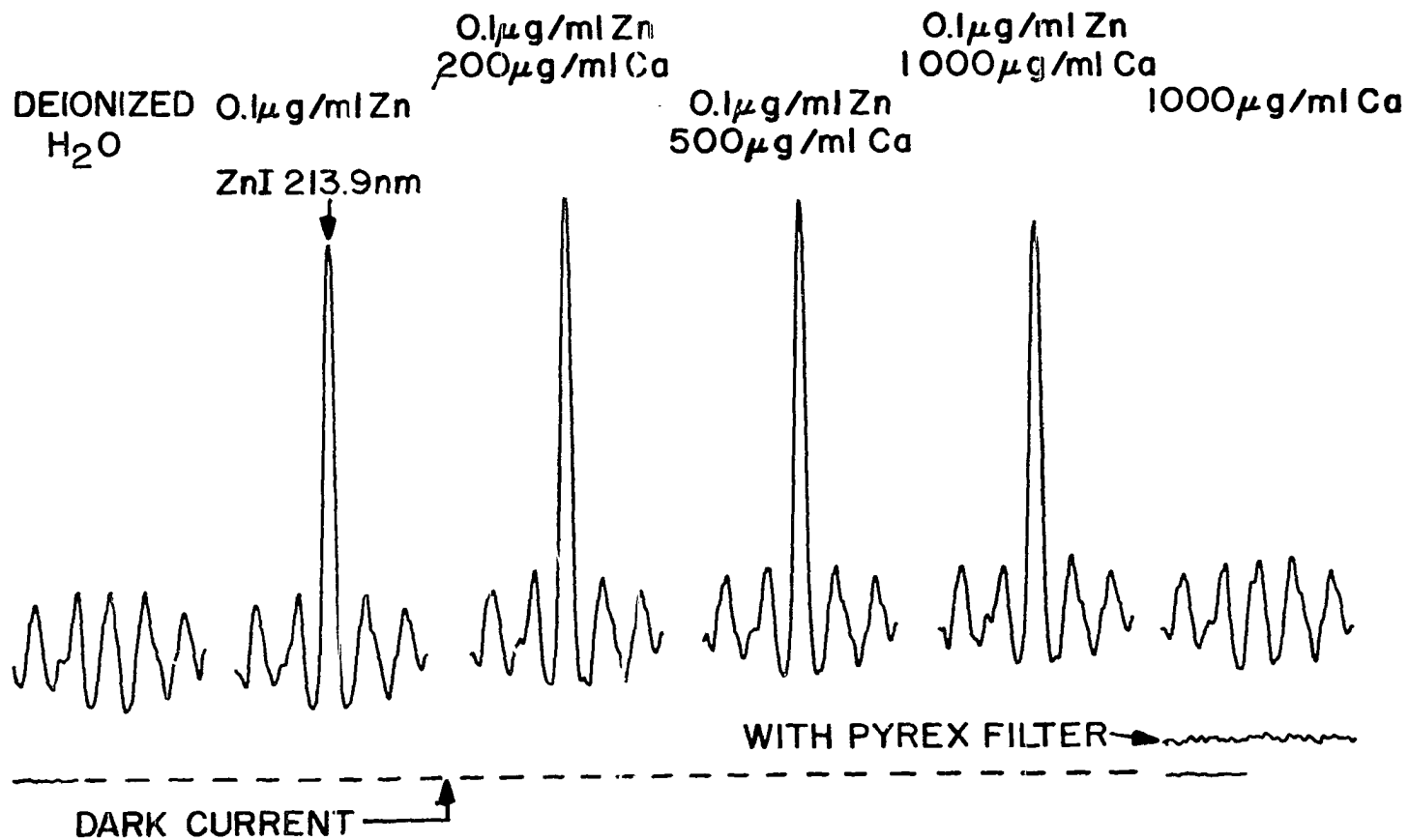
Figure 25. Effect of far scatter from Ca emission on the background signal observed with Spectrometer II-A in the region of the Zn I 213.9 nm line

of the performance of the spectrometers used to obtain the data in Figure 24 is not possible.

The stray light in spectrometer I-A, which was $\sim 2 \times 10^{-6}$ of the sum of the peak intensities of the Ca II 393.37 and 396.85 nm lines, produced a net signal equivalent to ~ 0.2 µg/ml Zn. Thus, a reduction to $\lesssim 2 \times 10^{-8}$ would be necessary to reduce the stray light from solutions containing 1000 µg/ml Ca to a net signal level less than that obtained with a solution containing Zn at the detection limit concentration (0.002 µg/ml). This level of rejection of far stray light is apparently attainable with some spectrometers presently available. However, such factors as grating efficiency, operating conditions of the ICP or other excitation source, and sample composition also play a role in determining the level of stray light rejection necessary for the reduction of stray light to a negligible level.

Knowledge of the specific radiations responsible for the stray light is a necessary prerequisite for the judicious selection of measures to eliminate the problems. To determine the origin of the stray light arising from calcium, several filters with known transmittances were placed in the optical path and the differences between the signals for solutions containing Ca and deionized H_2O (hereafter called the net signal) were measured. The results of these experiments are shown in Table VI. The principal origin of the

Table VI. Effect of filters on the stray light from Ca

Spectrometer	Sample nebulized	Normalized signal at a wavelength setting of 213.93 nm	Net signal[a]	Net signal[a] with borosilicate glass filter	Net signal[a] with CS-3-75 filter	Net signal[a] with CS-3-72 filter
I-A or I-C	H_2O	100				
I-A	1000 µg/ml Ca	193	93	80(91)[b]	25(89)[c]	∿0.1[d]
I-C	1000 µg/ml Ca	108	8	7(8)	2(7)	∿0
I-A	10,000 µg/ml Ca	388	288	227(258)	69(246)	∿1.3
I-C	10,000 µg/ml Ca	129	29	15(17)		

[a]Net signal = sample signal − signal for H_2O (with filter for 5th, 6th, and 7th columns).

[b]Values in parentheses are corrected for the transmittance of the borosilicate glass filter at 393.37 nm, i.e., Net ÷ transmittance of borosilicate glass filter.

[c]Values in parentheses are corrected for the transmittance of CS-3-75 filter at 393.37 nm (0.26) and 396.85 nm (0.31), weighted for the relative intensities of the Ca II 393.37 and 396.85 nm lines, i.e., Net ÷0.26.

[d]Transmittance of CS-3-72 filter was <10^{-4} at 393.37 nm and ∿0.8 from 490 to >750 nm.

stray light may be assigned with confidence if quantitative agreement is found between the net signal with no filter (column 4 of Table VI) and the net signals with several carefully chosen filters, after corrections for the transmittance of the filters at the suspected wavelength of the stray light (values in parentheses in columns 5 and 6 of Table VI). As shown in the fifth column of Table VI, the net signals observed for the 1000 μg/ml Ca solution were only slightly attenuated by a borosilicate glass filter (transmittance of $<10^{-4}$ at 213.86 nm). After correction for the transmittance of the borosilicate glass filter at 393.37 nm (or, because of the plateau in the transmittance curve of the filter, any wavelength between ∿350 nm and >750 nm), reasonable quantitative agreement was obtained with the net signals observed for the 1000 μg/ml Ca solution with no filter (column 4). Thus, the majority of the net signals for the 1000 μg/ml Ca solution were due to radiation passed by the borosilicate glass filter. The net signals for the 1000 μg/ml Ca solution were partially attenuated with the CS-3-75 filter (Corning Glass Works) as shown in the sixth column of Table VI. This filter is a sharp-cut filter with transmittances of <0.1 for wavelengths below 375 nm, 0.26 at 393.37 nm, 0.31 at 396.85 nm, and ⪞0.8 at wavelengths above 460 nm. After correction for the measured transmittances of the filter at the Ca II 393.37 and 396.85 nm lines,

weighted for the relative intensities of these lines,
reasonable quantitative agreement was found with the net
signals observed with no filter. For the CS-3-72 filter,
which is a sharp-cut, high wavelength pass filter with a
transmittance of $<10^{-4}$ at 396.85 nm, the net signals for
the 1000 µg/ml Ca solution were nearly completely attenu-
ated. This filter rejects the intense Ca lines at 393.37
and 396.85 nm but passes the radiation from the CaO and CaOH
bands in the visible. The data in column 7 show that only
a negligible net signal is observed, hence the major portion
of the stray light observed with the 1000 µg/ml Ca solutions
at a wavelength setting adjacent to the Zn I 213.86 nm line
with spectrometers I-A and I-C arose from the Ca II 393.37
and 396.85 nm lines.

It is evident from the data in column 4 of Table VI
that the net signals for 10,000 µg/ml Ca solutions were not
increased 10-fold over those observed for the 1000 µg/ml
solutions. Changes in the nebulization and transport
efficiencies, self-absorption of the Ca II lines, or shifts
in the real spectral background may have introduced a down-
ward bias in the expected increase in the net signal. On
the other hand, for spectrometer I-C, only half of the net
signal was observed for the 10,000 µg/ml Ca solution when
the borosilicate glass filter was inserted into the optical
path. Thus, for concentrations of Ca greater than ∿1000
µg/ml, either the stray light from other Ca lines became

more significant, or the real spectral background was affected by the introduction of solutions containing >1000 µg/ml Ca.

The effects of increasing concentrations of Mg in the nebulized solution on the background observed near the Zn I 213.86 nm line are shown in Figure 26. As in the case of Ca, the upward shifts in the background observed with increasing concentrations of Mg with these spectrometers, as well as the apparent change in structure for spectrometer I-A, were due to stray light as shown by the tracings with the CS-9-54 filter (Corning Glass Works) in the optical path. This filter is a sharp-cut, high-pass filter with transmittances of 0.05 at 213.86 nm and 0.86 at 280 nm. Thus, the CS-9-54 filter transmits most of the radiation from the very intense Mg II 279.55 and 280.27 nm lines, which are the principal sources of the stray light arising from appreciable concentrations of Mg in the ICP. When the stray light at 213.86 nm was expressed in terms of equivalent µg/ml Zn (to account for the differences in efficiencies of the gratings), the performance of spectrometer I-B was essentially the same as spectrometer I-C. Only ≲2% of the total stray light was observed in spectrometers I-B and I-C at 213.9 nm when the exit portion of the mirror was covered with black velvet. Thus, ∿98% of the stray light (difference between B' and A' in Figure 26) appeared to arise from
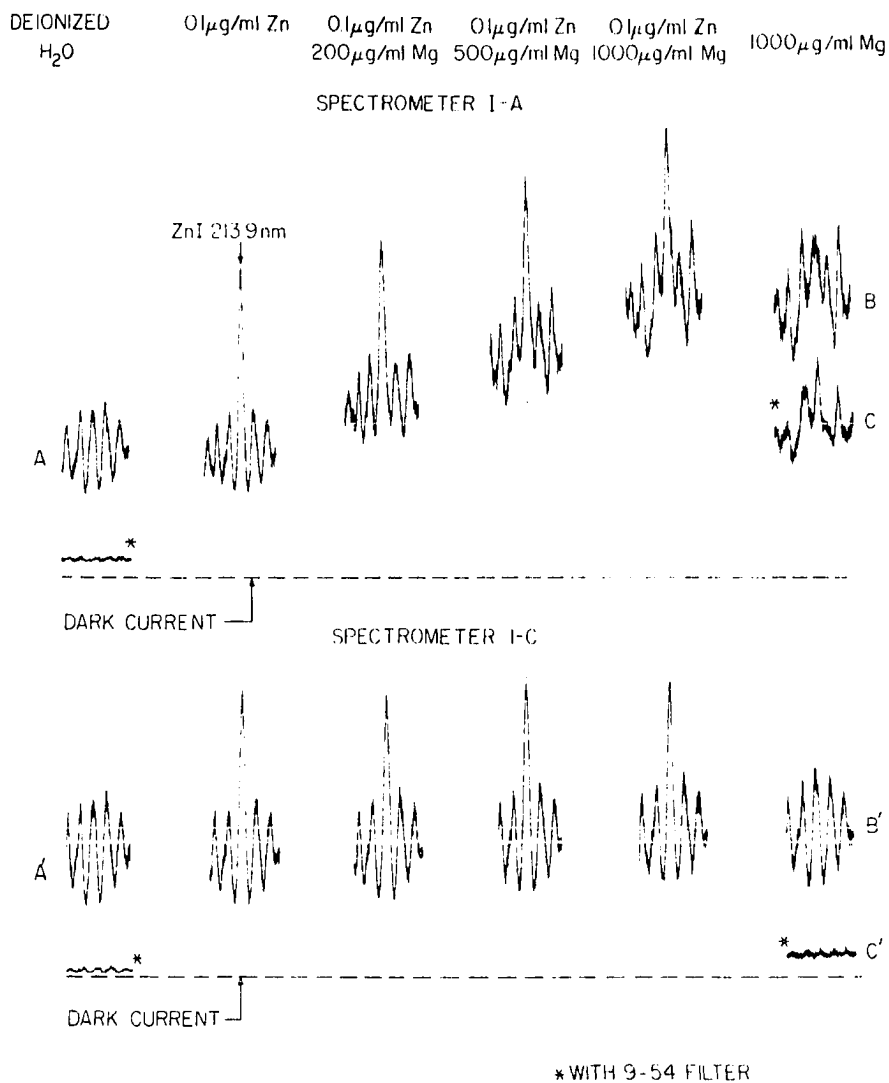
Figure 26. Effect of far scatter from Mg emission on the observed background signal in the region of the Zn I 213.9 nm line

grating scatter or from scattering from the exit portion of the mirror of the first order Mg II 279.55 and 280.27 nm lines (with possibly some contributions from the Mg I 285.2 line).

For spectrometer I-A the stray light level at a wavelength setting adjacent to the Zn I 213.86 nm line was $\sim 4 \times 10^{-6}$ of the measured peak intensities (first order) of the Mg II 279.55 and 280.27 nm lines. Because the stray light observed when solutions containing 1000 $\mu g/ml$ Mg were nebulized into the plasma produced a net signal equivalent to ~ 0.12 $\mu g/ml$ Zn, a reduction to $\gtrsim 7 \times 10^{-8}$ would be necessary at this Mg concentration to produce a net signal less than that obtained with a solution containing Zn at the detection limit concentration (0.002 $\mu g/ml$). This level of rejection of far stray is apparently attainable with some spectrometers presently available.

To eliminate the stray light contributions to the background signal adjacent to the Zn I 213.86 nm line, a uv interference filter (transmittances of 0.34 at 213.86 nm, ~ 0.004 at 279.6 nm, and 0.0002 at 393.4 nm; 78-2, Acton Research Corp., Acton, MA) was inserted in the optical path preceding the entrance slit of spectrometer II-B. No significant differences in the signals were observed for deionized H_2O and 1000 $\mu g/ml$ Ca or Mg solutions with a CS-9-54 filter in the optical path (in addition to the

interference filter). Thus, the interference filter reduced the stray light from longer wavelength Ca or Mg radiation to insignificant levels. The absence of stray light from radiation occurring within or below the bandpass of the filter was not unequivocally established. As shown by the normalized intensities in Table VII the addition of up to 1000 µg/ml Ca or Mg to the nebulized solution produced no significant change in the measured background signal, i.e., $\lesssim$1% of the background signal. The data in Table VI also indicate that the addition of up to 1000 µg/ml Li, 6900 µg/ml Na, or 20,000 µg/ml K produced no significant change in the background signal, although significant shifts were observed with the 5000 µg/ml Li and 23,000 µg/ml Na solutions. Depressions in the background signals from ICP's have been observed by Scott and Strasheim (136) for solutions containing K, Li, Mg or Ca (no corrections for the stray light were indicated) at 213.86 nm and by Dalager (137) for solutions containing Ca or Mg at several wavelength positions below 238.9 nm with interference filters immediately in front of the detectors. These discrepancies appear to be due to differences in operating conditions and require further study. For example, the data in Table VII were obtained with the capacitors of the impedance matching circuit at the positions which yielded the minimum reflected power meter reading ($\lesssim$5 W) with the introduction of deionized

Table VII. Effects of various elements on observed back-
ground signal with interference filter

Sample nebulized	Normalized signal of a wavelength setting of 213.93 nm
H$_2$O	100
200 µg/ml Ca	100.2 ± 1.4[a]
500 µg/ml Ca	99.6 ± 0.9
1000 µg/ml Ca	99.6 ± 1.0
200 µg/ml Mg	100.1 ± 0.8
500 µg/ml Mg	100.0 ± 1.2
1000 µg/ml Mg	100.9 ± 1.2
1000 µg/ml Li	100.3 ± 0.9
5000 µg/ml Li	106.1 ± 1.0
2300 µg/ml Na	99.7 ± 0.8
6900 µg/ml Na	99.4 ± 1.1
23,000 µg/ml Na	97.1 ± 1.2
100 µg/ml K	100.1 ± 1.3
1000 µg/ml K	99.5 ± 1.3
20,000 µg/ml K	100.4 ± 1.2

[a]Limits are the standard deviation.

H_2O. If the capacitors were readjusted to yield a reflected power of ∿15 W, depressions up to ∿14% of the background signals were observed which were accompanied by increases in the reflected power in apparent agreement with the observations of Scott and Strasheim (136). However, upward shifts in the spectral background adjacent to the Zn I 213.86 nm line were observed with spectrometer III with the introduction of solutions containing 200 to 1000 µg/ml Mg (but not Ca). For example, the shift observed with the 1000 µg/ml Mg solution was ∿7% of the signal observed without Mg. These shifts could not be attributed to stray light. Preliminary experiments have shown that various experimental parameters influence the relative magnitude of the shifts in the true spectral background, e.g., the radiofrequency power level, plasma gas flow rate, and the region from which the emission is sampled. Hence, the discrepancy between the above mentioned results from spectrometer III and the data in Table VII may be attributed to differences in the excitation sources. However, definitive investigations of the effects of various elements on the true spectral background will require high stray light rejection.

It is interesting to note that even without an interference filter, the stray light passed by a borosilicate glass filter with spectrometer I-A amounted to less than 1% of the background signal observed without the filter at

213.93 nm when solutions containing 5000 µg/ml Li, 23,000
µg/ml Na, or 20,000 µg/ml K were nebulized. The relatively
low stray light level may be attributed to several factors.
First, the high degree of ionization of the alkali elements
in the ICP leads to rare gas configurations, whose sensitive
lines occur in the vacuum ultraviolet region. Second, there
is a large wavelength separation between the most sensitive
atomic lines of these elements and the 213.93 nm wavelength
setting. Finally, S-13 photocathodes have low quantum
efficiency at the wavelengths of the sensitive atomic lines
of these elements.

Extraneous sources of stray light

Although grating imperfections have been identified
above as the primary source of stray light in some grating
spectrometers, improvements in the stray light character-
istics of gratings have increased the relative importance
of other extraneous sources of stray light. For example,
reflections and scattering of the Ca II 393.37 nm line in
the exit slit assembly of spectrometer I-A caused significant
levels of stray light as shown by the broad line (marked A)
in Figure 19.

As noted above, dispersed radiation that passes through
the appropriate exit slits of polychromators may undergo
scattering and reflection from the secondary mirrors employed
to deflect the radiation to the appropriate detector from

secondary mirror posts, and from other surfaces beyond the exit slit. To assess the magnitude of the stray light that eventually reaches the detectors from these sources, all of the exit slits in spectrometer II, except those of Ca II 393.37 and Mg II 279.55 nm lines were blocked. Although all exit slits other than those of Ca and Mg were blocked, it is still possible to scan each of the other 45 spectral lines across their appropriate blocked exit slits. This scanning action is achieved by moving the entrance slit along the Rowland circle to change the angle of incidence of the source radiation on the grating. During this experiment no signal should, of course, be observed in the blocked channels if stray light does not originate in the secondary optics. The recordings in Figures 27 and 28 definitely show that is not so. When solutions containing Ca and Mg were nebulized, it is seen that "pseudo lines" were recorded for the Tl I 377.57 and Fe 261.19 nm lines, at precisely the wavelength scanning position (slit dial position = -9.20 corresponding to the passage of the Ca II and Mg II lines through their respective exit slits. Similar scans were obtained for other programmed channels. Because the solutions contained no detectable Tl or Fe and the exit slits for these channels were blocked, these signals did not originate from characteristic Tl or Fe radiation passing through the exit slits. These signals, in fact, resulted from scattering and
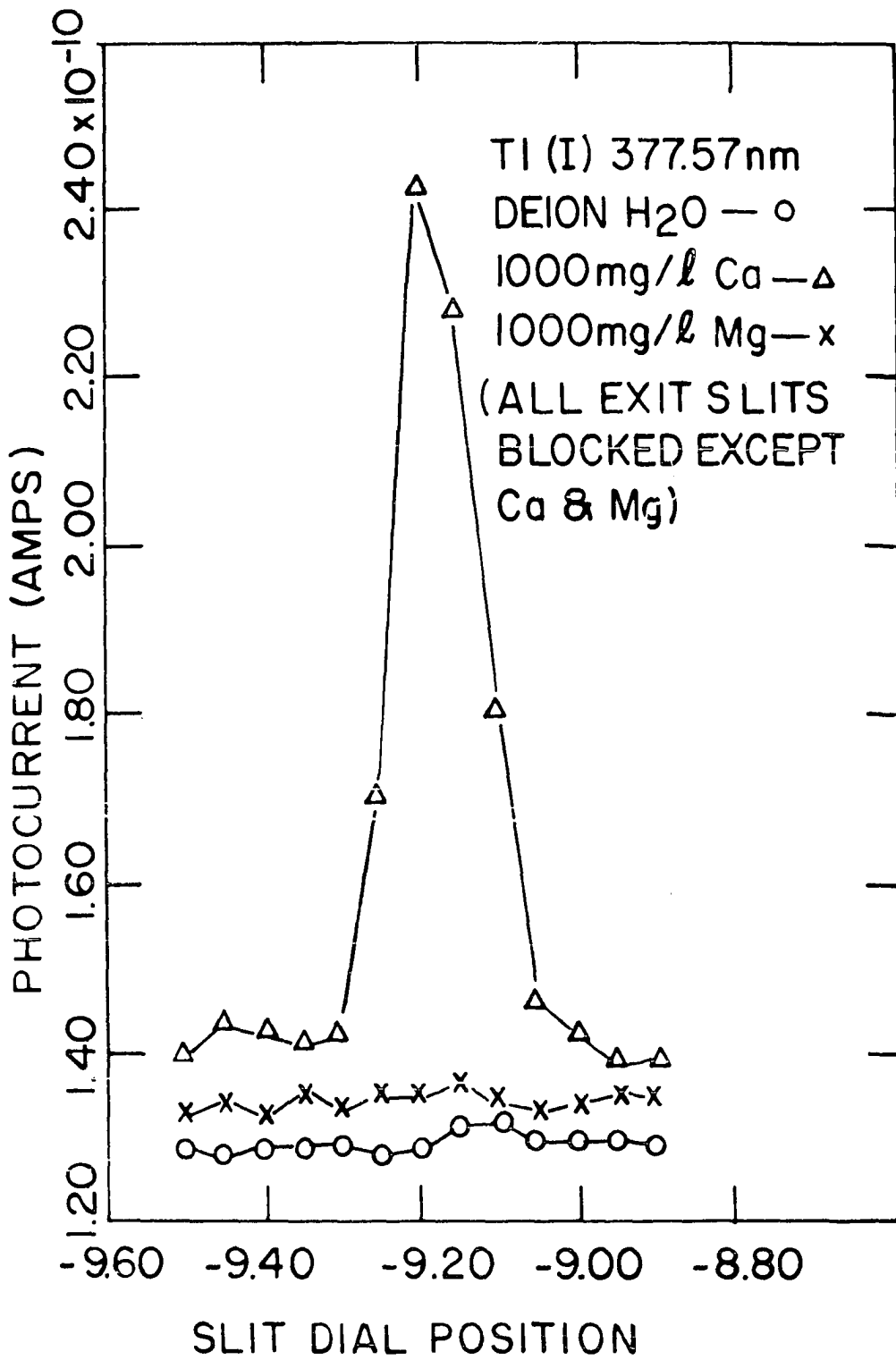
Figure 27. Stray light originating in the secondary optics
of spectrometer II-A measured on the Tl II
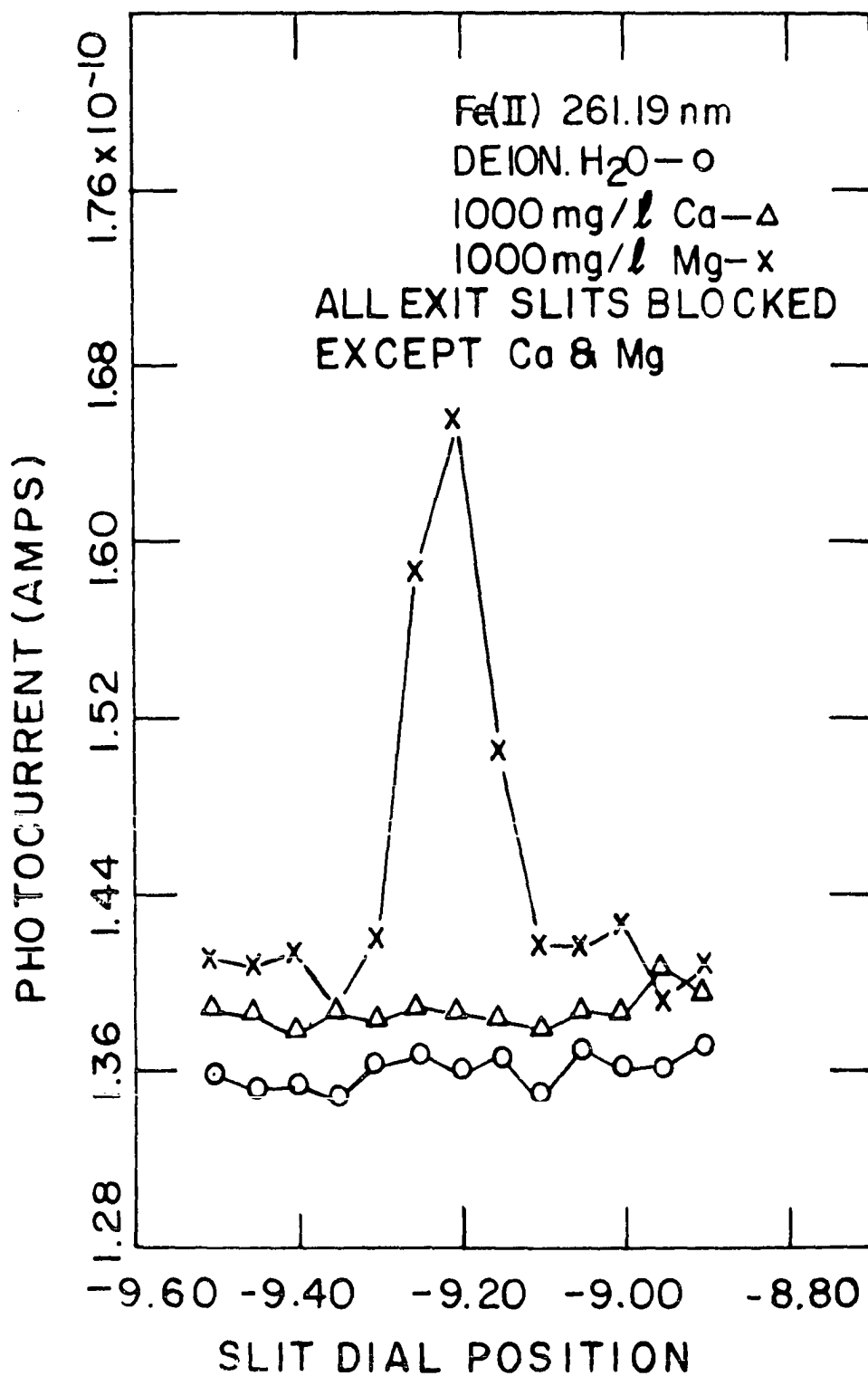377.57 nm channel

Figure 28. Stray light originating in the secondary optics
of spectrometer II measured on the Fe II
261.19 nm channel

reflections of the Ca and Mg ion line radiation in the secondary optics region during the transit of these lines across their respective exit slits.

In spectrometer II other extraneous sources of stray light were present in addition to that generated by scattering and reflection in the secondary optics of radiation passing through the exit slits. For example, the difference in the measured signals for the scans with deionized H_2O and the 1000 µg/ml Mg solutions in Figure 27 was essentially the same as that observed in another experiment with all of the exit slits blocked. Similarly, the signals observed for the 1000 µg/ml Ca solution with all exit slits blocked except for the Ca II and Mg II lines (Figure 27) at scan positions sufficiently removed from the -9.20 slit dial position, e.g., at -9.40, did not differ significantly from those observed with all of the exit slits blocked. A portion of these stray light signals apparently arose from radiation reflected from the bright metallic finish on the face of the exit slit jaws which escaped through the tubing and baffling leading to the entrance slit.

The stray light signals observed in spectrometer II for the 1000 µg/ml Ca or Mg solutions with all of the exit slits blocked except for the Ca II and Mg II lines ranged from an insignificant fraction of the total stray light signal with all slits opened to as much as a half of this total. However,

with improvements in the stray light characteristics of gratings, these other sources of stray light may become more significant, thus requiring higher quality engineering in the design and construction of polychromators.

The data presented above strongly suggest that the upward shifts in the measured background produced by relatively high concentrations of Ca reported previously by Borms et al. (138), Scott and Kokot (76), and Boumans and de Boer (139) were due to stray light rather than actual shifts in the true spectral background. The stray light effects documented above have undoubtedly occurred in other optical emission studies but have not been recognized because analyses were not performed near detection limit concentrations, or the effects of stray light were obscured by indirect effects on the real spectral background, or other interelement interactions caused far greater excursions in net line intensities.

It should be realized that upward shifts in the measured background may be produced not only by stray light arising from a few very intense lines but also by a large number of less intense lines or molecular bands. For instance, the introduction of solutions containing 1000 µg/ml of Fe, Mn, or Al produced a shift in the background (above that observed with the introduction of deionized H_2O only) adjacent to the Zn I 213.86 nm line equivalent to ∿0.2, ∿0.14, or ∿0.06 µg/ml Zn, respectively with spectrometer I-A. Since there are

large variations in the stray light characteristics of different spectrometers and even in gratings produced by the same technique, it is important to identify these effects with each spectrometer.

Solutions to the Stray Light Problem

Stray light levels may be decreased significantly through the use of "state of the art" gratings and optical components as well as through quality engineering in the design of spectrometers. For example, all nonoptic surfaces within a spectrometer should possess an optically flat black coating. Baffles should be located to trap the zero and other order radiations that are not used. In polychromators light tunnels and baffles may be necessary at appropriate locations in the secondary optics region to prevent optical "cross-talk" between channels. Stray light in the secondary optics region may also be reduced by elimination or temporary blockage of exit slits for intense lines of elements normally present in samples at varying high concentrations. However, reduction of stray light to insignificant levels for all sample types may not be possible even with "state of the art" single-pass spectrometers.

Normal interference correction procedures can be used to correct for stray light once the concomitants causing the stray light have been identified. Preliminary results (77) have revealed that empirical correction coefficients based

on a linear relationship with the interferent concentration do not generally provide valid corrections. These results imply that either correction curves should be established or the coefficients should be based on measured intensities of the parent line or lines. Direct reading polychromators simplify this task by allowing simultaneous measurement of the parent concomitant intensities from which appropriate correction coefficients may be calculated. Stray light arising from the cumulative effect of many elements or lines may, however, necessarily complicate the correction procedure.

Double monochromatization (129) provides a substantial reduction of stray light (the ratio of the stray light intensity to the parent line is squared) and should eliminate the need for corrections for stray light in nearly all situations. Prism predispersion will also provide significant reduction of stray light in many situations.

The judicious selection of the spectral response of the detectors may be used to good advantage in reducing stray light contributions. For example, solar blind photomultipliers employing Cs-Te or Rb-Te photocathodes may substantially reduce or eliminate the long wavelength stray light contributions from Ca in the determination of Zn or other elements with sensitive lines below $\sim$300 nm. However, no reduction can be expected for the stray light contribution

from Mg. Optical filters can also provide an effective means of stray light reduction. In many cases sufficient rejection of far stray light may be achieved with narrow bandpass interference filters placed immediately in front of the detectors in a polychromator (140,141) or in front of the entrance slit of a monochromator. As discussed in a previous section, the stray light at a wavelength setting of 213.93 nm arising from a solution containing 1000 µg/ml Ca or Mg was essentially eliminated with an interference filter in the optical path. Interference filters for the 190-230 nm region, which were placed immediately in front of the detectors in spectrometer II-B, eliminated the stray light from up to 1000 µg/ml Ca (140). Upward shifts in the true spectral background were also observed with solutions containing Mg in agreement with the observations with spectrometer III with the same ICP facility discussed above.

Wavelength scanning or modulation techniques (142-145) provide excellent background correction for constant or slowly varying background and should provide correction for baseline shifts in the background produced by stray light. It should be realized that stray light often possesses significant structure, e.g., Rowland ghosts as illustrated by the tracings in Figure 20, the far scatter with spectrometer I-A in Figures 24 and 26, and the "pseudo lines" originating from scattering and reflection in the secondary

optics region illustrated in Figures 27 and 28. It should
be recognized that wavelength scanning or modulation
techniques can compensate for shifts in the true spectral
background which may result from the wings of spectral lines
as illustrated in Figures 21 and 22, or from other sources
such as those discussed in the Introduction of this chapter.
Further research is needed to determine which approach in
this broad category provides the most valid background
correction. Careful consideration should be given to situ-
ations in which the background or background shift possesses
structure or in which a spectral line occurs near the
analysis line.

REFERENCES

1. S. Greenfield, I. Ll. Jones, and C. T. Berry, _Analyst_ (_London_), 89, 713 (1964).

2. R. H. Wendt and V. A. Fassel, _Anal. Chem._, 37, 920 (1965).

3. R. H. Wendt and V. A. Fassel, _Anal. Chem._, 38, 337 (1966).

4. V. A. Fassel, _Proc. 16th Coll. Spectr. Int._, Heidelberg, 1971, Adam Hilger, London, 1972, p. 63.

5. V. A. Fassel and R. N. Kniseley, _Anal. Chem._, 46, 1110A, 1155A (1974).

6. V. A. Fassel, ASTM Spec. Tech. Pub., in press.

7. S. Greenfield, H. McD. McGeachin, and P. B. Smith, _Talanta_, 23, 1 (1976).

8. S. Greenfield, I. Ll. Jones, H. McD. McGeachin, and P. B. Smith, _Anal. Chim. Acta_, 74, 225 (1975).

9. P.W.J.M. Boumans, _Z. Anal. Chem._, 279, 1 (1976).

10. IUPAC Information Bulletin: Appendices on Tentative Nomenclature, Symbols, Units, and Standards - No. 27, Nomenclature, Symbols, Units, and their Usage in Spectrochemical Analysis-III. Analytical Flame Spectroscopy and Associated Procedures, November, 1972.

11. R. Herrmann, C. Th. J. Alkemade, and P. T. Gilbert, "Chemical Analysis by Flame Photometry," Interscience, New York, N.Y., 1963, p. 300.

12. C. Th. J. Alkemade, _Anal. Chem._, 38, 1252 (1966).

13. S. Fukushima, _Mikrochim. Acta_, 1959, 596.

14. V. A. Fassel and D. A. Becker, _Anal. Chem._, 41, 1522 (1969).

15. M. Servigne and M. Guerin de Montgareuil, _Chim. Anal._, 36, 115 (1954).

16. R. E. Popham and W. G. Schrenk, "Developments in Applied Spectroscopy," E. L. Grove and A. J. Perkins, Eds., Plenum Press, New York, Vol. 7A, 1969, p. 189.

17. C. Th. J. Alkemade and M. H. Voorhuis, $\underline{Z}$. $\underline{Anal}$. $\underline{Chem}$., $\underline{163}$, 91 (1968).

18. W. H. Foster and D. N. Hume, $\underline{Anal}$. $\underline{Chem}$., $\underline{31}$, 2033 (1959).

19. D. A. Becker, Ph.D. Thesis, Iowa State University, Ames, IA, 1970.

20. G. R. Kornblum and L. de Galan, $\underline{Spectrochim}$. $\underline{Acta}$, $\underline{Part}$ $\underline{B}$, $\underline{28}$, 139 (1973).

21. F. Alder and J. M. Mermet, $\underline{Spectrochim}$. $\underline{Acta}$, $\underline{Part}$ $\underline{B}$, $\underline{28}$, 421 (1973).

22. J. M. Mermet, $\underline{Spectrochim}$. $\underline{Acta}$, $\underline{Part}$ $\underline{B}$, $\underline{30}$, 383 (1975).

23. J. M. Mermet, $\underline{C}$. $\underline{R}$. $\underline{Acad}$. $\underline{Sc}$. $\underline{Paris}$, $\underline{Ser}$. $\underline{B}$, $\underline{281}$, 273 (1974).

24. D. J. Kalnicky, Ph.D. Thesis, Iowa State University, Ames, IA, 1976.

25. D. J. Kalnicky, V. A. Fassel, and R. N. Kniseley, submitted for publication in $\underline{Appl}$. $\underline{Spectrosc}$.

26. P.W.J.M. Boumans in "Analytical Emission Spectroscopy," E. L. Grove, Ed., Vol. 1, Part 2, Chapter 6, Marcel Dekker, New York, 1972.

27. S. Murayama, $\underline{Spectrochim}$. $\underline{Acta}$, $\underline{Part}$ $\underline{B}$, $\underline{25}$, 191 (1970).

28. K. Kitagawa and T. Takeuchi, $\underline{Anal}$. $\underline{Chim}$. $\underline{Acta}$, $\underline{60}$, 309 (1972).

29. M. Marinkovic and B. Dimitrijevic, $\underline{Spectrochim}$. $\underline{Acta}$, $\underline{Part}$ $\underline{B}$, $\underline{23}$, 257 (1968).

30. M. Marinkovic and T. J. Vickers, $\underline{Appl}$. $\underline{Spectrosc}$., $\underline{25}$, 319 (1971).

31. H. Schirrmeister, $\underline{Spectrochim}$. $\underline{Acta}$, $\underline{Part}$ $\underline{B}$, $\underline{23}$, 709 (1968).

32. H. Schirrmeister, $\underline{Spectrochim}$. $\underline{Acta}$, $\underline{Part}$ $\underline{B}$, $\underline{24}$, 1 (1969).

33. P.W.J.M. Boumans and F. J. de Boer, Spectrochim. Acta, Part B, 30, 309 (1975).

34. P.W.J.M. Boumans and F. J. de Boer, Spectrochim. Acta, Part B, in press.

35. M. H. Abdallah, J. M. Mermet, and C. Trassy, submitted for publication in Anal. Chim. Acta.

36. G. W. Dickinson, Ph.D. Thesis, Iowa State University, Ames, IA, 1969.

37. G. W. Dickinson and V. A. Fassel, Anal. Chem., 41, 1021 (1969).

38. T. B. Reed, J. Appl. Phys., 32, 821, 2534 (1961).

39. T. B. Reed, Int. Science and Tech., June 1962, p. 42.

40. M. Riemann in "Emissionspektroskopie," R. Ritschl and G. Holdt, Eds., Akademie-Verlag, Berlin, Germany, 1964, p. 173.

41. R. Woodriff, Appl. Spectrosc., 22, 207 (1968).

42. J. D. Chase, J. Appl. Phys., 40, 318 (1969).

43. J. D. Chase, J. Appl. Phys., 42, 4870 (1971).

44. M. L. Thorpe, NASA Technical Report No. NASA CR-1143, 1968.

45. B. Waldie, Conference Proceedings International Round Table on the Study and Applications of Transport Phenomena in Thermal Plasmas, Odeillo-Fontromeu, France, Sept. 1975, IV-9.

46. M. I. Boulos, Conference Proceedings International Round Table on the Study and Applications of Transport Phenomena in Thermal Plasmas, Odeillo-Fontromeu, France, Sept. 1975, IV-7.

47. M. I. Boulos, IEEE Trans. Plasma Sci., PS-4, No. 1, 28 (1976).

48. A. I. Leont'ev and E. A. Tsalko, Teplofiz. Vys. Temp., 7, 715 (1969); High Temp. 7, 654 (1970).

49. P. Rosenblatt and V. K. Lamer, Phys. Rev., 70, 385 (1946).

50. Yu. P. Raizer, Usp. Fiz. Nauk, 99, 687 (1969);
    Sov. Phys. Usp., 12, 777 (1970).

51. A. C. West, V. A. Fassel, and R. N. Kniseley,
    Anal. Chem., 45, 1586 (1973).

52. R. H. Scott, V. A. Fassel, R. N. Kniseley, and
    D. E. Nixon, Anal. Chem., 46, 75 (1974).

53. C. C. Butler, R. N. Kniseley, and V. A. Fassel,
    Anal. Chem., 47, 825 (1975).

54. C. Veillon and M. Margoshes, Spectrochim. Acta, Part B,
    23, 503 (1968).

55. P.W.J.M. Boumans, F. J. de Boer, and J. W. Raiter,
    Philips Tech. Rev., 33, 50 (1973).

56. P.W.J.M. Boumans and F. J. de Boer, Spectrochim. Acta,
    Part B, 27, 391 (1973).

57. R. K. Winge, V. A. Fassel, R. N. Kniseley, and
    W. L. Sutherland, Pittsburgh Conference on Analytical
    Chemistry and Applied Spectroscopy, Cleveland, Ohio
    March 1974, No. 433.

58. Len West, Plasma-Therm, Inc., Kresson, NJ, personal
    communication, 1976.

59. R. G. Schleicher and R. M. Barnes, Anal. Chem., 47,
    724 (1975).

60. R. N. Kniseley, H. Amenson, C. C. Butler, and
    V. A. Fassel, Appl. Spectrosc., 28, 285 (1974).

61. S. Murayama, H. Matsuno, and M. Yamamoto, Spectrochim.
    Acta, Part B, 23, 513 (1968).

62. W. Tappe and J. van Calker, Z. Anal. Chem., 198, 13
    (1963).

63. H. Kawaguchi, M. Hasegawa, and A. Mizuike, Spectrochim.
    Acta, Part B, 27, 205 (1972).

64. S. E. Valente and W. G. Schrenk, Appl. Spectrosc., 24,
    197 (1970).

65. H. C. Hoare and R. A. Mostyn, Anal. Chem., 39, 1153
    (1967).

66. G. F. Kirkbright, A. F. Ward, and T. S. West,
    Anal. Chim. Acta, <u>62</u>, 241 (1972).

67. G. F. Kirkbright, A. F. Ward, and T. S. West,
    Anal. Chim. Acta, <u>64</u>, 353 (1973).

68. G. F. Larson, V. A. Fassel, R. H. Scott, and
    R. N. Kniseley, _Anal. Chem._, <u>47</u>, 238 (1975).

69. W. F. Meggers, C. H. Corliss, and B. F. Scribner, "Table
    of Spectral-Line Intensities," Part 1, NBS Monograph
    32, Washington, D.C., 1961.

70. R. N. Kniseley, C. C. Butler, and G. E. Holland,
    Ames Laboratory, USERDA, Iowa State University,
    Ames, IA, unpublished data.

71. D. J. Kalnicky, R. N. Kniseley, and V. A. Fassel,
    Spectrochim. Acta, Part B, <u>30</u>, 511 (1975).

72. J. M. Mermet and J. Robin, _Anal. Chim. Acta_, <u>70</u>, 271
    (1975).

73. W. B. Barnett, V. A. Fassel, and R. N. Kniseley,
    Spectrochim. Acta, Part B, <u>23</u>, 643 (1968).

74. R. N. Kniseley, V. A. Fassel, and C. C. Butler,
    Clin. Chem. (Winston-Salem, N.C.), <u>19</u>, 807 (1973).

75. S. Greenfield, H. McD. McGeachin, and P. B. Smith,
    Anal. Chim. Acta, <u>84</u>, 67 (1976).

76. R. H. Scott and M. L. Kokot, _Anal. Chim. Acta_, <u>75</u>,
    257 (1975).

77. R. K. Winge, Ames Laboratory, USERDA, Iowa State
    University, Ames, IA, unpublished data.

78. K. W. Olson, W. J. Haas, Jr., and V. A. Fassel,
    submitted for publication in _Anal. Chem._

79. P.W.J.M. Boumans, F. J. de Boer, F. J. Dahmen,
    H. Hoelzel, and A. Meier, _Spectrochim. Acta, Part B_,
    <u>30</u>, 449 (1975).

80. H. J. Issaq and L. P. Morgenthaler, _Anal. Chem._, <u>47</u>,
    1661 (1975).

81. E. Bădărău, M. Giurgea, G. H. Giurgea, and A.T.H. Trutia,
    Spectrochim. Acta, <u>11</u>, 411 (1956).

82. R. Mavrodineanu and R. C. Hughes, _Spectrochim. Acta_, 19, 1309 (1963).

83. S. Greenfield, H. McD. McGeachin, and P. B. Smith, _Talanta_, 22, 553 (1975).

84. R. K. Skogerboe and G. N. Coleman, _Anal. Chem._, 48, 611A (1976).

85. S. Murayama, _J. Appl. Phys._, 39, 5478 (1968).

86. J. B. Willis, _Spectrochim. Acta, Part B_, 25, 487 (1970).

87. J. van Calker and W. Tappe, _Arch. Eisenhuettenwes._, 34, 679 (1963).

88. W. Jantsch, Dissertation, Technische Hochschule, München, 1970.

89. W. Kessler, _Glastechn. Ber._, 44, 479 (1971).

90. D. F. Sermin, Applied Research Laboratories, Lausanne, Internal Report, May 1973.

91. K. Govindaraju, G. Mevelle, and C. Chouard, _Anal. Chem._, 48, 1325 (1976).

92. C. D. West and D. N. Hume, _Anal. Chem._, 36, 412 (1964).

93. A. C. West, V. A. Fassel, and R. N. Kniseley, _Anal. Chem._, 45, 2420 (1973).

94. J. D. Cobine and D. A. Wilber, _J. Appl. Phys._, 22, 835 (1951).

95. S. Lanz, W. Lochte-Holtgreven, and G. Traving, _Z. Physik_, 176, 1 (1963).

96. J. Janča, _Czech. J. Phys._, B17, 761 (1967).

97. G. Pforr, _Proc. 14th Coll. Spectr. Int._, Debrechen, 1967, Adam Hilger, London, 1968, p. 687.

98. W. Slavin, _Anal. Chem._, 35, 561 (1963).

99. F.J.J. Clarke, _J. Res. Nat. Bur. Stand._, A, 76A, 375 (1972).

100. R. Mavrodineanu, _J. Res. Nat. Bur. Stand._, A, 76A, 405 (1972).

101. S. R. Goode and S. R. Crouch, Anal. Chem., 46, 181 (1974).

102. J. N. Demas and G. A. Crosby, J. Phys. Chem., 75, 991 (1971).

103. W. H. Melhuish, J. Res. Nat. Bur. Stand., A, 76A, 547 (1972).

104. W. B. Barnett and H. L. Kahn, Anal. Chem., 44, 935 (1972).

105. T. C. Rains, M. S. Epstein, and O. Menis, Anal. Chem., 46, 207 (1974).

106. R. F. Stamm and C. F. Salzman, Jr., J. Opt. Soc. Amer., 43, 126 (1953).

107. R.C.C. Leite and S.P.S. Porto, J. Opt. Soc. Amer., 54, 981 (1964).

108. IUPAC Commission on Spectrochemical and Other Optical Procedures for Analysis, Pure Appl. Chem., 30, 653 (1972); Appl. Spectrosc., 28, 398 (1974).

109. H. A. Rowland, Phil. Mag., 35, 397 (1893).

110. G. W. Stroke in "Handbuch der Physik", Vol. 29, S. Flügge, Ed., Springer-Verlag, Berlin, Germany, 1967, pp. 533-564, 648-652.

111. R. M. Barnes and R. F. Jarrell in "Analytical Emission Spectroscopy", E. L. Grove, Ed., Vol. I, Pt. 1, Marcel Dekker, New York, 1971, p. 243.

112. A. J. Mitteldorf, Spex Speaker, X(3), 5 (1965).

113. H. P. Palenius, C. E. Magnussow, and P. O. Zetterberg, J. Opt. Soc. Amer., 62, 1525 (1972).

114. J. V. Kline and D. W. Steinhaus, Appl. Opt., 7, 2015 (1968).

115. T. Lyman, Phys. Rev., 16, 257 (1903).

116. F. A. Jenkins and H. E. White in "Fundamentals of Optics", 2nd ed., McGraw-Hill, New York, 1950, p. 320.

117. M. Françon, "Diffraction", Pergamon Press, New York, 1966, p. 111.

118. M. V. Klein, "Optics," J. Wiley & Sons, Inc., New York, 1970, p. 335.

119. P. Jacquinot and B. Roizen-Dossier in "Progress in Optics," E. Wolf, Ed., Vol. III, Chap. II, North-Holland, Amsterdam, 1964, pp. 42, 50.

120. A. Couder and P. Jacquinot, C. R. Acad. Sci. Paris, 208, 1639, 1939.

121. N. L. Alpert, Appl. Opt., 1, 437 (1962).

122. J. E. Tyler and R. C. Smith, J. Opt. Soc. Amer., 56, 1390 (1966).

123. A. Watanabe and G. C. Tabisz, Appl. Opt., 6, 1132 (1967).

124. C. M. Penchina, Appl. Opt., 6, 1029 (1967).

125. J. J. Mitteldorf and D. O. Landon, Appl. Opt., 7, 1431 (1968).

126. J. K. Pribram and C. M. Penchina, Appl. Opt., 7, 2005 (1968).

127. I. I. Sobel'man, "Introduction to the Theory of Atomic Spectra," Pergamon Press, Elmsford, NY, 1972, pp. 377-465.

128. A. P. Thorne, "Spectrophysics," Chapman and Hall, Ltd., London, 1974, pp. 249-283.

129. D. Landon and S.P.S. Porto, Appl. Opt., 4, 762 (1965).

130. P. Frank, P. Hahn-Weinheimer, and G. Markl, Appl. Spectrosc., 25, 529 (1971).

131. C. G. James and T. M. Sugden, Proc. Roy. Soc., Ser. A, 227, 312 (1955).

132. B. E. Buell in "Flame Emission and Atomic Absorption Spectrometry," J. A. Dean and T. C. Rains, Eds., Vol. 1, Marcel Dekker, New York, 1969, p. 274.

133. R. D. Cowan and G. H. Dieke, Rev. Mod. Phys., 20, 418 (1948).

134. J. D. Winefordner, W. W. McGee, J. M. Mansfield, M. L. Parsons, and K. E. Zacha, Anal. Chim. Acta, 36, 25 (1966).

135. C. S. Rann, _Spectrochim. Acta, Part B_, _23_, 245 (1968).

136. R. H. Scott and A. Strasheim, _Anal. Chim. Acta_, _76_, 71 (1975).

137. P. D. Dalager, Applied Research Laboratories, Sunland, personal communication, 1976.

138. A.G.J.M. Borms, G. R. Kornblum, and L. de Galan, _Third Int. Cong. of Atomic Absorption and Atomic Fluorescence Spect._, Paris, 1971, Halsted Press, New York, p. 53.

139. P.W.J.M. Boumans and F. J. de Boer, _Proc. Anal. Div. Chem. Soc. (London)_, _12_, 133 (1975).

140. J. M. Katzenberger, Ames Laboratory, USERDA, Iowa State University, Ames, IA, unpublished data.

141. G. V. Alexander and L. T. McAnulty, 1975 Pacific Conference on Chemistry and Spectroscopy, North Hollywood, CA, October 1975, No. 13.

142. W. Snelleman, T. C. Rains, K. W. Yee, H. D. Cook, and O. Menis, _Anal. Chem._, _42_, 394 (1970).

143. G. M. Hieftje and R. J. Sydor, _Appl. Spectrosc._, _26_, 624 (1972).

144. R. K. Skogerboe, G. N. Coleman, P. J. Lamothe, S. J. Freeland, and F. T. Varcoe, Federation of Analytical Chemistry and Spectroscopy Societies Second National Meeting, Indianapolis, IN, October 1975, No. 126.

145. R. K. Skogerboe, P. J. Lamothe, G. J. Bastiaans, S. J. Freeland, and G. N. Coleman, _Appl. Spectrosc._, _30_, 495 (1976).

ACKNOWLEDGMENTS